Modeling and Simulation of concentrated suspensions of short, rigid and flexible fibers

Rabih Mezher

Thèse de Doctorat

Rabih MEZHER

Mémoire présenté en vue de l'obtention du
grade de Docteur de l'École centrale de Nantes
sous le label de l'Université de Nantes Angers Le Mans

École doctorale : Sciences pour l'ingénieur, géosciences et architecture

Discipline : Mécanique des solides, des matériaux des structures et des surfaces
Unité de recherche : Institut de recherche en Génie civil et Mécanique

Soutenue le 8 décembre 2015

Modélisation et Simulation de suspensions concentrées de fibres courtes, rigides et flexibles

JURY

Président :	**M. Roland KEUNINGS**, Professeur, Université Catholique de Louvain - Belgique
Rapporteurs :	**M. Gilles REGNIER**, Professeur des universités, ENSAM Paris
	M. Ivan IORDANOFF, Professeur des universités, ENSAM Bordeaux
Examinateurs :	**M. Gilles AUSIAS**, Maître de conférences (HDR), Université de Bretagne - Sud
	M. Christophe BINETRUY, Professeur des universités, École Centrale de Nantes - GeM
Directeur de thèse :	**M. Francisco CHINESTA**, Professeur des universités, École Centrale de Nantes - GeM
Co-directeurs de thèse :	**Mme Emmanuelle ABISSET - CHAVANNE**, Maître de conférences, École Centrale de Nantes - GeM
	M. Julien FÉREC, Maître de conférences, Université de Bretagne - Sud

Remerciements

C'était le 4 avril 2012 à la bibliothèque de l'INSA de Lyon que je t'ai rencontré pour la première fois. Nous avons discuté pour une bonne trentaine de minutes. Et avant que tu es parti tu m'as dit: "Rabih, je pense qu'on va faire une belle thèse ensemble". Et bien, Paco, je pense que nous avons fait une belle thèse ensemble. Je ne sais par où dois-je commencer pour exprimer mes remerciements et mes appréciations te concernant. Tout d'abord je dois te remercier pour m'avoir donné l'opportunité de travailler avec toi, de découvrir un domaine extraordinaire dans le monde de la physique et d'accomplir mon rêve. Grâce à ton humanité, ta sympathie et ta gentillesse permanante, tu m'as permis de construire une grande passion pour le domaine de la physique et de la rhéologie. Je suis très heureux d'avoir eu la chance de bénéficier au niveau scientifique, humain et social de ton immense expérience. Tu étais toujours présent pour remédier aux problèmes que j'ai rencontrés durant la thèse. Aussi, tu acceptais et améliorais toujours mes suggestions et idées lors de nos nombreuses discussions dans ton bureau. Tu m'as fait preuve d'une totale confiance, et tu étais toujours à l'écoute et en mode actif. Je n'oublie jamais comment tu m'a encouragé à découvrir les différentes briques de la thèse. Avec ton sens de l'apprentissage, tu m'as motivé encore plus, et je suis devenu prêt à m'engager dans n'importe quelle idée sans avoir le moindre doute et sans avoir peur. Je souhaite vivement remercier Francisco Chinesta pour son amitié et lui exprimer ma plus profonde gratitude. Encore je me permets de te dire "Merci" dans ta langue maternelle : "Gracias".

Je passes en ce moment vers mes encadrants à Lorient: Julien Férec et Gilles Ausias. Je les remercie vivement pour leur amitié et les nombreuses discussions que nous avons eues et faites lors de leurs nombreuses visites à l'Ecole Centrale de Nantes. Je n'oublie jamais les choses qu'ils m'ont appris lors de mon séjour, qu'ils ont extrèmement faciliter, à l'Université de Bretagne Sud. Il m'ont bien formé dans le domaine de la simulation numerique directe et pour ça je leur doit une gratitude infinie. Ils ont contribué dans le deuxième, troisième et quatrième chapitre de cette thèse. Notamment ils ont toujours offert des idées originales dans la thèse et des solutions pour beaucoup de problèmes. Grâce à eux je suis capable aujourd'hui de présenter le fruit de cette thèse et d'être présent dans ce monde de la recherche.

Je n'oublie pas de remercier Emmanuelle Abisset-Chavanne.

Je tiens à remercier les membres du jury pour avoir accepter de participer à l'évaluation de ma thèse. Pour moi, c'est un honneur d'avoir un jury qui est une référence dans les travaux de ma thèse. Vous avez apporté les remarques, critiques et les éléments nécessaires qui rendent ce travail plus complet. Et pour cela je suis vraiment reconnaissant.

4

Il ne faut pas aussi oublié de remercier Adrien Leygue, qui est un dictionnaire et une encyclopédie de méthodes numériques. Il m'a beaucoup aidé à résoudre les principaux problèmes numériques dans cette thèse. Il était toujours à l'écoute et prêt à offrir et partager ses expériences avec moi, que se soit dans le domaine numérique ou dans le domaine rhéologique. Adrien je te remercie infiniment pour ton immense aide et ton savoir scientifique illimité.

Au delà des horizons nantais et du travail, je tiens à remercier vivement ma famille pour son soutien infini lors de ces trois années. Mes chers **parents** vous m'avez toujours donné de la motivation. Sans cette dernière et sans vous tout le fruit de cette aventure n'était pas possible. MERCI. Mon **frère** Haitham, tu étais toujours présent et à l'écoute pour m'aider dans les situations stressantes. Tu m'as poursuis pendant les beaux et les frustrants moments. Tu as contribué dans cette thèse sur le plan humain, moral et même technique. MERCI.

Encore, je me déplace vers mes amis qui m'ont aider beaucoup lors de la préparation du pot. Merci à chacun de vous pour votre présence et pour avoir assister à ma soutenance de thèse. J'apprécie tous vos efforts ce jour là.

Finalement, je remercie particulièrement mon ami et mon second **frère** Moustafa. Aussi tu m'as accompagné durant ces trois années et m'a soutenu dans toutes les situations et les difficultés que j'ai rencontrées. Je n'oublierai jamais tes encouragements.

PBS Job Id: 31/10/2015 rabih.ec-nantes.fr
Job Name: Thèse
Execution terminated
Exit-status = statut terminé
resources-used.mem = 223 Gb
resources-used.vmem = 223 Gb
resources-used.walltime = 26280 hours (3 years)

"THE TWO MOST IMPORTANT DAYS IN YOUR LIFE ARE THE DAY YOU ARE BORN AND THE DAY YOU FIND OUT WHY"

. *A ma famille*

Résumé

Les suspensions de nanoparticules - en particulier nanofibres et nanotubes - sont de plus en plus utilisées dans le cadre du développement de matériaux fonctionnels. Afin d'optimiser l'utilisation de ces matériaux et leurs procédés de fabrication, une connaissance fine de la microstructure et de son évolution lors d'un écoulement est primordiale. Pour cela, l'étude des suspensions se divise en deux axes de recherche : le régime dilué où la concentration est faible et chaque particule peut être décrite seule, et le régime concentré où l'on ne peut plus négliger l'interaction entre les particules, ni la formation d'agrégats. Le premier type de suspensions est bien connu ; le second reste encore problématique.

Pour une description plus précise de la physique fine qui agit à l'échelle microscopique, des modèles basés sur la Simulation Numérique Directe (ou DNS) sont développés. Une DNS est basée sur le calcul dans un volume représentatif, du mouvement d'une centaine de fibres (particules) et de leurs interactions, à l'échelle microscopique lorsqu'un écoulement de cisaillement simple est appliqué. Ainsi les suspensions sont considérées avec des interactions entre les fibres et l'évolution statistique d'une population de fibres (forces d'interaction et le nombre de contacts entre les fibres) est décrite. Durant la thèse un code de calcul intensif 3D basé sur la DNS a été développé. Ce code calcule la cinématique associée aux suspensions de fibres concentrées (contenues dans un volume élémentaire) et prend en compte les forces d'interactions présentes à chaque pas de temps.

Il existe une autre approche plus simplifiée à l'échelle mésoscospique pour traiter le régime concentré: la théorie cinétique. Cela est possible grâce à une fonction de densité de probabilité qui représente la probabilité de trouver une particule avec une orientation à un temps donné, dans l'espace. Lorsque la concentration du système devient très élevée, on considère un agrégat de fibre (au lieu de considérer une fibre, on suit l'évolution d'un agrégat composé de fibres enchevêtrées).

Mots clés: Simulation Numérique Directe, Théorie Cinétique, Rhéologie, Modélisation Numérique, Mécanique des Fluides

Abstract

Suspensions involving nanoparticles such as nanofibers and nanotubes are widely used today in the development of functional materials. In order to optimize the usage of these materials and their manufacturing processes, a fine knowledge of the microstructure's evolution in a flow is required. Thus, the study of such suspensions is divided into two main categories: the dilute regime where the concentration is low enough to describe each particle independently from its neighbors and the concentrated regime where the interaction between particles can no longer be neglected, nor the formation of aggregates (or clusters). The first type of suspensions is well known and treatable; the second one remains difficult to study. For a more precise and fine description of the physics at the microscopic scale, a solution consists in performing a Direct numerical simulation (or DNS). DNS is based on the computation, in a representative volume, of the motion of several hundreds of fibers and their interactions. It is a step by step process which derives kinematics as well as macroscopic properties, while taking into account the forces applied on each fiber at the microscopic scale. Thus the suspensions are considered along with interaction forces acting on each fiber and a statistical description is built (number of interactions, magnitude of forces, elastic energy...). During the thesis an extensive 3D simulation code based on DNS has been developed. It takes into account the kinematics of the concentrated fiber suspensions as well as the interaction forces involved.

Another more simple way to simulate concentrated fiber suspensions in a given flow is to use kinetic theory approaches. The kinetic theory incorporates a statistical orientation distribution function, which represents the probability of having a particle in a given physical space, having a certain orientation, at a given time. The simplicity of this theory is that it ignores the individuality of the entities (particles, fibers, nanotubes, ...), by introducing a probability function that acts on the mesoscopic scale. Thus, when the concentration of the fibers is high enough, a cluster of fibers can be considered and the rheological properties can then be calculated.

Key words: Direct Numerical Simulation, Kinetic Theory, Rheology, Numerical Modeling, Fluid Mechanics

Résumé développé

Aujourd'hui, les matériaux polymères composites renforcés par des fibres sont des matériaux importants dans un large éventail d'applications grâce à leurs propriétés mécaniques, électriques, et thermo-physiques intéressantes. Dans les processus industriels qui font intervenir l'écoulement, des fibres sont normalement présentes en suspensions dans une matrice polymère et constituent le renfort principal. La problématique principale est la compréhension du comportement mécanique de ces suspensions associé à leur microstructure, afin d'aboutir à une bonne description de la rhéologie et optimiser le procédé pour obtenir la meilleure microstructure.

Cependant il est souvent difficile de prédire expérimentalement ce comportement. C'est pourquoi, il s'avère nécessaire de faire des simulations numériques pour prédire l'évolution de la cinématique des suspensions. En général la concentration, l'orientation des fibres et le rapport de forme sont les paramètres clés, affectant la géométrie finale et les propriétés des pièces produites. Les paramètres principaux régissant le comportement rhéologique complexe des suspensions de fibres, outre la concentration et l'évolution de l'orientation, sont la distribution spatiale, les propriétés mécaniques des fibres/de la matrice, et les mécanismes d'interactions de type fibre-fibre et fibre-fluide (écoulement).

Si la concentration du système est assez faible, on peut supposer que le champ de vitesse de l'écoulement n'est pas perturbé par la présence des fibres. Les fibres sont suffisamment éloignées les unes des autres, de manière qu'elles n'interagissent pas entre elles. L'augmentation de la concentration des fibres - mène à des interactions hydrodynamiques - parce que la densité élevée des fibres dans le volume est suffisante pour perturber l'écoulement. Ici les fibres interagissent ensemble par l'intermédiaire de contacts directs. La distance moyenne entre les fibres devient du même ordre de grandeur que le diamètre des fibres et les fibres agissent l'une sur l'autre par des effets hydrodynamiques.

Dans cette thèse l'objectif est d'étudier les suspensions concentrées de fibres, puisqu'elles représentent le cas le plus réaliste dans les processus industriels. Dans le premier chapitre, une étude bibliographique sur les suspensions de fibres est faite. Leurs divers modèles théoriques dans la littérature, les différentes échelles utilisées pour l'étude de tels suspensions et les trois régimes de concentration principaux sont présentés et expliqués.

Dans les deuxième, troisième et quatrième chapitres, on présente un modèle à l'échelle microscopique qui décrit au mieux les interactions complexes de type fibre-fibre et permet d'adresser la physique fine impliquée dans de telles interactions riches et intenses. Ici on décrit la simulation numérique directe (DNS): la DNS est basée sur le calcul dans

un volume représentatif, du mouvement d'une centaine de fibres et de leurs interactions, à l'échelle microscopique. La DNS, dans ces chapitres, est appliquée pour des fibres de longueurs différentes qui suivent une loi de distribution normale (avec une longueur moyenne et un écart type). Le fluide est newtonien et on considère un écoulement de cisaillement simple. Au sein de cet écoulement, la cinématique des fibres et les propriétés macroscopiques ont été obtenues. L'originalité ici, est l'introduction de l'élasticité et la flexion des fibres. On note que les fibres sont supposées rigides tant qu'on ne s'intéresse pas à l'énergie élastique qu'elles peuvent stocker. Si les fibres sont infiniment rigides, donc aucune énergie élastique sera stockée. Les fibres sont supposées subir des petites déformations, sous l'action des moments fléchissants issus des forces d'interactions, quand elles deviennent plus flexible. Pour cette raison, leur cinématique sera la même que celle des fibres rigides. A partir delà, on a tiré beaucoup de résultats et conclusions. Tout d'abord on est arrivé à distinguer deux régimes dans l'évolution de la cimématique: une phase transitoire où l'orientation évolue d'un état isotrope à un état où la plupart des fibres sont alignées, ce qui constitue le régime stationnaire. Pour les différences de contraintes normales N_1^+ et N_2^+, on a lié leur comportement dans la zone transitoire avec le changement brusque des orientations des fibres, dû à la nature du cisaillement. Ce comportement était en accord avec des mesures expérimentales vues dans la littérature. Les signes de N_1^+ et N_2^+ ont été discutés et c'était prouvé que N_2^+ ne peut pas être considérée négligeable devant N_1^+ dans le cas de suspensions concentrées avec la présence d'interactions entre les fibres. Ensuite, les évolutions statistiques ont été étudiées: l'énergie élastique et le nombre des interactions. Lorsque l'écoulement a été inversé, le nombre d'interactions a diminué et par conséquent les fibres ont perdu leur tendance à être alignées, et cela a été démontré par l'évolution de la viscosité dans le sens inverse. Pour l'énergie élastique, des pics apparaissent au début de la simulation lorsque les fibres ont brusquement changé leur orientation où l'élasticité des suspensions est activée. Lorsque les fibres étaient presque alignées, l'élasticité diminuait et les suspensions subissaient une relaxation avec des interactions relativement faibles. On a comparé le nombre total d'interactions N_I avec le nombre moyen théorique d'interactions par fibre N_C. Il a été constaté que la différence entre N_I et N_C dépend de la distance critique autorisée entre deux fibres (la distance critique permise entre deux fibres est la distance limite au-dessous de laquelle on considère une interaction entre elles). La même allure de courbe pour N_I que pour N_C a été obtenue mais avec un décalage de nN_C (n étant le nombre total des fibres). Puis en variant cet espacement, le nombre d'interactions prédit par la simulation était proche de celui donné par la théorie. Finalement les effets du changement des longueurs des fibres, leur diamètre et le taux de cisaillement sur l'évolution de l'énergie élastique ont été également analysés et interprétés. Lorsque la longueur moyenne des fibres a augmenté, les fibres ont devenues beaucoup plus susceptibles de se fléchir. Ainsi, elles emmagasinent au plus de l'énergie élastique. Inversement si le diamètre des fibres diminue, les fibres deviennent plus épaisses et vont donc perdre leur flexibilité résultant en une énergie élastique beaucoup plus basse. En augmentant la valeur du cisaillement, l'intensité des interactions devient plus importante. C'est à dire que les forces d'interactions plus intenses mènent les fibres à être encore plus élastiques et stocker d'avantage d'énergie.

Le cinquième chapitre discute des modèles basés à l'échelle mésoscopique, une échelle intermédiaire entre l'échelle microscopique et l'échelle macroscopique. Ici tous les mod-

èles ont été définis dans le cadre de la théorie cinétique. La théorie cinétique est une approche micro-macro qui permet de considérer le système à l'échelle mésoscopique tout en conservant la physique fine nécessaire à la description de la microstructure et de son évolution. Cela est possible grâce à l'introduction d'un certain nombre de coordonées de conformation. L'approche proposée pour construire les modèles peut être résumée en trois points : (i) la microstructure est définie à l'échelle micro, via l'introduction de différents paramètres de conformation, et son évolution est obtenue à partir de l'écriture de l'équilibre ; (ii) une fonction de distribution est introduite à l'échelle méso, représentant la fraction de particules présentant une certaine conformation à un certain temps et en un certain point de l'espace. Cette fonction contient par définition toute les informations sur la microstructure ; (iii) les propriétés macroscopiques de la suspension sont ensuite calculées à partir des différents moments de la distribution. Après avoir montrée que cette approche permet de retrouver l'équation de Jeffery pour les suspensions diluées, elle est appliquée aux suspensions concentrées présentant des agrégats de fibres, agrégats dans un premier temps rigides puis déformables. Ensuite, afin de rendre compte de toutes les physiques mises en jeu dans le cas de ces suspensions concentrées, l'élasticité des agrégats ainsi que les effets aléatoires dus aux interactions hydrodynamiques entre agrégats sont introduits dans le modèle. Des différents modèles ont été proposés dans la littérature. Des effets d'élasticité et de mémoire évanescente ont été introduits dans le modèle des agrégats déformables de fibres. C'était une première suggestion et approche pour essayer d'expliquer l'étirement subit par un agrégat de fibre, observé expérimentalement. Le modèle le plus réaliste (agrégats déformables) associé aux effets de mémoire (élasticité avec la diffusion Brownienne), a montré que l'élasticité était inactive dans le cas d'un écoulement de cisaillement simple. Dans ce type d'écoulement, l'état stationnaire est atteint et donc la configuration de référence coïncidait avec la configuration actuelle. Toutefois, dans ces travaux on a supposé des physiques particulières, associées à des hypothèses bien phénoménologiques (rigidité des agrégats, déformabilité des agrégats, diffusion Brownienne, élasticité et effets mémoires). Et on a essayé de décrire et justifier les observations expérimentales des agrégats de fibres par ces hypothèses. Et à cause de ces considérations hypothétiques, il s'avère important de valider tous ces modèles d'agrégats. La DNS est un candidat qui permet la validation de ces modèles. Dans des travaux futurs, des agrégats de fibres peuvent être créés à l'échelle microscopique. Après les simulations numériques dans le cadre de la DNS seront comparées avec les modèles de la théorie cinétique afin de conclure sur la validité, et la crédibilité des hypothèses faîtes dans ces modèles.

Finalement dans le dernier chapitre on conclut sur la validité et la crédibilité des modèles utilisés. On présente également les perspectives et les futurs travaux à venir.

Contents

I

General introduction

Today, fiber reinforced polymer composites are important materials in a wide range of applications because of their interesting mechanical, electrical, thermo-physical properties and their cost efficient processing [1]. The study of the rheology of suspensions is considered to be a challenge in modern industrial applications. The fluid-particle or particle-particle interactions, the motion and rotation of particles strongly modify the behavior of the suspending fluid and are difficult physical phenomena to observe, measure and model. In this thesis, the rheology of fiber suspensions is modeled, and analyzed from the point of view of these physical phenomena.

Fiber suspensions are used in industrial processes that involve flow. As examples of these processes one can mention the Sheet Molding Compound (SMC) and the Glass Mat Thermoplastics (GMT) processes. These are widely used in the automotive or electrical industries to produce semi-structural and lightweight parts. The key problem nowadays is understanding the coupling between the mechanical behavior of these suspensions and their microstructure in order to possess a good description of the rheology of such materials and optimize composites manufacturing. However it is often difficult to predict these behaviors and descriptions. That is why, the main emphasis in modern fiber suspension science is to model and simulate real industrial processes. In general, the fiber content (i.e. concentration), the evolution of fiber orientation during the forming process and the aspect ratio strongly affect the final geometry and the properties of the produced parts [2, 3].

The main structural parameters governing the complex rheological behavior of fiber suspensions are the fiber concentration, orientation and spatial distribution, the mechanical properties of the fibers and the matrix, and the matrix-fiber or fiber-fiber interaction mechanisms. The deformation mode of the suspension depends on its concentration regime. If the concentration is low enough then it is assumed that the perturbation of the flow field in the matrix near a fiber is not affected by the presence of the others because the fibers are sufficiently far apart from each other. Increasing the concentration, leads to fibers with hydrodynamic interactions because of the flow field perturbations surrounding the fibers. When the system gets too concentrated with fibers, the average distance between the fibers is of the order of the fiber's diameter so that fibers interact through hydrodynamic and also direct contact effects. Fiber suspensions involved in SMC and GMT belong to this last category. The high concentration and the fiber orientation make fibers strongly entangled, bent and experience multiple contacts with their neighbors.

In this thesis the objective is to study concentrated fiber suspensions, since they represent the most realistic scenario in industrial processes. In the first chapter, a detailed bibliographic study on the different scales for simulating fiber suspensions and the three main regimes that exist are presented. Then in the second, third and fourth chapter, a simulation model is proposed to better describe complex fiber-fiber interactions where the simulations allow to address the fine physics involved in rich and intense interactions. The fifth chapter will discuss another model based on a theory that has the capability of addressing macroscopic systems, through the use of a distribution function where the necessary physical variables are incorporated. Finally, the conclusions and perspectives of this work are discussed from the point of view of the credibility and reliability of the used models,

and the challenging future works to come.

<div style="text-align: right; font-size: 3em;">**1**</div>

Bibliographic study

Contents

1.1   Introduction

Fiber suspensions can be described at different scales: the microscopic scale, related to individual fibers, the mesoscopic scale which considers a population of fibers within a local representative volume, and the macroscopic scale related to the forming process and the final part itself.

Theoretical models not only depend on the chosen scale of description, but also on the concentration regime considered. In the dilute regime, fiber-fiber interactions are neglected altogether. These interactions are usually taken into account in the form of a phenomenological randomizing mechanism when the suspension is semi-dilute. In the concentrated regimes, such a phenomenological approach is no longer appropriate. Indeed, when the concentration and fiber length become large enough, richer microstructures can be observed: entangled systems exhibiting numerous and intense interactions, and dense (either rigid or deformable) clusters of fibers immersed in the suspending fluid,

with specific kinematics and often complex aggregation/disaggregation kinetics.

It is well known that the process-induced microstructure determines the mechanical or functional properties of the final part. Thus, the development of accurate models and efficient computational solvers is crucial. Industrial applications usually involve semi-concentrated or concentrated short fiber suspensions. These applications are thus characterized by a high fiber content, strong interactions, confinement and fiber bending mechanisms. They call for theoretical models that go much beyond the dilute regime.
Most currently available process simulation tools implement *ad hoc* modifications of the classical Jeffery model developed for the dilute regime.

1.2   The three main description scales

Suspensions of particles can be described at the microscopic scale by tracking the motion of each individual particle in the system. In order to circumvent the difficulties (more computational than conceptual) related to simulations at the microscopic scale where too many particles are present, coarser models were introduced [4].

Mesoscopic kinetic theory models result from the coarsening of microscopic descriptions. In kinetic theory models, the individuality of the particles is lost in favor of a statistical description that substitutes the entities by a series of conformation coordinates [5, 6]. For example, when considering a suspension of rods, the mesoscopic description consists in giving the fraction of rods that at a random position and time are oriented along a certain direction. This information is contained in the probability distribution function (PDF) whose conservation balance results in the so-called Fokker-Planck equation.

The Fokker-Planck equation governs the flow-induced evolution of conformation. Being highly-dimensional, it cannot be solved by means of standard mesh-based discretization techniques. Solution procedures based on the use of particles at the mesoscopic scale have been extensively developed by many authors [7, 8, 9, 10, 11, 12, 13, 14]. On the other hand, there are few works on the solution of the Fokker-Planck equation with standard discretization techniques [15, 16].

At the macroscopic scale, the PDF is substituted by some of its moments [17, 18]. Here, the level of detail and the involved physics are sacrificed in favour of computational efficiency. The equations governing the time evolution of these moments usually involve the usage of approximations [19] whose impact on the results can be important [20, 21].

1.3   The three main suspension regimes

1.3.1   Dilute and semi-dilute suspensions

Models concerning dilute and semi-dilute suspensions have been addressed in numerous theoretical and numerical studies. The theories describing these type of suspensions are now well established for suspensions of rigid fibers in Newtonian fluids.

Most of the models existing today are based on the fundamental works of Jeffery and Batchelor. Jeffery [22] studied the motion of a rigid small ellipsoidal particle in an infinite incompressible Newtonian solvent, with no external forces or torques or Brownian motion, and determined the stress state near the particle. After the proposed model by Jeffery, different new models for suspensions of ellipsoids in the dilute or semi-dilute regime appeared [23, 24, 25]. The works in [26, 27] gave a general framework for mechanical models for suspensions. Then the slender body theories were developed to determine the force applied on a particle and particle flow interaction [28]. Finally in these works, the modeling of the behavior of semi-dilute suspensions of aligned fibers was done [29]. Following these works, Dinh and Armstrong [30] generalized this last problem to arbitrary orientation distribution.

Shaqeh, Koch, and co-workers [31, 32, 33] further developed the semi-dilute theory and validated it either with experimental studies [34] or numerical simulation [35, 36]. It is important to notice that these works lead to a common expression for the macroscopic stress tensor of the suspensions. Moreover, they considered fiber orientation by using mesoscopic descriptors called orientation tensors [37] which are compact, and give an efficient macroscopic measurement of fiber orientation. The orientation of the fibers in a given system, has an influence on the behavior of the suspensions. This influence is accounted for the coupling constitutive expressions of the stress tensor with a set of equations modeling the change of the orientation tensors during the flow [23, 37, 38, 39]. In most cases, this system of equations is based on an extension of the fundamental problem of the orientation evolution of a slender particle suspended in an infinite incompressible Newtonian fluid for the dilute or semi-dilute regimes [22, 31, 40, 41, 42, 43, 44]. To simplify the calculations, higher order orientation tensors (such as the fourth order orientation tensor) were usually expressed in terms of the second order orientation tensor. These approximations are known as closure approximations [17, 37, 38, 45, 46, 47]. The issues raised by closure approximations have attracted a lot of attention during the past two decades. These issues remain challenging to this day. For example, some closure approximations could cause kinematic or thermodynamic anomalies [39, 48], whereas others are more or less relevant depending on the local flow and the current orientation of fibers.

To summarize, in the case of dilute or semi-dilute suspensions of short fibers, the three main scales have been extensively considered, and without major difficulties or challenges to model the associated systems. Note that, all of the approaches that have been mentioned here are devoted to Newtonian suspending fluids.

1.3.2 Concentrated suspensions

As soon as the concentration in the system increases, difficulties begin to appear. In the semi-dilute regime, fiber-fiber interactions occur, but in general they can be accurately modeled by introducing a randomizing diffusion term in Jeffery's model [49]. There is a wide literature concerning dilute and semi-dilute suspensions, addressing modeling, [26, 38, 47, 50, 51] flows [18, 52, 53, 54], and rheology [55, 56]. These models describe

quite well the experimental observations. In fact, semi-dilute models have been applied to describe the rheology of concentrated fiber suspensions, even though the description of local mechanisms of interactions between fibers remain inappropriate for such materials. Hence, it was shown in previous works [35] that the predicted viscosities of the theories and simulations based on hydrodynamic fiber-fiber interactions were not compatible with experimental measurements. This incompatibility is due to the leading role of mechanical contacts between fibers in the concentrated regime, that have been neglected in semi-dilute models.

The origin and nature of these mechanical contacts or interactions, were further investigated with Newtonian fiber suspensions [57] and non-Newtonian fiber or fiber bundle suspensions [3, 58]. The results of these studies emerged the following proof: fiber-fiber contact efforts are ruled by friction and lubrication mechanisms; the last one is linked to the deformation of a thin amount of entrapped matrix in the contact zones. Following these studies, several numerical studies have been carried out to understand the behavior of concentrated suspensions and model their macroscopic rheology [36, 41, 59, 60, 61].

When the concentration increases even further, the fiber-fiber interactions become so intense that they must be taken into account appropriately, as for example in the model proposed in [62]. Recent experiments suggest that short fibers in concentrated suspensions align more slowly as a function of strain than the models based on Jeffery's equation predict [63]. In order to address this issue, Wang et al. [63] proposed the use of a strain reduction factor, but this approach violates the principle of objectivity. Later, the same authors proposed an objective model by decoupling the time evolution of both the eigenvalues and the eigenvectors of the second-order orientation tensor [64]. In [65], an anisotropic rotary diffusion is proposed that accounts for the fiber-fiber interactions; the model parameters were selected by matching the experimental steady-state orientation in simple shear flow and by requiring stable steady states and physically realizable solutions.

The most complex scenario is that of the concentrated flow regime involving entangled suspensions or dense clusters immersed into the suspending fluid, exhibiting specific kinematics and complex aggregation/disaggregation mechanisms [66]. The first natural question is how to describe such systems. At the macroscopic scale, one could try to fit some power-law constitutive equation, however, this description does not hold for the microstructure. At the microscopic scale, numerical simulations describing complex fiber-fiber interactions can be carried out in small enough representative volumes [67, 68, 69, 70]. These methods are known as direct numerical simulations.

A first attempt to describe dilute suspensions composed of rigid and deformable clusters from a micromechanical point of view was proposed in [10]. Later, kinematic predictions for rigid and deformable clusters were compared with direct numerical simulation in [71]. An enriched description of the kinematics of rigid clusters within a multi-scale framework was addressed in [72].

Finally, entangled systems involving moderately long fibers are generally described by using some *ad hoc* adaptations of the Folgar-Tucker model [49]. This model, however,

has its origins in the Jeffery equation whose validity is by construction restricted to the dilute regime. For this reason, the validity of these models must be confirmed from both the theoretical and experimental viewpoints. Moreover, when the fiber length and the number of interactions per fiber increase, bending mechanisms are activated. Some attempts at modeling rod bending exist, and most of them consider the rod composed of rigid segments connected by springs activated by bending [10, 11, 73, 74]

1.4 Characteristics of fiber suspensions

A number of physical parameters have to be known in order to understand and predict the flow behavior and the rheology of fiber suspensions.

1.4.1 Aspect ratio and fiber shape

Whatever the shape of a fiber, it is characterized by an aspect ratio which will be denoted by r. To understand the meaning of r one must consider a specific shape for the fibers. For example if a fiber is modeled by a cylinder or a prolate spheroid (i.e. an ellipsoid with two equal short axes), then the aspect ratio is just the ratio of the fiber length to its diameter. The two limiting cases are: the length greatly exceeds the diameter, then fibers have an infinite aspect ratio and the diameter greatly exceeds the length, then the particles are no longer considered as fibers, but disks. If the fiber has an arbitrary shape, then other dimensions (then the length and diameter) have to be defined to better describe its aspect ratio. The aspect ratio is an important parameter that is directly related to the concentration of the system. In fact for a fixed concentration, a system becomes more concentrated if the length (i.e. aspect ratio) of the fibers increases relatively to the diameter (Figure 1.1). Conversely, if the diameter increases (i.e. aspect ratio decreases) relatively to the length then a system is considered less concentrated.

1.4.2 Concentration

Knowing the concentration of the fibers in the suspending fluid is a key element to determine the average distance between fibers and thus the concentration regime. From an industrial point of view, it is usually the mass fraction that defines this concentration. In rheology, it is the volume fraction denoted by ϕ which sets the concentration. ϕ is defined as the ratio of the average volume occupied by the fibers, to the total volume of the system. ϕ is also linked with the average aspect ratio of the fibers. Table 1.1 illustrates the three cases where ϕ is related with r and the concentration regime that results from these relationships. Figure 1.1 shows the limits of the three regimes as functions of ϕ and r where one concludes that most commercial composite materials lie within the concentrated regime.

Relationship between ϕ and r	$\phi \leq \dfrac{1}{r^2}$	$\dfrac{1}{r^2} \leq \phi \leq \dfrac{1}{r}$	$\phi \geq \dfrac{1}{r}$
Regime	dilute	semi-dilute	concentrated

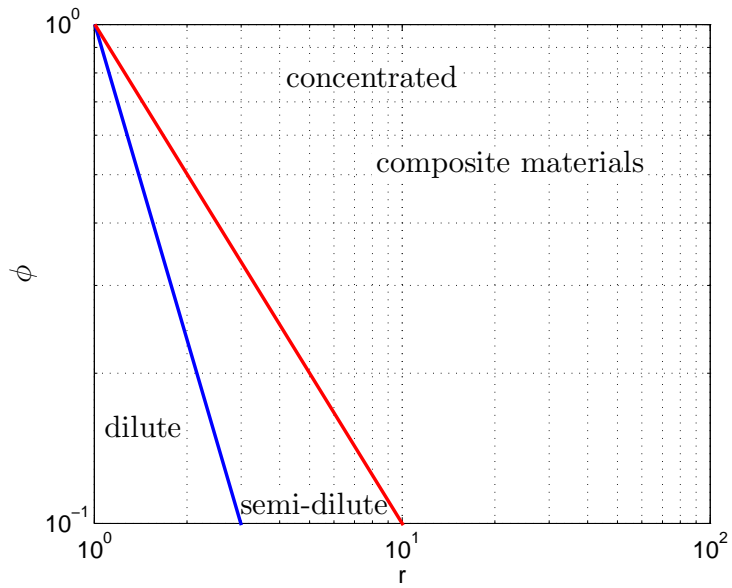Table 1.1: Criteria for the three concentration regimes

Figure 1.1: The limits of the three regimes

1.5 Résumé du chapitre

Les suspensions fibres peuvent être décrites à différentes échelles: l'échelle microscopique liée à chaque fibre, l'échelle mésoscopique qui considère une population de fibres dans un volume représentatif local, et l'échelle macroscopique. Les modèles qui existent dans la littérature dépendent de ces trois échelles, et surtout de la concentration volumique des fibres dans le système.

A l'échelle microscopique, chaque fibre dans le système sera suivie en terme de cinématique; tandis qu'à l'échelle mésoscopique, la démarche est simplifiée en disant que toutes les coordonnées nécessaires pour l'étude du système sont incluses dans une seule fonction de densité de probabilité. Cette fonction donne donc, la probabilité de trouver une fibre avec ces coordonnées dans l'espace et à chaque instant donné. A l'échelle macroscpique on remplace cette fonction par des moments (tenseurs d'orientations), tout en disposant des approximations de fermeture adéquates.

Il existe trois régimes de concentration pour les suspensions de fibres:
- le régime dilué où la concentration est très faible, de manière à traiter chaque fibre indépendamment des autres; là l'orientation de chaque fibre est donnée par l'équation de Jeffery sans interaction;
- le régime semi-dilué (ou semi-concentré) où quelques interactions sont présentes: des interactions entre les fibres et le fluide dues aux bombardements des molécules du fluide et des interactions entre les fibres elles mêmes. Les derniers types d'interactions sont rares dans le cas semi-dilué et normalement la cinématique est donnée ici en ajoutant un terme de diffusion additionnel dans le modèle de Jeffery;
- le régime concentré où des intenses interactions entre les fibres existent et ne peuvent pas être négligées. Le cas le plus complexe est la formation d'une microstructure de fibres enchevêtrées: des agrégats de fibres. Il existe beaucoup de modèles dans la littérature pour la description des systèmes concentrés que ce soit à l'échelle microscopique (simulations numériques directes), ou mésoscopique/macroscopique.

Finalement, les caractéristiques intrinsèques des suspensions de fibres sont discutés: le rapport de forme des fibres et leur concenration. Le rapport de forme pour des fibres cylindriques ou ellipsoidales, est simplement le rapport entre la longueur et le diamètre des fibres. Pour une longeur très grande devant le diamètre les fibres seront caractérisées par un rapport de forme infini. Le cas contraire, résulte en des particules sous formes de disques. Si les fibres ont une forme quelconque, il faut donc définir d'autres critères (autres que la longueur et le diamètre). La concentration est définie comme étant le rapport entre le volume moyen occupé par les fibres et le volume total du système. Elle permet de connaître dans quel limite de régime de concentration le système se trouve et ainsi savoir quel modèle le décrit au mieux.

II

An introduction to direct numerical simulations (DNS)

One way of studying the kinematics of fiber suspensions and their macroscopic properties is to conduct a direct numerical simulation (or DNS for abbreviation). A DNS is based on the computation, in a representative volume, of the motion of several hundreds of fibers and their interactions. It is a step by step process which derives kinematics as well as macroscopic properties, while taking into account the forces applied on each fiber at the microscopic scale [67]. DNS allows a precise description of the fine physics involved at the microscopic scale. Few works used DNS in order to better describe complex fiber-fiber interactions [75, 76, 68, 69]. And in [76, 68, 69] DNS dealt with rigid fibers considered free of any type of elasticity or bending.

In the following chapters, the micro-mechanical model based on DNS is developed in the framework of microscopic descriptions. Concentrated suspensions are considered. Unlike previous works [77, 78, 79] where fibers had the same aspect ratio, fibers having a distribution of lengths is described. In fact, the assumption of fibers with a distribution of lengths is closer to real industrial composites [80]. Then the kinematic of the fibers immersed in a Newtonian fluid under simple shear flow is studied. Macroscopic properties (normal stress growth functions) are investigated. The main originality is the introduction of elasticity due to the fibers bending: the interaction forces acting on each fiber are calculated along with the number of interactions between fibers and a statistical description is built. The forces are assumed to induce a torque leading to a physical bending of the fibers and an elastic energy is then calculated and recovered. This energy is supposed to be stored within the suspension during the evolution of the fibers kinematics and the intense interactions involved. Note that the fibers are supposed to be rigid, as long as elasticity is not considered in the analysis. Hence, for infinite rigid fibers, no elastic energy is stored. The fibers are supposed to exhibit small deformations when they are more and more flexible. For this reason, their kinematics will be the same as the rigid fibers.

The numerical algorithms used to solve and integrate the different equations in the model are detailed.

Finally the main numerical results are discussed.

2

DNS Micro-mechanical model

Contents

The objective of this chapter is to present the necessary elements, describing the DNS model at the microscopic scale. The micro-mechanical model presented here concerns concentrated fiber suspensions and involves the interactions between particles (for the detailed calculations of the different governing equations presented in this chapter, the reader can refer to Appendix A).

2.1 Main assumptions

The main assumptions and hypothesis of this model are :
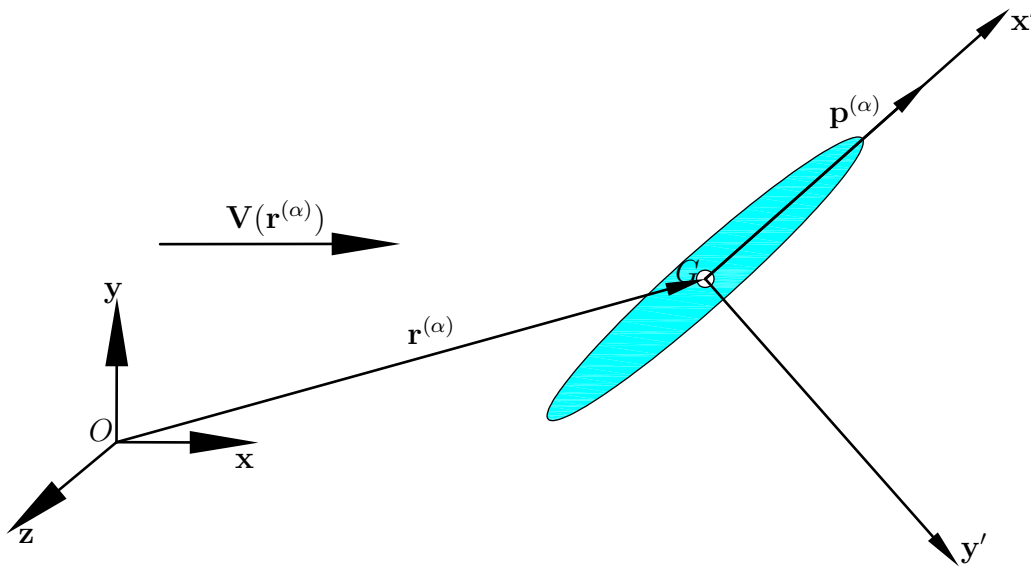
Figure 2.1: Schematic representation of the fiber in the spatial system of the laboratory

1. The suspending fluid is Newtonian, incompressible and the flow is laminar;

2. The velocity field and its gradient are assumed to be homogeneous in the considered volume, thus it is not affected by the particle's presence and its orientation;

3. The mass of the fibers is negligible, thus the inertia of the fibers are not considered in this study;

4. Fibers are considered to have different lengths;

5. The long-range hydrodynamic interactions are considered along with short-range hydrodynamic interactions between fibers;

6. Initially and before the simulation is started, the fibers are homogeneously distributed in the considered volume and they are not in any state of interaction.

The position of the center of gravity G for a fiber denoted by α is at $\mathbf{r}^{(\alpha)}$ (Figure 2.1) with:

$$\mathbf{r}^{(\alpha)} = x^{(\alpha)}\mathbf{x} + y^{(\alpha)}\mathbf{y} + z^{(\alpha)}\mathbf{z}, \tag{2.1}$$

$\mathbf{x}$, $\mathbf{y}$ and $\mathbf{z}$ represent respectively the three unit vectors related to the three space coordinates (in the three dimensionnal axis system). $x^{(\alpha)}$, $y^{(\alpha)}$ and $z^{(\alpha)}$ are the coordinates of the center of gravity of fiber α. In the literature, the shape of the studied particles can be restricted to either spheres, ellipsoids or cylinders. In this model, each fiber is modeled by an ellipsoid (i.e. prolate spheroid) having a length of $l^{(\alpha)}$ along the long revolution axis and a diameter d along the normal axes (Figure 2.2). All the fibers are considered to have the same diameter d. Thus the aspect ratio of the fibers can be defined by $r^{(\alpha)}$ such as:

$$r^{(\alpha)} = \frac{l^{(\alpha)}}{d} \tag{2.2}$$

Since the suspensions are considered concentrated, then the volume concentration ϕ is related with the aspect ratio as:

$$\phi \geq \frac{1}{r} \tag{2.3}$$
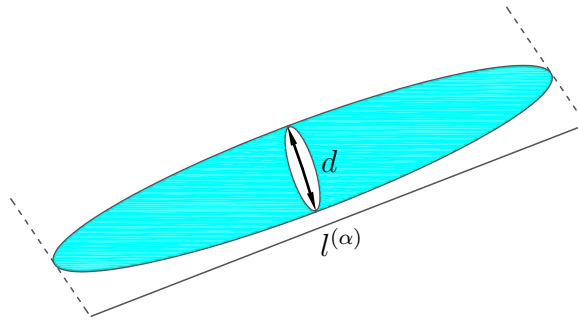
Figure 2.2: Fiber modeled by a prolate spheroid

where r is the average aspect ratio. The more r is important (i.e. long fibers), the more the system is considered concentrated for a fixed value of ϕ. In this model the fibers are supposed to be sufficiently long (i.e. $r > 1$) and close to being cylindrical.

A fixed axis system $(O, \mathbf{x}, \mathbf{y}, \mathbf{z})$ is defined relative to the reference of the laboratory and a local axis system $(G, \mathbf{x}', \mathbf{y}', \mathbf{z}')$ is defined relative to the reference of each fiber (Figure 2.1). The shear field, is imposed by considering a simple shear flow with a shear rate $\dot{\gamma}$. The velocity field is:

$$\mathbf{V}^T(\mathbf{x}) = (V_1, V_2, V_3) = (\dot{\gamma}y, 0, 0) \tag{2.4}$$

(throughout the entire text, "T" denotes the transpose of any vector or matrix) and is defined in each point of space.

In systems dealing with simple shear flow, axis $\mathbf{x}$ is associated with the first direction of the flow velocity field (V_1 in equation (2.4)), axis $\mathbf{y}$ is associated with the velocity gradient and axis $\mathbf{z}$ is associated with the vorticity (Figure 2.1). The velocity gradient is given by:

$$\nabla \mathbf{V} = \frac{\partial V_m}{\partial x_n} = \begin{bmatrix} 0 & \dot{\gamma} & 0 \\ 0 & 0 & 0 \\ 0 & 0 & 0 \end{bmatrix} \tag{2.5}$$

m=1, 2 and 3 defines the index for the three components of $\mathbf{V}(\mathbf{x})$, and n=1, 2 and 3 defines the index for the three space coordinates. When the velocity field is uniform in the considered volume, then the flow velocity field at position $\mathbf{r}^{(\alpha)}$ can be written as:

$$\mathbf{V}(\mathbf{r}^{(\alpha)}) = \nabla \mathbf{V} \cdot \mathbf{r}^{(\alpha)} \tag{2.6}$$

The rate of strain tensor is written as:

$$\mathbf{D} = \frac{1}{2} \left(\nabla \mathbf{V} + (\nabla \mathbf{V})^T \right) \tag{2.7}$$

and the vorticity tensor is given by:

$$\mathbf{W} = \frac{1}{2} \left(\nabla \mathbf{V} - (\nabla \mathbf{V})^T \right) \tag{2.8}$$

The direction or orientation of a fiber is defined by the unit vector $\mathbf{p}^{(\alpha)}$ such as $\mathbf{p}^{(\alpha)} = p_1^{(\alpha)} \mathbf{x} + p_2^{(\alpha)} \mathbf{y} + p_3^{(\alpha)} \mathbf{z}$. $p_1^{(\alpha)}$, $p_2^{(\alpha)}$, and $p_3^{(\alpha)}$ are the coordinates of the orientation vector.
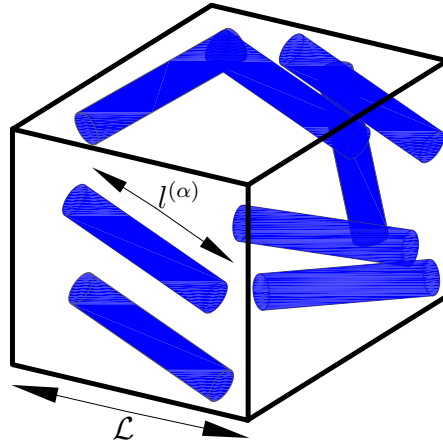
Figure 2.3: Representative elementary volume (REV)

The position of G relative to the fluid is given by a vector that will be denoted by $\mathbf{q}$. The relative velocity of G with respect to the fluid is thus given by:

$$\dot{\mathbf{q}}^{(\alpha)} = \dot{\mathbf{r}}^{(\alpha)} - \mathbf{V}(\mathbf{r}^{(\alpha)}) = \dot{\mathbf{r}}^{(\alpha)} - \dot{\gamma}y^{(\alpha)}\mathbf{x} \tag{2.9}$$

$\boldsymbol{\Omega}$ is the rotating velocity of the fluid in the flow field $\mathbf{V}(\mathbf{r}^{(\alpha)})$ given by:

$$\boldsymbol{\Omega} = \frac{1}{2}\left(\nabla \times \mathbf{V}\right) = \frac{1}{2}\varepsilon_{ijk}\frac{\partial}{\partial x_j}V_k \tag{2.10}$$

Where "$\times$" is the cross product and ε_{ijk} is the Levi-Civita permutation tensor.

2.2   Representative elementary volume

One way of simulating the behavior of fiber suspensions, at the microscopic scale is to consider a representative elementary volume (or REV). DNS is done here in a REV containing the fibers and the fluid. The volume considered is a cubic reference cell (Figure 2.3) having a size:

$$\mathcal{L} = \mathcal{L}_x = \mathcal{L}_y = \mathcal{L}_z \tag{2.11}$$

$\mathcal{L}$ has to be chosen in a way to be smaller then the dimension of the macroscopic system. However, $\mathcal{L}$ has to be larger than the dimension $l^{(\alpha)}$ of each fiber in order to obtain a homogeneous mechanical behavior inside the volume (i.e. if the fibers are initially placed outside the reference cell, the information on the evolution of the kinematics, interaction and associated macroscopic properties will be lost). If this is not the case, then the behavior of the suspensions (kinematics, interactions, etc...) will strongly fluctuate from one volume to another [81]. In the DNS performed here, hundreds of fibers are considered in the REV.

2.3   Fiber motion equations

When interactions between fibers are neglected (dilute case), the fibers are subjected to the effects of the hydrodynamic forces and torques from the surrounding fluid. However,

once the system is considered concentrated, the right physical description for defining interaction forces have to be taken into account in order to consider fiber-fiber interactions.

2.3.1 Fiber translation

The force exhibited by the fluid on the fiber (for ellipsoidal fibers [82]) depends on the relative velocity of G with respect to that of the fluid and a resistance tensor such as:

$$\mathbf{F}^{(\alpha)} + \boldsymbol{\zeta}^{(\alpha)} \cdot \dot{\mathbf{q}}^{(\alpha)} = 0 \tag{2.12}$$

Where $\mathbf{F}^{(\alpha)}$ is the resultant force acting on the fiber and $\boldsymbol{\zeta}^{(\alpha)}$ is the resistance tensor relating the applied force $\mathbf{F}^{(\alpha)}$ and the relative velocity $\dot{\mathbf{q}}^{(\alpha)}$ in the shear flow. According to assumption 5, there are only short-range forces acting on the fibers. Thus $\mathbf{F}^{(\alpha)}$ should be equal to the sum of the interactions forces when a fiber is in contact with its closest neighbor.
For an ellipsoidal fiber, Kim and Karilla [82] derived the expression of the resistance tensor $\boldsymbol{\zeta}^{(\alpha)}$ as follows:

$$\zeta_{jk}^{(\alpha)} = -3\pi\eta_0 l^{(\alpha)} \left[X_A^{(\alpha)} p_j^{(\alpha)} p_k^{(\alpha)} + Y_A^{(\alpha)} \left(\delta_{jk} - p_j^{(\alpha)} p_k^{(\alpha)} \right) \right] \tag{2.13}$$

Where p_j and p_k are the components of $\mathbf{p}$ and index j and k denote the direction of space ($j = 1$, 2 or 3 and $k = 1$, 2 or 3). η_0 is the viscosity of the suspending fluid, $X_A^{(\alpha)}$ and $Y_A^{(\alpha)}$ are functions of the prolate spheroid aspect ratio [82]: the first coefficient is defined for a flow parallel to the axis of revolution (axis $\mathbf{x}'$) and the second coefficient is defined for a flow perpendicular to the axis of revolution (axis $\mathbf{y}'$); δ_{jk} is defined as the Kronecker delta symbol, [83]:

$$\begin{cases} \delta_{jk} = 1 & (j = k) \\ \delta_{jk} = 0 & (j \neq k) \end{cases} \tag{2.14}$$

Then $\dot{\mathbf{q}}^{(\alpha)}$ for fiber α can be written as:

$$\dot{\mathbf{q}}^{(\alpha)} = -\boldsymbol{\zeta}^{(\alpha)^{-1}} \cdot \mathbf{F}^{(\alpha)} \tag{2.15}$$

When they are no short-range forces acting on the fiber (other than the hydrodynamic force), it would move in the flow like a force-free single independent fiber. This case is expressed by the following equation:

$$\dot{\mathbf{q}}^{(\alpha)} = \mathbf{0} \tag{2.16}$$

Neglecting the inertia forces, this leads to:

$$\dot{\mathbf{r}}^{(\alpha)} = \mathbf{V}(\mathbf{r}^{(\alpha)}) \tag{2.17}$$

Thus, in this case the center of gravity will move at the same velocity as the suspending fluid.

2.3.2   Fiber rotation

Neglecting fiber-fiber interactions

When fiber-fiber interactions are neglected, the rotational motion of the fibers is supposed to be only caused by the deformation of the fluid once the shear rate is applied. The deformation of the fluid due to the presence of the velocity field induces a torque given by $\mathcal{H}^{(\alpha)} : \mathbf{D}$. The relative motion of the fiber with respect to that of the fluid produces a torque written as: $\boldsymbol{\xi}^{(\alpha)} \cdot \boldsymbol{\omega}^{(\alpha)}$. Here $\boldsymbol{\xi}^{(\alpha)}$ and $\mathcal{H}^{(\alpha)}$, are the rotating resistance tensors. They represent the friction due to the rotation of the fibers and the deformation of the fluid respectively. They are written as [82]:

$$\xi_{jk}^{(\alpha)} = -\pi\eta_0 l^{(\alpha)} \left[X_C^{(\alpha)} p_j^{(\alpha)} p_k^{(\alpha)} + Y_C^{(\alpha)} \left(\delta_{jk} - p_\alpha^{(\alpha)} p_k^{(\alpha)} \right) \right] \tag{2.18}$$

$$\mathcal{H}_{ijk}^{(\alpha)} = -\pi\eta_0 l^{(\alpha)3} Y_H^{(\alpha)} \left(\varepsilon_{ikl} p_j^{(\alpha)} + \varepsilon_{jkl} p_i^{(\alpha)} \right) p_l^{(\alpha)} \tag{2.19}$$

where $X_C^{(\alpha)}$, $Y_C^{(\alpha)}$ and $Y_H^{(\alpha)}$ are functions of the fiber's aspect ratio. Since inertia effects are neglected, the balance of torques can be written as:

$$\boldsymbol{\xi}^{(\alpha)} \cdot \boldsymbol{\omega}^{(\alpha)} + \mathcal{H}^{(\alpha)} : \mathbf{D} = \mathbf{0} \tag{2.20}$$

The relative rotational velocity is then expressed as:

$$\boldsymbol{\omega}^{(\alpha)} = -\boldsymbol{\xi}^{(\alpha)-1} \cdot \left(\mathcal{H}^{(\alpha)} : \mathbf{D} \right) = -\frac{Y_H^{(\alpha)}}{Y_C^{(\alpha)}} \varepsilon_{ikl} p_j p_l D_{kj} \tag{2.21}$$

Where the inverse of $\boldsymbol{\xi}^{(\alpha)}$ is found to be [82]:

$$\xi_{jk}^{(\alpha)-1} = -\frac{1}{\pi\eta_0 l^{(\alpha)3}} \left[\frac{1}{Y_C^{(\alpha)}} \delta_{jk} + \left(\frac{1}{X_C^{(\alpha)}} - \frac{1}{Y_C^{(\alpha)}} \right) p_j^{(\alpha)} p_k^{(\alpha)} \right] \tag{2.22}$$

Then the evolution of the fiber's orientation in time is given by the equation:

$$\dot{\mathbf{p}}^{(\alpha)} = -\mathbf{p}^{(\alpha)} \times \left(\boldsymbol{\omega}^{(\alpha)} - \boldsymbol{\Omega} \right) \tag{2.23}$$

It can be shown that, the time evolution of the orientation is equal to the Jeffery's equation :

$$\dot{\mathbf{p}} = \dot{\mathbf{p}}_J^{(\alpha)} = \mathbf{W} \cdot \mathbf{p}^{(\alpha)} + \lambda^{(\alpha)} \left[\mathbf{D} \cdot \mathbf{p}^{(\alpha)} - \left(\mathbf{D} : \mathbf{p}^{(\alpha)} \otimes \mathbf{p}^{(\alpha)} \right) \mathbf{p}^{(\alpha)} \right] \tag{2.24}$$

where $\dot{\mathbf{p}}_J^{(\alpha)}$ is the Jeffery orientation time evolution. $\lambda^{(\alpha)}$ is a function of the aspect ratio of fiber α.

$$\lambda^{(\alpha)} = \frac{Y_H^{(\alpha)}}{Y_C^{(\alpha)}} = \frac{r^{(\alpha)2} - 1}{r^{(\alpha)2} + 1} \tag{2.25}$$

For an infinite aspect ratio, $\lambda \to 1$ and equation (2.24) becomes:

$$\dot{\mathbf{p}} = \dot{\mathbf{p}}_J^{(\alpha)} = \mathbf{W} \cdot \mathbf{p}^{(\alpha)} + \left[\mathbf{D} \cdot \mathbf{p}^{(\alpha)} - \left(\mathbf{D} : \mathbf{p}^{(\alpha)} \otimes \mathbf{p}^{(\alpha)} \right) \mathbf{p}^{(\alpha)} \right] \tag{2.26}$$
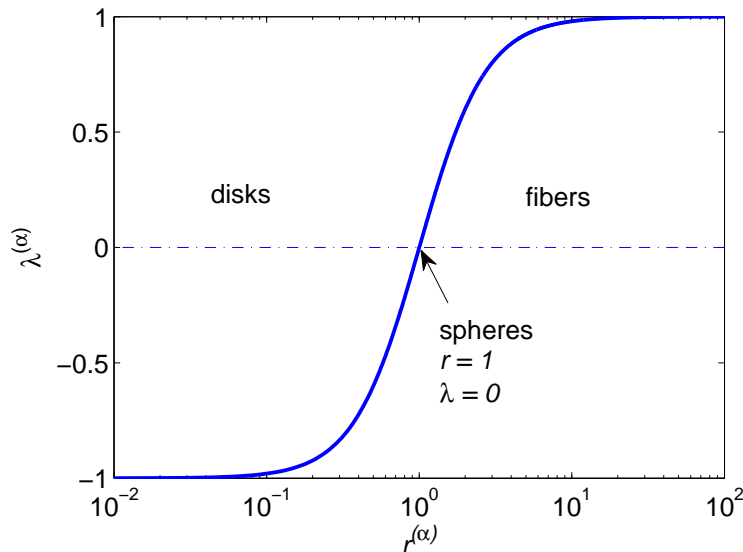
Figure 2.4, shows the evolution of λ for various particle shapes. For fibers (the studied case here), $\lambda > 0$.

Figure 2.4: λ as a function of the aspect ratio

Fiber-fiber interactions

When the system becomes concentrated enough, fiber-fiber interactions occur. Thus, short-range forces will appear on the fibers as they interact together. Before detailing the micro-mechanical model with interactions, the type of interactions between fibers has to be defined, as well as the geometry of interaction at the nearest interaction point between a couple of fibers.

There are two types of interactions considered via two type of forces: a lubrication force occurs when two fibers move close to each other. For spherical particles, the lubrication forces are intense enough to prevent the spheres from overlapping. However, for fibers the lubrication forces are not as strong as those between two spheres, thus fibers can touch each other. As a result the contact force has to be considered when fibers are touching. The shearing lubrication force is supposed to be much smaller than the squeezing one. The surface of the fibers is assumed smooth and the friction force small when fibers get into contact. This is why, only normal components of forces to the fiber's axis are taken into account here.

The resulting interaction force on fiber α will be written as:

$$\mathbf{F}^{(\alpha)} = \sum_{\beta \neq \alpha} F_c^{(\alpha,\beta)} \mathbf{n}^{(\alpha,\beta)} + \sum_{\mu \neq \alpha} F_{lb}^{(\alpha,\mu)} \mathbf{n}^{(\alpha,\mu)} \tag{2.27}$$

Equation (2.27) shows that $\mathbf{F}^{(\alpha)}$ is divided into two sums: the first one groups all fibers denoted by β in contact with fiber α and here $F_c^{(\alpha,\beta)}$ is the magnitude of the contact force; the second one groups all fibers denoted by μ in lubrication with fiber α and here $F_{lb}^{(\alpha,\mu)}$ is the magnitude of the lubrication force. It follows that $\mathbf{n}^{(\alpha,\beta)}$ and $\mathbf{n}^{(\alpha,\mu)}$ are the normal vectors to the axis of fibers in contact with fiber α and fibers in lubrication with fiber α
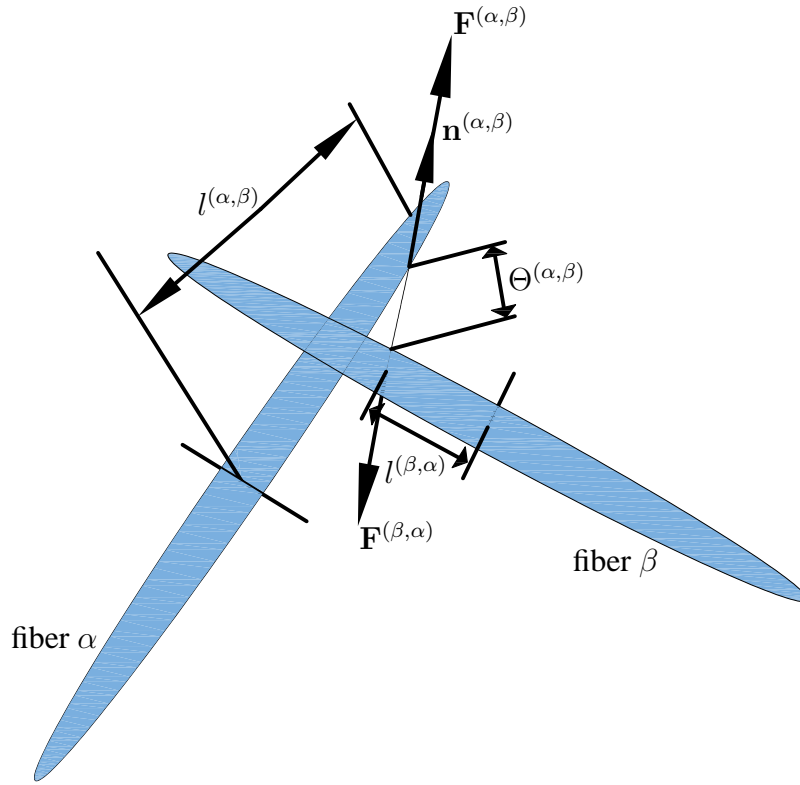
Figure 2.5: Contact or lubrication between two fibers α and β

respectively. The resulting forces will now induce another torque which is:

$$\mathbf{T}^{(\alpha)} = l^{(\alpha,\beta)}\mathbf{p}^{(\alpha)} \times \mathbf{F}^{(\alpha,\beta)} \tag{2.28}$$

where $l^{(\alpha,\beta)}$ is the distance from the center of gravity of fiber α to the point of interaction with another fiber denoted by β (Figure 2.5), and $\mathbf{F}^{(\alpha,\beta)}$ is the resultant force applied to the couple of fibers (α, β). The balance of torques now writes:

$$\mathbf{T}^{(\alpha)} + \boldsymbol{\xi}^{(\alpha)} \cdot \boldsymbol{\omega}^{(\alpha)} + \boldsymbol{\mathcal{H}}^{(\alpha)} : \mathbf{D} = 0 \tag{2.29}$$

Thus:

$$\boldsymbol{\omega}^{(\alpha)} = -\boldsymbol{\xi}^{(\alpha)^{-1}} \cdot \left(\mathbf{T}^{(\alpha)} + \boldsymbol{\mathcal{H}}^{(\alpha)} : \mathbf{D}\right) \tag{2.30}$$

$\boldsymbol{\omega}^{(\alpha)}$ can now be expressed by using equation (2.29) and (2.30):

$$\boldsymbol{\omega}^{(\alpha)} = \frac{1}{\pi\eta_0 l^{(\alpha)^3}Y_C^{(\alpha)}}\mathbf{p}^{(\alpha)}\times\left(\sum_{\beta\neq\alpha}l^{(\alpha,\beta)} F_c^{(\alpha,\beta)}\mathbf{n}^{(\alpha,\beta)}+\sum_{\mu\neq\alpha}l^{(\alpha,\mu)} F_{lb}^{(\alpha,\mu)}\mathbf{n}^{(\alpha,\mu)}\right)-\frac{Y_H^{(\alpha)}}{Y_C^{(\alpha)}}\varepsilon_{ikl}p_jp_lD_{kj} \tag{2.31}$$

The torque $\mathbf{T}^{(\alpha)}$ is obtained using equation (2.28):

$$\mathbf{T}^{(\alpha)} = \mathbf{p}^{(\alpha)} \times \left(\sum_{\beta\neq\alpha}l^{(\alpha,\beta)} F_c^{(\alpha,\beta)}\mathbf{n}^{(\alpha,\beta)} + \sum_{\mu\neq\alpha}l^{(\alpha,\mu)} F_{lb}^{(\alpha,\mu)}\mathbf{n}^{(\alpha,\mu)}\right) \tag{2.32}$$

Then using equations (2.8), (2.23), (2.31), and the fact that :
$\mathbf{p}^{(\alpha)} \times \left(\mathbf{p}^{(\alpha)} \times \mathbf{n}^{(\alpha,\beta)}\right) = -\mathbf{n}^{(\alpha,\beta)}$, the evolution of the fiber's orientation is obtained as follows:

$$\dot{\mathbf{p}}^{(\alpha)} = \frac{1}{\pi\eta_0 l^{(\alpha)3} Y_C^{(\alpha)}} \left(\sum_{\beta \neq \alpha} l^{(\alpha,\beta)} F_c^{(\alpha,\beta)} \mathbf{n}^{(\alpha,\beta)} + \sum_{\mu \neq \alpha} l^{(\alpha,\mu)} F_{lb}^{(\alpha,\mu)} \mathbf{n}^{(\alpha,\mu)} \right) + \dot{\mathbf{p}}_J^{(\alpha)} \qquad (2.33)$$

Using equations (2.15) and (2.27) it can be shown that:

$$\dot{\mathbf{q}}^{(\alpha)} = \frac{1}{3\pi\eta_0 l^{(\alpha)} Y_A^{(\alpha)}} \left(\sum_{\beta \neq \alpha} F_c^{(\alpha,\beta)} \mathbf{n}^{(\alpha,\beta)} + \sum_{\mu \neq \alpha} F_{lb}^{(\alpha,\mu)} \mathbf{n}^{(\alpha,\mu)} \right) \qquad (2.34)$$

Finally the time evolution of the position of the center of gravity of fiber α writes:

$$\dot{\mathbf{r}}^{(\alpha)} = \dot{\gamma} y^{(\alpha)} \mathbf{x} + \frac{1}{3\pi\eta_0 l^{(\alpha)} Y_A^{(\alpha)}} \left(\sum_{\beta \neq \alpha} F_c^{(\alpha,\beta)} \mathbf{n}^{(\alpha,\beta)} + \sum_{\mu \neq \alpha} F_{lb}^{(\alpha,\mu)} \mathbf{n}^{(\alpha,\mu)} \right) \qquad (2.35)$$

The interactions between fibers take place according to a specified configuration. The next section will detail this configuration.

2.3.3 Distance between two fibers

The configuration of interaction is defined by the nearest distance or gap between the fibers, when interactions happen. For two fibers α and β, the normal perpendicular to their plane through the orientations $\mathbf{p}^{(\alpha)}$ and $\mathbf{p}^{(\beta)}$ is written as:

$$\mathbf{n}^{(\alpha,\beta)} = \pm \frac{\mathbf{p}^{(\alpha)} \times \mathbf{p}^{(\beta)}}{\|\mathbf{p}^{(\alpha)} \times \mathbf{p}^{(\beta)}\|} \qquad (2.36)$$

where the sign in equation (2.36) is chosen such as the distance decreases when fiber β moves along the positive direction of $\mathbf{n}^{(\alpha,\beta)}$ [41]. The distance from the mass center of fiber α to the interaction point with fiber β is $l^{(\alpha,\beta)}$ and the distance from the mass center with fiber β to the interaction point with fiber α is $l^{(\beta,\alpha)}$ (Figure 2.5) such as:

$$
\begin{aligned}
l^{(\alpha,\beta)} &= \frac{-(\mathbf{r}^{(\alpha)} - \mathbf{r}^{(\beta)}) \cdot \mathbf{p}^{(\alpha)} + \left[(\mathbf{r}^{(\alpha)} - \mathbf{r}^{(\beta)}) \cdot \mathbf{p}^{(\beta)}\right] \left(\mathbf{p}^{(\alpha)} \cdot \mathbf{p}^{(\beta)}\right)}{1 - \left(\mathbf{p}^{(\alpha)} \cdot \mathbf{p}^{(\beta)}\right)^2} \\
l^{(\beta,\alpha)} &= \frac{-(\mathbf{r}^{(\beta)} - \mathbf{r}^{(\alpha)}) \cdot \mathbf{p}^{(\beta)} + \left[(\mathbf{r}^{(\beta)} - \mathbf{r}^{(\alpha)}) \cdot \mathbf{p}^{(\alpha)}\right] \left(\mathbf{p}^{(\beta)} \cdot \mathbf{p}^{(\alpha)}\right)}{1 - \left(\mathbf{p}^{(\alpha)} \cdot \mathbf{p}^{(\beta)}\right)^2}
\end{aligned} \qquad (2.37)
$$

In the case of high aspect ratio prolate spheroids, the gap between two fibers $\Theta^{(\alpha,\beta)}$ (Figure 2.5) is [84]:

$$\Theta^{(\alpha,\beta)} = (\mathbf{r}^{(\alpha)} - \mathbf{r}^{(\beta)}) \cdot \mathbf{n}^{(\alpha,\beta)} - \frac{d}{2}\sqrt{1 - 4\frac{l^{(\alpha,\beta)2}}{l^{(\alpha)2}}} - \frac{d}{2}\sqrt{1 - 4\frac{l^{(\beta,\alpha)2}}{l^{(\beta)2}}} \qquad (2.38)$$

2.3.4   Interaction forces

Lubrication forces

When two fibers approach, a lubrication force occurs. In previous works [68], the authors proposed a power law behavior to describe the relationship between the force and the deformation and was applied in a 2D model. However in the model presented here, the study is done in 3D. The lubrication force $\mathbf{F}_{lb}^{(\alpha,\beta)}$ was thus calculated within a linear approach given by Yamane et al [84]:

$$\mathbf{F}_{lb}^{(\alpha,\beta)} = -K\Theta^{(\alpha,\beta)}\dot{\Theta}^{(\alpha,\beta)}\mathbf{n}^{(\alpha,\beta)} = F_{lb}^{(\alpha,\beta)}\mathbf{n}^{(\alpha,\beta)} \tag{2.39}$$

with:

$$K = \frac{3\pi\eta_0 d^2}{\Theta^{(\alpha,\beta)}\|\mathbf{p}^{(\alpha)} \times \mathbf{p}^{(\beta)}\|} \tag{2.40}$$

$\dot{\Theta}^{(\alpha,\beta)}$ is the relative velocity between two nearest interaction points, projected on the normal $\mathbf{n}^{(\alpha,\beta)}$:

$$\begin{aligned}
\dot{\Theta}^{(\alpha,\beta)} &= \left[\dot{\mathbf{q}}^{(\alpha)} + \dot{\gamma}y^{(\alpha)}\mathbf{x} + l^{(\alpha,\beta)}\left(\boldsymbol{\omega}^{(\alpha)} - \boldsymbol{\Omega}\right) \times \mathbf{p}^{(\alpha)} - \dot{\mathbf{q}}^{(\beta)} - \dot{\gamma}y^{(\beta)}\mathbf{x}\right. \\
&\quad \left. - l^{(\beta,\alpha)}\left(\boldsymbol{\omega}^{(\beta)} - \boldsymbol{\Omega}\right) \times \mathbf{p}^{(\beta)}\right] \cdot \mathbf{n}^{(\alpha,\beta)} \\
&= \left(\dot{\mathbf{q}}^{(\alpha)} - \dot{\mathbf{q}}^{(\beta)} + l^{(\alpha,\beta)}\dot{\mathbf{p}}^{(\alpha)} - l^{(\beta,\alpha)}\dot{\mathbf{p}}^{(\beta)}\right) \cdot \mathbf{n}^{(\alpha,\beta)} + \dot{\gamma}\left(y^{(\alpha)} - y^{(\beta)}\right)n_x^{(\alpha,\beta)}
\end{aligned} \tag{2.41}$$

where $n_x^{(\alpha,\beta)}$ is the x component of $\mathbf{n}^{(\alpha,\beta)}$. Using equations (2.15), (2.33), (2.34) and (2.39) in equation (2.41), the lubrication forces are determined as follows:

$$\begin{aligned}
&\frac{1}{K\Theta^{(\alpha,\beta)}}F_{lb}^{(\alpha,\beta)} + \frac{1}{3\pi\eta_0 l^{(\alpha)}Y_A^{(\alpha)}}\left(\sum_{\mu\neq\alpha}F_c^{(\alpha,\mu)}\mathbf{n}^{(\alpha,\mu)}\cdot\mathbf{n}^{(\alpha,\beta)} + \sum_{\nu\neq\alpha}F_{lb}^{(\alpha,\nu)}\mathbf{n}^{(\alpha,\nu)}\cdot\mathbf{n}^{(\alpha,\beta)}\right) \\
&- \frac{1}{3\pi\eta_0 l^{(\beta)}Y_A^{(\beta)}}\left(\sum_{\theta\neq\beta}F_c^{(\beta,\theta)}\mathbf{n}^{(\beta,\theta)}\cdot\mathbf{n}^{(\alpha,\beta)} + \sum_{\chi\neq\beta}F_{lb}^{(\beta,\chi)}\mathbf{n}^{(\beta,\chi)}\cdot\mathbf{n}^{(\alpha,\beta)}\right) \\
&+ \frac{1}{\pi\eta_0 l^{(\alpha)3}Y_C^{(\alpha)}}\left(\sum_{\mu\neq\alpha}l^{(\alpha,\mu)}F_c^{(\alpha,\mu)}\mathbf{n}^{(\alpha,\mu)}\cdot\mathbf{n}^{(\alpha,\beta)} + \sum_{\nu\neq\alpha}l^{(\alpha,\nu)}F_{lb}^{(\alpha,\nu)}\mathbf{n}^{(\alpha,\nu)}\cdot\mathbf{n}^{(\alpha,\beta)}\right) \\
&- \frac{1}{\pi\eta_0 l^{(\beta)3}Y_C^{(\beta)}}\left(\sum_{\theta\neq\beta}l^{(\beta,\theta)}F_c^{(\beta,\theta)}\mathbf{n}^{(\beta,\theta)}\cdot\mathbf{n}^{(\alpha,\beta)} + \sum_{\chi\neq\beta}l^{(\beta,\chi)}F_{lb}^{(\beta,\chi)}\mathbf{n}^{(\beta,\chi)}\cdot\mathbf{n}^{(\alpha,\beta)}\right) \\
&= -\left(l^{(\alpha,\beta)}\dot{\mathbf{p}}_J^{(\alpha)} - l^{(\beta,\alpha)}\dot{\mathbf{p}}_J^{(\beta)}\right)\cdot\mathbf{n}^{(\alpha,\beta)} - \dot{\gamma}\left(y^{(\alpha)} - y^{(\beta)}\right)n_x^{(\alpha,\beta)}
\end{aligned} \tag{2.42}$$

Before solving the system given by equation (2.42), the contact forces (in case contact forces exist) have to be determined.

Contact forces

Contact forces are assumed to occur if the gap between two close fibers is equal to zero and if $F_c^{(\alpha,\beta)} \neq 0$. In previous works, authors focused on introducing simple conditions to impose the contact, because a complex description of contact forces is diffcult to generate

[36, 85]. The condition considered here uses equation (2.38) and takes the following form [67]:

$$\frac{d}{dt}\left[\left(\mathbf{r}^{(\alpha)} - \mathbf{r}^{(\beta)}\right) \cdot \mathbf{n}^{(\alpha,\beta)}\right] = \dot{\Theta}^{(\alpha,\beta)} = 0 \tag{2.43}$$

with $\Theta^{(\alpha,\beta)} \approx 0$. This condition is only valid if the fiber that is in contact has a null relative velocity along direction $\mathbf{n}^{(\alpha,\beta)}$. It physically means that two fibers in contact cannot overlap or pass through each other. They maintain a steady distance between them at the contact point, when the gap is almost equal to zero.

In general, to solve system (2.42) the groups of fibers in interaction with the pair of fibers α and β have to be found. The first group is all the fibers in interaction with fiber α and is referred to indexes μ and ν in equation (2.42). The second group is all the fibers in interaction with fiber β and is referred to indexes θ and χ in equation (2.42). There is one unknown force for each pair of fibers, because the forces acting on the two fibers are equal in magnitude but opposite in direction. All forces for these two groups are coupled and should be solved together with all the interactions in the suspension.

If there are only fibers in contact (no lubrication), then the system (2.42) have to be solved but without the term $\frac{1}{K\left(\Theta^{(\alpha,\beta)}\right)}F_{lb}^{(\alpha,\beta)}$, with condition (2.43) imposed in equation (2.41).

2.4 Macroscopic descriptors of the suspensions

2.4.1 Orientation tensor

Now that the orientation evolution has been well defined with the interaction forces, the orientation state of the fibers can be described by orientation tensors. These tensors give a statistical average for the orientation of a fiber population, according to a specific direction [17]. For a population of fibers, a distribution orientation function $\psi(\mathbf{p})$ describes the state of the fibers orientation in the fluid. In the litterature, the orientation state of a population of fibers is given by the second and fourth order orientation tensors $\mathbf{a_2}$ and $\mathbf{a_4}$ respectively [17]:

$$\mathbf{a_2} = \int_{\mathbf{p}^{(\alpha)}} \mathbf{p}^{(\alpha)} \otimes \mathbf{p}^{(\alpha)} \psi(\mathbf{p}^{(\alpha)}) d\mathbf{p}^{(\alpha)} \tag{2.44}$$

$$\mathbf{a_4} = \int_{\mathbf{p}^{(\alpha)}} \mathbf{p}^{(\alpha)} \otimes \mathbf{p}^{(\alpha)} \otimes \mathbf{p}^{(\alpha)} \otimes \mathbf{p}^{(\alpha)} \psi(\mathbf{p}^{(\alpha)}) d\mathbf{p}^{(\alpha)} \tag{2.45}$$

where "$\otimes$" denotes the tensor product.

The interesting tensor from a kinematic point of view is $\mathbf{a_2}$, because it is the most used in the literature. However, $\mathbf{a_4}$ is a crucial tensor when calculating the stress growth functions. When dealing with a discrete population of hundreds of fibers, the integral in expression (2.44) can be replaced by a discrete sum. Hence, for a total number of fibers n this tensor will be calculated, in the DNS framework as:

$$\mathbf{a}_{jk} = \frac{1}{n}\sum_{\alpha=1}^{n} p_j^{(\alpha)} p_k^{(\alpha)} \tag{2.46}$$

where p_j and p_k are two components of $\mathbf{p}$; $\mathbf{a}_{jk}$ are the components of the second order orientation tensor. Index j and k denote the direction of space (j=1, 2 or 3 and k=1, 2 or
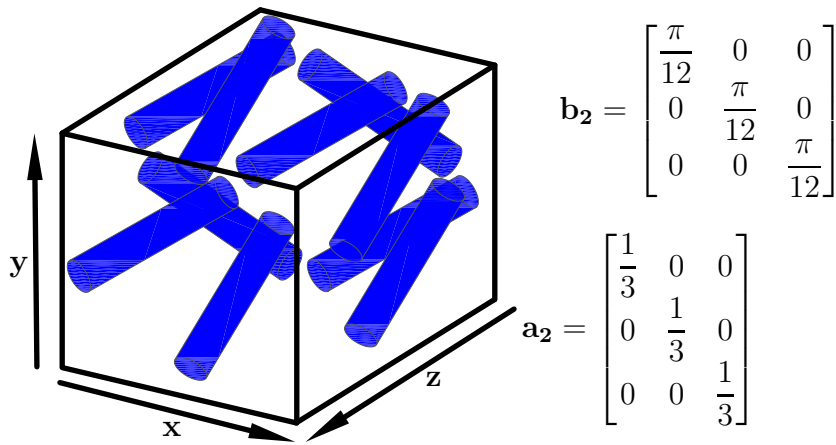
$$\mathbf{b_2} = \begin{bmatrix} \dfrac{\pi}{12} & 0 & 0 \\ 0 & \dfrac{\pi}{12} & 0 \\ 0 & 0 & \dfrac{\pi}{12} \end{bmatrix}$$

$$\mathbf{a_2} = \begin{bmatrix} \dfrac{1}{3} & 0 & 0 \\ 0 & \dfrac{1}{3} & 0 \\ 0 & 0 & \dfrac{1}{3} \end{bmatrix}$$

Figure 2.6: Example of an isotropic orientation state

$$\mathbf{b_2} = \begin{bmatrix} 0 & 0 & 0 \\ 0 & 0 & 0 \\ 0 & 0 & 0 \end{bmatrix}$$

$$\mathbf{a_2} = \begin{bmatrix} 1 & 0 & 0 \\ 0 & 0 & 0 \\ 0 & 0 & 0 \end{bmatrix}$$
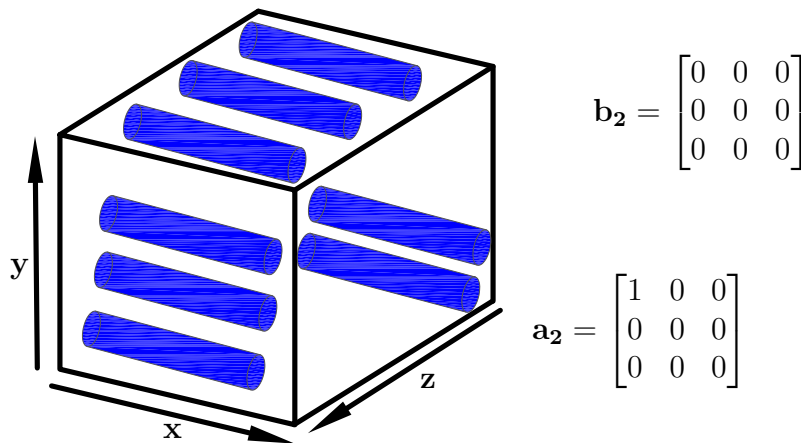
Figure 2.7: Example of an aligned orientation state

3). The orientation tensor, preserves a unit trace through time, and is fully symmetric (i.e. $a_{11}+a_{22}+a_{33} = 1$ and $a_{jk} = a_{kj}$ respectively). Figures 2.6 and 2.7 detail some component values of $\mathbf{a_2}$ for particular orientation states. For an isotropic state, the fibers are oriented in all given directions along the primary space axes (Figure 2.6). For an aligned state, the fibers are all aligned along the $\mathbf{x}$ direction (Figure 2.7).

In the DNS performed here, the initial state is generated in a way that all the fibers in the REV are in an almost isotropic state (the generation of the initial state will be detailed in the following chapter, describing the numerical implementation methods and used algorithms).

2.4.2   Probability of interaction and interaction tensor

So far the interactions between fibers has been explained but nothing has been said about the probability of having interactions between them. This section will discuss another tensor, characterizing this probability: the interaction tensor.

When fibers interact together, they are crossed one over the other and their orientations

will form an angle. For a pair of fibers this could be expressed as:

$$\|\mathbf{p}^{(\alpha)} \times \mathbf{p}^{(\beta)}\| > 0 \tag{2.47}$$

Equation (2.47) simply means that if two fibers are perfectly parallel, the probability of interaction is equal to zero since it is not possible to have an interaction according to equation (2.36). If one considers a test fiber having an orientation $\mathbf{p}^{(\alpha)}$, the interaction probability is defined as the probability of finding a fiber in a volume of fluid adjacent to the test fiber [86, 87] (the fiber must not be parallel to the test fiber in order to possibly interact). For the sake of simplicity the test fiber is represented by a segment of length $ds^{(\alpha)}$ (Figure 2.8). When another fiber having an orientation $\mathbf{p}^{(\beta)}$ and segment length $ds^{(\beta)}$ is crossing the test fiber, it will be intersecting it in an infinitesimal volume dV above or below the test fiber. This volume will depend on the angle formed by the two fibers. From Figure 2.8 the two cases are presented: whether the second fiber in interaction with the test fiber is in the above or below surface area of the test fiber, dV will be equal to the fiber's diameter multiplied by the surface of the parallelogram formed by the two fibers intersecting that is $\|\mathbf{p}^{(\alpha)} \times \mathbf{p}^{(\beta)}\|$ [87]:

$$dV = 2d(ds^{(\alpha)} ds^{(\beta)})\|\mathbf{p}^{(\alpha)} \times \mathbf{p}^{(\beta)}\| \tag{2.48}$$

Finally the probability of interaction is obtained by multiplying equation (2.48) by the number of fibers per unit volume N and by integrating along all possible fibers having orientation $\mathbf{p}^{(\beta)}$:

$$P = 2Nd \int_{\mathbf{p}^{(\beta)}} \|\mathbf{p}^{(\alpha)} \times \mathbf{p}^{(\beta)}\| \psi_{\mathbf{p}^{(\beta)}} d\mathbf{p}^{(\beta)} ds^{(\alpha)} ds^{(\beta)} \tag{2.49}$$

$\psi_{\mathbf{p}}^{(\beta)}$ being the statistical orientation distribution function. This probability could be related to a tensor that describes the interaction state [62] and is valid for fibers with high aspect ratios (i.e. $r \gg 1$). The interaction tensor denoted by $\mathbf{b_2}$ gives a statistical average for the probability and/or the number of interactions involved. This tensor is given by [62]:

$$\mathbf{b_2} = \int_{\mathbf{p}^{(\alpha)}} \int_{\mathbf{p}^{(\beta)}} \mathbf{p}^{(\alpha)} \otimes \mathbf{p}^{(\beta)} \|\mathbf{p}^{(\alpha)} \times \mathbf{p}^{(\beta)}\| \psi_{\mathbf{p}^{(\alpha)}} \psi_{\mathbf{p}^{(\beta)}} d\mathbf{p}^{(\alpha)} d\mathbf{p}^{(\beta)} \tag{2.50}$$

Then since a large number of fibers is considered in this discrete particle-based simulation, $\mathbf{b_2}$ can be evaluated with the following summation [88]:

$$b_{ik} = \frac{1}{n^2} \sum_{\alpha=1}^{n} \sum_{\beta=1}^{n} \|\mathbf{p}^{(\alpha)} \times \mathbf{p}^{(\beta)}\| p_i^{(\alpha)} p_k^{(\alpha)} \tag{2.51}$$

where indexes i and k have the same meaning as in equation (2.46). Note that unlike the orientation tensor, the components of $\mathbf{b_2}$ distinguish a random and a biaxial orientation state. Figures 2.6 and 2.7 present some component values of $\mathbf{b_2}$ for come particular orientation states. If fibers are almost perfectly aligned in one direction, say the $\mathbf{x}$ direction (Figure 2.6) then they will be parallel to each other. Hence, no interaction is possible between them and the interaction tensor will have null components (a null probability).
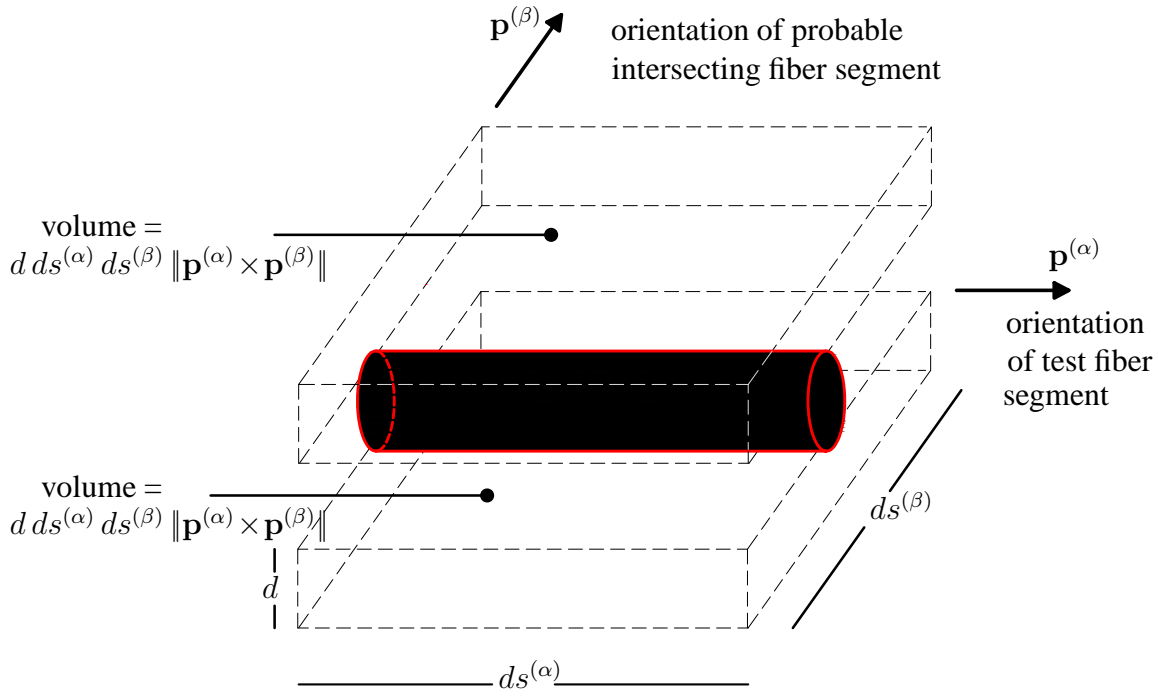
Figure 2.8: Two volumes (above or below) containing the second interacting fiber with the first test fiber

In previous works [62, 89], $\mathbf{b_2}$ has been related to the average number of interactions per fiber N_C as follows:

$$N_C = \frac{8}{\pi} r\phi f + 4\phi (g + 1) \tag{2.52}$$

where $f = \text{trace}(\mathbf{b_2}) = \int_{\mathbf{p}^{(\alpha)}} \int_{\mathbf{p}^{(\beta)}} \|\mathbf{p}^{(\alpha)} \times \mathbf{p}^{(\beta)}\| \psi_{\mathbf{p}^{(\alpha)}} \psi_{\mathbf{p}^{(\beta)}} d\mathbf{p}^{(\alpha)} d\mathbf{p}^{(\beta)}$

and $g = \int_{\mathbf{p}^{(\alpha)}} \int_{\mathbf{p}^{(\beta)}} \|\mathbf{p}^{(\alpha)} \cdot \mathbf{p}^{(\beta)}\| \psi_{\mathbf{p}^{(\alpha)}} \psi_{\mathbf{p}^{(\beta)}} d\mathbf{p}^{(\alpha)} d\mathbf{p}^{(\beta)}$

For slender fibers (i.e. $r \gg 1$), N_C reduces to:

$$N_C = \frac{8}{\pi} r\phi f \tag{2.53}$$

2.5   Macroscopic properties

The hydrodynamic forces and torques applied by the fluid at each fiber, induce a stress in the considered volume. Moreover, when concentrated suspensions are dealt with, the contribution of the lubrication and contact forces to the stress have to be considered. The following section will detail the resulting normal stress growth functions, shear stress growth coefficient and the elastic energy respectively.

2.5.1 Normal stress growth functions and shear stress growth coefficient

For suspensions free of interactions (diluted suspensions), each fiber can be considered independently from the others [22]. Thus to obtain the total stress in the suspensions it suffices to define the stress induced by a single fiber. The contribution of the suspensions to stress depends on the geometrical shape of the fibers. For a single prolate spheroid α, the hydrodynamic (or H for abbreviation) stress tensor $\boldsymbol{\sigma}^H$ is defined by Kim and Karilla as follows [82]

$$
\begin{aligned}
\sigma_{ij}^{H(\alpha)} &= \frac{5}{6}\pi\eta_0 l^{(\alpha)^3} \left(X_M^{(\alpha)}\Gamma_{ijkl}^{(0)} + Y_M^{(\alpha)}\Gamma_{ijkl}^{(1)} + Z_M^{(\alpha)}\Gamma_{ijkl}^{(2)} \right) D_{kl} \\
&+ \frac{1}{2}\pi\eta_0 l^{(\alpha)^3} Y_H^{(\alpha)} \left(\varepsilon_{ikl}p_j^{(\alpha)} + \varepsilon_{jkl}p_i^{(\alpha)} \right) p_l^{(\alpha)}\omega_k^{(\alpha)}
\end{aligned}
\tag{2.54}
$$

The contribution of the non-hydrodynamic (or NH for abbreviation) interactions to the effective stress is written as:

$$
\begin{aligned}
\sigma_{ij}^{NH(\alpha)} &= m^{(\alpha)}\dot{q}_i^{(\alpha)}\dot{q}_j^{(\alpha)} \\
&+ \frac{1}{2}\sum_{\beta=1}^{n}F^{(\alpha,\beta)} \left[\left(r_i^{(\alpha)} - r_i^{(\beta)}\right) n_j^{(\alpha,\beta)} + n_j^{(\alpha,\beta)} \left(r_i^{(\alpha)} - r_i^{(\beta)}\right) \right]
\end{aligned}
\tag{2.55}
$$

where $F^{(\alpha,\beta)}$ denotes the magnitude of either a lubrication force or a contact force [90] and $m^{(\alpha)}$ is the mass of the fiber (assumed negligible). The effective stress tensor takes the following form:

$$
\boldsymbol{\sigma}^f = \frac{1}{\rho}\sum_{\alpha=1}^{n} \left(\boldsymbol{\sigma}^{H(\alpha)} - \boldsymbol{\sigma}^{NH(\alpha)} \right)
\tag{2.56}
$$

where ρ is the total volume of the representative volume. The total stress in the suspensions can be written as [82]:

$$
\boldsymbol{\sigma} = -\Xi\mathbf{I} + 2\eta_0\mathbf{D} + \boldsymbol{\sigma}^f
\tag{2.57}
$$

where Ξ is the hydrodynamic pressure and $\mathbf{I}$ the unit tensor (identity matrix; throughout the text the identity matrix is denoted by $\mathbf{I}$, however its components are represented by the Kronecker delta symbol δ_{jk} previously defined in section 2.3, equation (2.14)). It is then possible to define the suspensions apparent viscosity η (or the shear stress growth coefficient) by:

$$
\eta = \frac{\sigma_{12}}{\dot{\gamma}}
\tag{2.58}
$$

Finally the first and second normal stress growth functions are respectively:

$$
\begin{aligned}
N_1^f &= \sigma_{11}^f - \sigma_{22}^f; & N_2^f &= \sigma_{22}^f - \sigma_{33}^f \\
N_1 &= \sigma_{11} - \sigma_{22}; & N_2 &= \sigma_{22} - \sigma_{33}
\end{aligned}
\tag{2.59}
$$

Note that all stress tensors defined in this section are symmetric (i.e. $\sigma_{ij}^f = \sigma_{ji}^f$ and $\sigma_{ij} = \sigma_{ji}$). And since the suspending fluid is Newtonian then it results: $N_1^f = N_1$ and $N_2^f = N_2$.

2.5.2 Elastic Energy

The mechanism of bending associated with the flexibility and elasticity of fibers, was evidenced in recent experimental studies made on glass fiber reinforced concrete [91]. It also appears in dry glass fiber projection (GFP) on a wall, where the bending of the fiber was analyzed when it rebounds off the wall. Thus here, in order to introduce a type of elasticity in the suspensions, we can assume that fibers bend under the effect of their interactions. A possible explanation of this effect is that the components of the forces can contribute to the bending of the fiber when it is subjected to contact and lubrication forces.

This would be similar to a simple beam theory problem of a fixed beam, since only one interaction (i.e. one force) per fiber is enough to activate fiber bending (because hydrodynamic forces and their resulting torques also apply on the fibers [70]).

Before proceeding with the elastic analysis, it is essential to express the necessary components in the reference system of the fiber. To do so a transformation of coordinates from the reference system of the laboratory $(O, \mathbf{x}, \mathbf{y}, \mathbf{z})$ to the reference system of the fiber has to be done. Since the orientation $\mathbf{p}$ is a unit vector, its time derivative $\dot{\mathbf{p}}$ is orthogonal to it. It is possible to construct the reference system of the fiber $(G, \mathbf{x}', \mathbf{y}', \mathbf{z}')$, where the three unit vectors related to the three space coordinates (in the three dimensional axis system $\mathbf{x}'$, $\mathbf{y}'$, and $\mathbf{z}'$) are respectively: $\mathbf{x}' = \mathbf{p}$, $\mathbf{y}' = \dfrac{\dot{\mathbf{p}}}{\|\dot{\mathbf{p}}\|}$ and $\mathbf{z}' = \dfrac{\mathbf{p} \times \dot{\mathbf{p}}}{\|\mathbf{p} \times \dot{\mathbf{p}}\|}$. Then any vector $\mathbf{S} = S_x \mathbf{x} + S_y \mathbf{y} + S_z \mathbf{z}$ in the reference system of the laboratory can be written in the reference system of the fiber by the following transformation:

$$\begin{bmatrix} s_x \\ s_y \\ s_z \end{bmatrix}_{\text{fiber}} = \begin{bmatrix} \mathbf{x} \cdot \mathbf{x}' & \mathbf{x} \cdot \mathbf{x}' & \mathbf{z} \cdot \mathbf{x}' \\ \mathbf{x} \cdot \mathbf{y}' & \mathbf{y}' \cdot \mathbf{y} & \mathbf{z} \cdot \mathbf{y}' \\ \mathbf{x} \cdot \mathbf{z}' & \mathbf{y} \cdot \mathbf{z}' & \mathbf{z} \cdot \mathbf{z}' \end{bmatrix} \begin{bmatrix} S_x \\ S_y \\ S_z \end{bmatrix}_{\text{laboratory}} \tag{2.60}$$

The components of the forces will be denoted by F_y and F_z in the reference system attached to the fiber $(G, \mathbf{x}', \mathbf{y}', \mathbf{z}')$ (Figure 2.9), and the force vector acting on fiber α is denoted by $\mathbf{F}$ where the indexes "lb", "c" and "(α, β)" have been omitted for the sake of simplicity. The component F_x is not considered inducing mainly buckling, here ignored. Elastic analysis is carried out within the standard linear elastic beam theory: the F_y component will induce a bending torque M_z and the F_z component will induce a bending torque M_y (Figure 2.9). Then knowing the distance l (that is $l^{(\alpha,\beta)}$) from each interaction point to the center of the fiber, these resulting torques can be evaluated for each point on the fiber; the torque being a function of x, the coordinate related to the fiber's axis (Figure 2.9). For example if a force is acting at a position A on the fiber (Figure 2.9), and the fiber's center of gravity is taken at position G, then the torques acting in each position of the segment $[GA]$ result:

$$\mathbf{M}(x) = (l - x)\mathbf{p} \times \mathbf{F} \tag{2.61}$$

Continuing the analysis in the second segment $[BG]$, the torques result now (with $x < 0$ in the segment region $[BG]$):

$$\mathbf{M}(x) = (l - x)\mathbf{p} \times \mathbf{F} - x\mathbf{p} \times \mathbf{F}^H \tag{2.62}$$

Note that the hydrodynamic force $\mathbf{F}^H$ (where the superscript "H" refers to its hydrodynamic nature) acts on the center G of the fiber, hence leading to the hydrodynamic torque
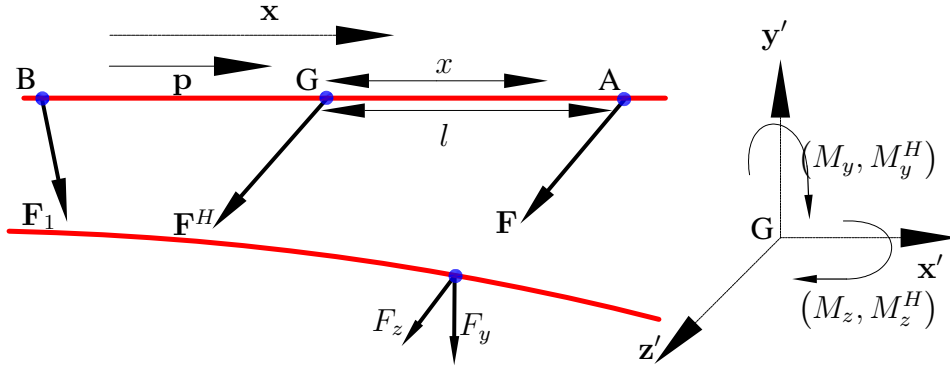
Figure 2.9: Fiber bending under the effect of contact and lubrication forces

$\mathbf{M}^H$ and its components contributing to the bending M_y^H and M_z^H. The bending torques are assumed to be coupled with the fiber's elasticity and it is assumed that the physical bending of the fibers lead to the storage of an elastic energy. Finally the elastic energy stored in each fiber can be calculated as:

$$u = \int_{\frac{-L}{2}}^{\frac{L}{2}} \left(\frac{M_z^2(x)}{EI_z} + \frac{M_y^2(x)}{EI_y} \right) dx \tag{2.63}$$

where L is the total length of the fiber. I_z and I_y are the relative quadratic torque of the fiber's section that for cylindrical fibers result:

$$I_z = I_y = \frac{\pi d^4}{64} \tag{2.64}$$

E being the Young modulus of the fiber (modulus of elasticity).
Again when dealing with discrete simulations, the integral in equation (2.63) is replaced by a sum. Hence, the elastic energy resulting on one fiber is written as:

$$u = \sum_i \left(\frac{M_z^2(x_i)}{EI_z} + \frac{M_y^2(x_i)}{EI_y} \right) \Delta x \tag{2.65}$$

Then the total elastic energy for all the fibers which are bending is simply:

$$U = \sum_{\alpha=1}^{n} \left[\sum_i \left(\frac{M_z^2(x_i)}{EI_z} + \frac{M_y^2(x_i)}{EI_y} \right) \Delta x \right] \tag{2.66}$$

2.6   Résumé du chapitre

Quand les suspensions de fibres deviennent concentrées, les théories à l'échelle méso-scopique ne permettent plus d'avoir une description précise de la physique fine qui agit à l'échelle microscopique de la fibre. Ainsi, une façon d'étudier la cinématique et la rhéolo-gie de ces suspensions à l'échelle microscopique est de faire une simulation numérique directe (ou SND). Une SND est basée sur le calcul dans un volume représentatif, du mou-vement d'une centaine de fibres et de leurs interactions, à l'échelle microscopique. Dans les travaux antérieurs, l'élasticité associée à la flexion des fibres n'a pas été considérée: les fibres ont été considérées purement rigides et sans effets de flexion lorsque des forces d'interactions se manifestaient suite à un contact entre deux fibres. Dans le cadre de la théorie des corps élancés, l'élasticité des suspensions est introduite en prenant compte que les forces qui agissent sur chaque fibre mènent à la flexion des fibres. Ainsi, cette flexion donne lieu à un comportement élastique physique illustré quantitativement par une én-ergie élastique emmagasinée à l'intérieur des suspensions.

Dans ce chapitre, les éléments théoriques de la DNS sont développés dans le cadre de la mécanique des fluides. Tout d'abord les principales hypothèses sont énoncées. En-suite, le volume représentatif représentant le milieu physique des fibres est décrit. Ensuite les équations de mouvement des fibres en translation et rotation sont détaillées à l'échelle microscopique (évolution temporelle de l'orientation des fibres et de la position du centre de gravité), avec les éléments nécessaires pour le calcul des forces d'interactions. La dis-tance entre deux fibres est définie, à partir de travaux précedents. De plus, on présente les expressions des propriétés macroscopiques (tenseur d'orientation, tenseur d'interaction, différence des contraintes normales, viscosité apparente). Finalement on définit l'énergie élastique dans le cadre de la théorie des poutres.

3

Numerical implementation and algorithm

Contents

This chapter will detail the numerical implementation of the micro-mechanical model and the algorithm used to perform the simulations. The numerical methods used from the generation of an initial state of concentrated fiber suspensions until the final time evolution of the kinematics/interactions, are discussed.

3.1 Generating the initial state

The parameters that are initially entered and controlled throughout this process are: the lengths of the fibers (with a standard mean deviation since different lengths are used

with a distribution law) their diameter, the total number of fibers n, the number of fibers in each direction of the REV, and the concentration ϕ. A *MATLAB* processing program was developed in order to generate the initial configuration of the fibers.

3.1.1   Fiber position

Fibers are homogeneously distributed in the REV described before (Figure 2.3), in a way to respect the following condition for their positions:

$$\sum_{\alpha=1}^{n} \mathbf{r}^{(\alpha)} = \mathbf{0} \tag{3.1}$$

and they are not touching each other (i.e initially no interactions are allowed). The axis system $(O, \mathbf{x}, \mathbf{y}, \mathbf{z})$ defined relative to the reference of the laboratory is supposed to be in the center of the REV. The program starts by dividing the 3D space according to the number of fibers in each direction; then the positions of center of gravity of each fiber are found by meshing the volume into three grids (Figure 3.2).
The average volume of one prolate spheroid (i.e. one fiber) is given by:

$$V_p = \frac{4\pi < l > d^2}{3} \tag{3.2}$$

where $< l >$ is the average length of the fibers.
The lengths of the fibers follow a normal distribution law with the mean length $< l >$ and a standard deviation σ respectively. Figure 3.1 shows an example of the distribution function for the aspect ratio where a mean length of $< l >= 20$ mm, a standard deviation of $\sigma = 3$ mm and an arbitrary total number of fibers was used.
 It is possible to define the number of fibers per direction (i.e. the number of fibers along
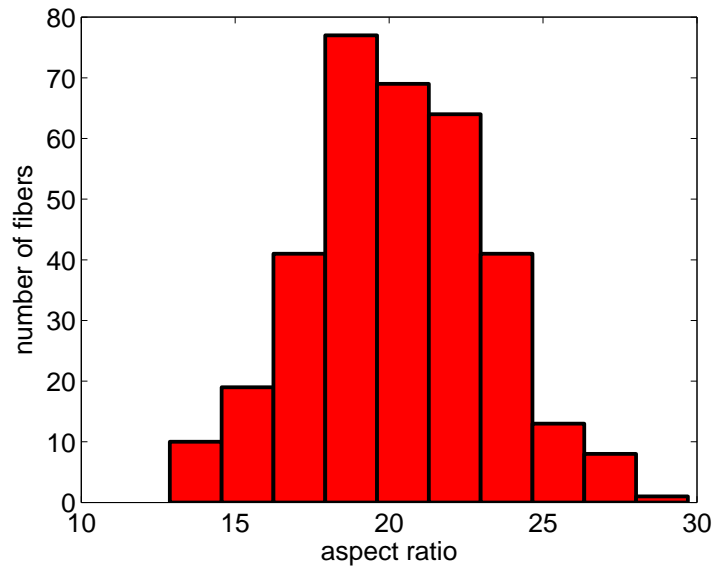

Figure 3.1: Aspect ratio normal distribution function

the **x**, **y** and **z** direction) as follows:

$$\mathcal{L} = h n_{x,y,z} \tag{3.3}$$

where $n_{x,y,z}$ is the number of fibers along one direction, and h is the initial gap between them (Figure 3.2). In this illustrative example, $n_{x,y,z} = 5$ and it is well visible in the **x**
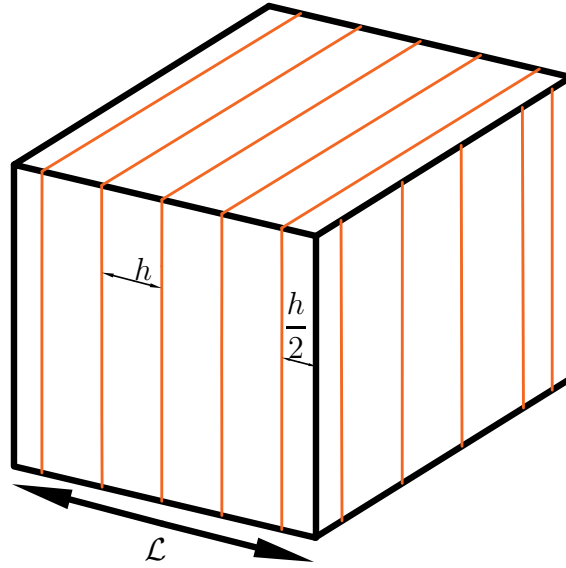

Figure 3.2: The REV dimensions as a function of h

direction that $\mathcal{L} = 5h$. Thus 5 fibers are being distributed here on each direction and the total number of fibers is $n = n_{x,y,z}^3$. The total volume of the REV can be expressed as:

$$V_{REV} = \mathcal{L}^3 = (h n_{x,y,z})^3 \tag{3.4}$$

Using equations (3.2) and (3.4) it is possible to numerically define h for a given concentration ϕ with respect to condition (2.3) as follows:

$$\phi = \frac{n V_p}{V_{REV}} = \frac{n V_p}{(h n_{x,y,z})^3} \Rightarrow h = \left(\frac{n V_p}{\phi n_{x,y,z}^3} \right)^{\frac{1}{3}} \tag{3.5}$$

Thus, the gap between the fibers will depend on the entered parameters (lengths, diameter, number of fibers per direction and concentration). For each new group of parameters ($<l>, \sigma, d, n_{x,y,z}, \phi$), there will be a new initial state to generate.

3.1.2 Fiber orientation

The orientation $\mathbf{p}^{(\alpha)}$ of each fiber must vary within a unit sphere of radius $R = 1$ (Figure 3.3) [92]. Thus, to chose the components of the orientation, a random vector named **J** is generated whose components (i.e. J_1, J_2 and J_3) are such as:

$$\begin{cases} 0 \leq J_1 \leq R \\ 0 \leq J_2 \leq R \\ 0 \leq J_3 \leq R \end{cases} \tag{3.6}$$

then for each fiber $\mathbf{p}^{(\alpha)}$ will be considered equal to:

$$\mathbf{p}^{(\alpha)} = \frac{2\mathbf{J} - \mathbf{O}}{\|2\mathbf{J} - \mathbf{O}\|} \tag{3.7}$$

where $\mathbf{O}$ is such as $O_1 = O_2 = O_3 = 1$. The numerator of equation (3.7), simply means that the components of $\mathbf{p}^{(\alpha)}$ are inside the unit sphere depicted in Figure 3.3. Then $2\mathbf{J} - \mathbf{O}$ is divided by its norm to insure a unit orientation vector.

To generate a set of n randomly oriented fibers distributed isotropically in the REV, the
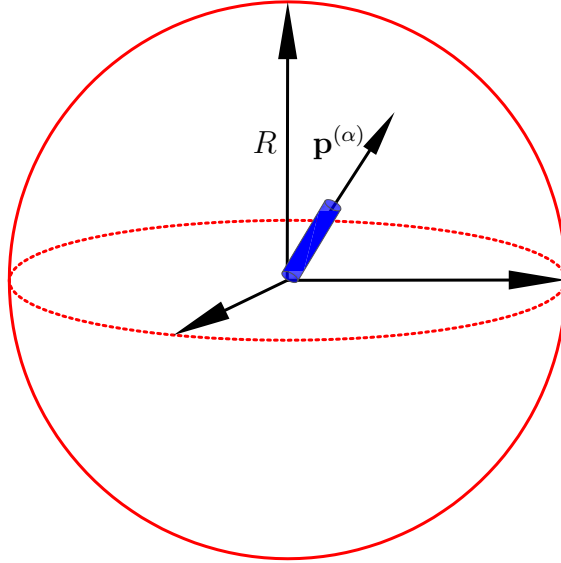

Figure 3.3: Fiber in the sphere of radius R

random orientations are made with respect to condition (3.6). Then each fiber is checked for avoiding interaction with another one. Therefore, a cutoff distance defined by [93]:

$$r_c = <l> + \sigma \tag{3.8}$$

is used to judge if a fiber is probable to interact with another one. This cutoff distance simply means that fibers lying outside the sphere of radius r_c do not influence the tested fiber. Hence, if the distance between the centers of two close fibers, say fiber α and fiber β is less than r_c, then the fibers could be in lubrication or contact. This is illustrated quantitatively in the following, and qualitatively in Figure 3.4:

$$\|\mathbf{r}^{(\alpha)} - \mathbf{r}^{(\beta)}\| < r_c \tag{3.9}$$

where a 2D representation has been used to simplify the concept. In this example one can notice that fiber β lies in the cutoff sphere and thus could interact with fiber α. However, fiber ν cannot interact with fiber α because it is located outside the r_c range.

These fibers are supposed to be in interaction, once condition (3.9) has been verified, the distance at the interaction point is such that $\Theta^{(\alpha,\beta)}$ is less a fraction of the fibers diameter d [41] and if that point falls between the ends of both fibers. The last condition is written
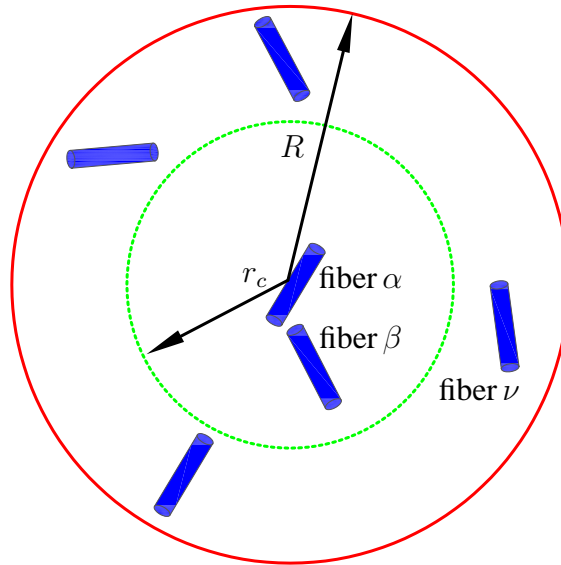
Figure 3.4: The cutoff sphere and the probable interacting fibers

as:

$$
\begin{aligned}
\left| l^{(\alpha,\beta)} \right| &\leq \frac{l^{(\alpha)}}{2} \\
\\
\left| l^{(\beta,\alpha)} \right| &\leq \frac{l^{(\beta)}}{2}
\end{aligned}
\tag{3.10}
$$

The program starts with one initial fiber α randomly oriented at $\mathbf{p}^{(\alpha)}$. Subsequently another fiber β is randomly oriented at $\mathbf{p}^{(\beta)}$. They are then checked for overlap (i.e. for interaction). If the pair of fibers α and β do not overlap then fiber β is accepted as a new fiber. If this is not the case, fiber β has to be repositioned by randomly selecting a new $\mathbf{p}^{(\beta)}$, while maintaining the same position $\mathbf{r}^{(\beta)}$. The selection of a new $\mathbf{p}^{(\beta)}$ is repeated up to a maximum number of trials, until the overlap condition is released. In all the production runs, the maximum number of tries for a new fiber to be placed within the REV with no overlapping was fixed to $Q = 10^4$. When the number Q is exceeded and the new placed fiber overlaps with previously placed fibers, then the programs stops and resets (the whole operation is restarted from the beginning).

3.1.3 Fibers located near the REV boundaries

Another thing that is considered while generating the fibers in the original REV, is that the fibers are allowed to extend outside the reference cell. This must be allowed, because it is impractical to consider walls at the boundaries of the REV, because this would produce nonrandom packing near the walls [92, 94]. In other terms, this is why, the gap between the boundaries of the REV and the last/first fiber placed in the REV is equal to $\frac{h}{2}$: no fibers are placed on the boundaries. Instead, the reference cell is replicated throughout space [95, 96, 93]. With this consideration if the fibers in the original cell
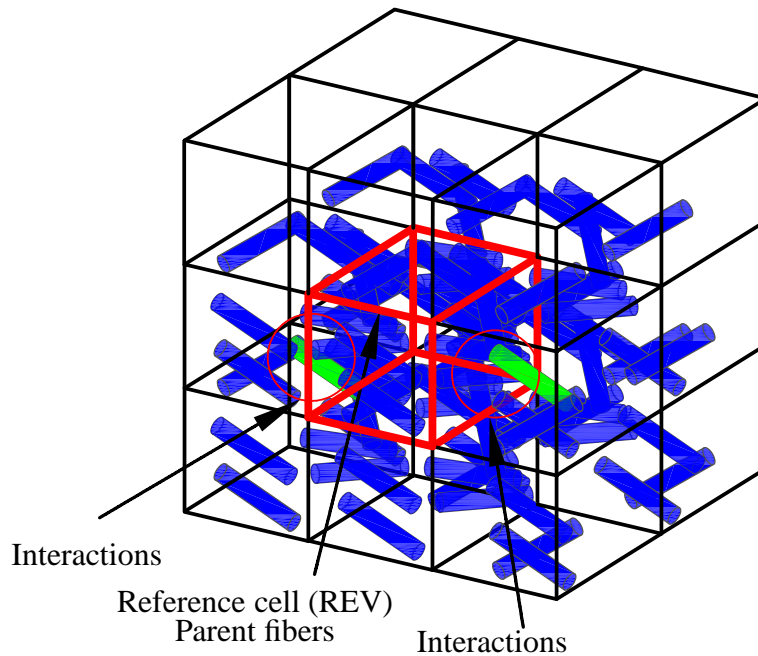
Figure 3.5: Reference cell (in highlighted thick red line) surrounded by neighboring cells

are named parent fibers, then the fibers sticking outside of the cell can interact with other fibers from the neighboring cells. Therefore, each new fiber β and its 26 image fibers, lying in the 26 neighboring cells have to be checked for overlapping with all previously placed parent fibers α. This is shown in Figure 3.5.

Note that the velocity gradient $\nabla \mathbf{V}$ is the same in all the cells. Finally, the steps to generate the initial state is resumed in the algorithm chart of Figure 3.6.

3.2 Deriving the kinematics evolution with the interactions

Having generated the initial state of the suspensions with the description above, it is now possible to numerically apply a simple shear flow, with respect to equation (2.4). Before detailing the numerical integration of the governing kinematic and interactions equations (i.e. equations (2.33), (2.34) and (2.35)), the numerical criteria for considering the two type of interactions (i.e. lubrication and contact) has to be detailed.

Starting from the initial state the *MATLAB* program starts by calculating the Jeffery orientation evolution for all n fibers with respect to equation (2.24). Then a function will find the fibers which are interacting at an instant t. The search for the interacting fibers is done according to section 3.1. The couple of fibers which are found to be in contact are stored at first independently from those which are in lubrication according to conditions (3.12) and (3.11). After that the corresponding normal vectors (equation (2.36)) are calculated. Finally, the system given by (2.42) have to be solved in order to derive all the existing forces.
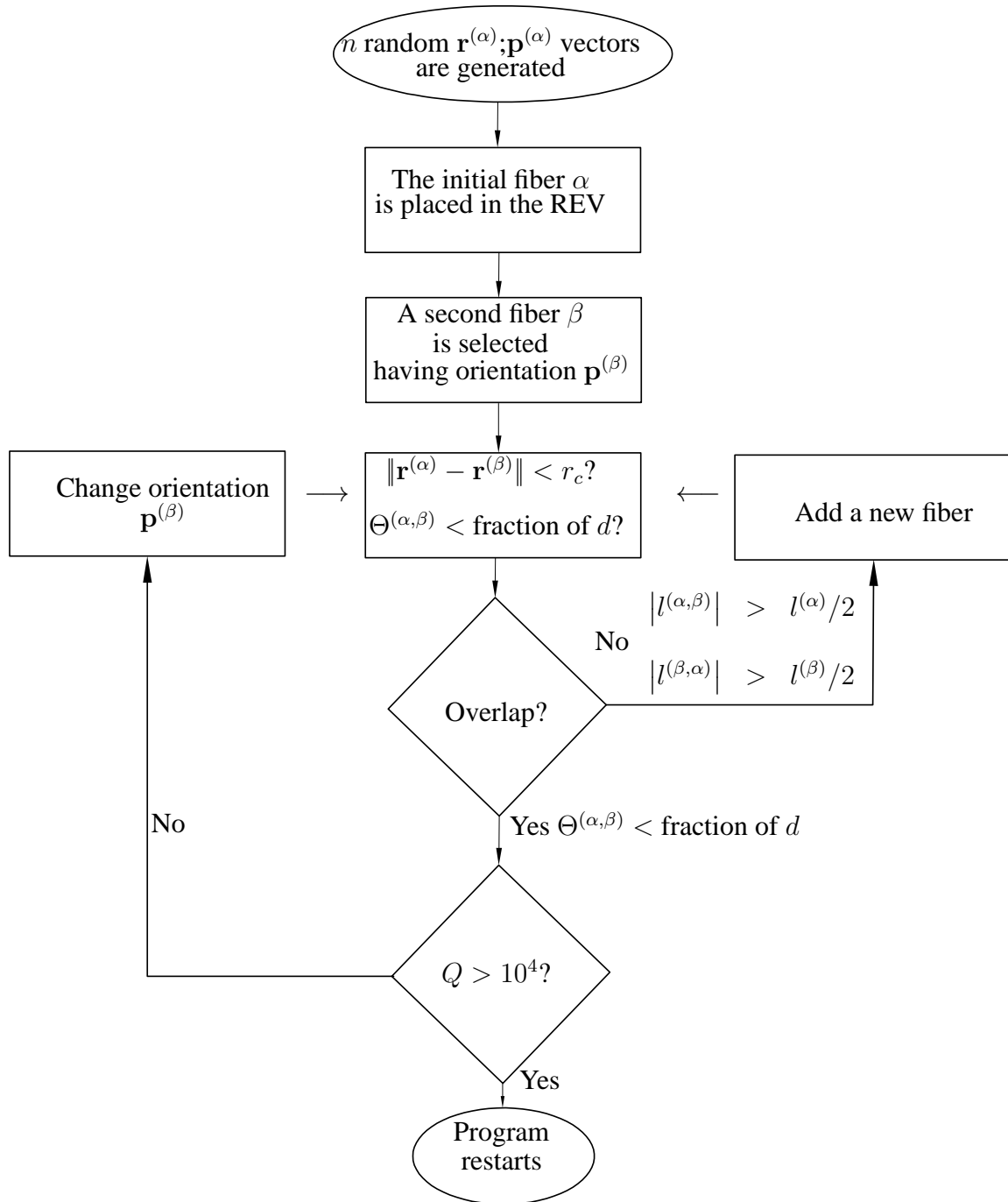
Figure 3.6: Algorithm chart for generating the initial state

3.2.1   Numerical criteria for interactions

Lubrication criteria

Since the suspensions are concentrated, it is logical to consider that if the distance between two fibers is less then a fraction of d, then a lubrication force is assumed to occur. In this study the lubrication condition that was used is:

$$\Theta^{(\alpha,\beta)} < \frac{d}{\Lambda} \qquad (3.11)$$

($\Theta^{(\alpha,\beta)}$ is the distance between two fibers) where Λ is the parameter used. In the simulations that have been performed Λ was set to 10^2.

Contact criteria

In section 2.3.4 the contact was defined according to equation (2.43). The distance was considered to be approximately equal to zero at the contact point. However, it is numerically difficult to simulate fibers that are not passing through each other when contact takes place between them. Thus $\Theta^{(\alpha,\beta)}$ can take a negative value numerically. And a contact happen when the following condition apply :

$$\Theta^{(\alpha,\beta)} \leq 0 \qquad (3.12)$$

3.2.2   Deriving the interaction forces

To further detail the numerical scheme used to solve system (2.42), the following simple example is considered. A couple of fibers α and β are found to be in interaction such as: fiber α is in interaction with fibers β and another fiber ν (Figure 3.7). And it is assumed that fibers α and β are in contact while fibers α and ν are in lubrication. It is clear from this example that there are are two unknowns (two interaction points thus two forces): $F_1 = F_c^{(\alpha,\beta)}$ and $F_2 = F_{lb}^{(\alpha,\nu)}$. If the number of interactions is denoted by N_I , it must be equal to the number of forces (i.e. in this case $N_I = 2$). The algorithm used finds the common fiber existing in couples of interacting fibers. In this simple example, the common fiber is α existing in the couples : (α,β) and (α,ν). Thus the first equation to be solved corresponding to the couple of fibers (α,β) is written (with respect to (2.42)) as:

$$
\begin{aligned}
&\frac{1}{3\pi\eta_0 l^{(\alpha)} Y_A^{(\alpha)}} \left(F_1 \mathbf{n}^{(\alpha,\beta)} \cdot \mathbf{n}^{(\alpha,\beta)} + F_2 \mathbf{n}^{(\alpha,\nu)} \cdot \mathbf{n}^{(\alpha,\beta)} \right) - \frac{1}{3\pi\eta_0 l^{(\beta)} Y_A^{(\beta)}} \left(F_1 \mathbf{n}^{(\beta,\alpha)} \cdot \mathbf{n}^{(\alpha,\beta)} \right) \\
&+ \frac{1}{\pi\eta_0 l^{(\alpha)3} Y_C^{(\alpha)}} \left(l^{(\alpha,\beta)} F_1 \mathbf{n}^{(\alpha,\beta)} \cdot \mathbf{n}^{(\alpha,\beta)} + l^{(\alpha,\nu)} F_2 \mathbf{n}^{(\alpha,\nu)} \cdot \mathbf{n}^{(\alpha,\beta)} \right) \\
&- \frac{1}{\pi\eta_0 l^{(\beta)3} Y_C^{(\beta)}} \left(l^{(\beta,\alpha)} F_1 \mathbf{n}^{(\beta,\alpha)} \cdot \mathbf{n}^{(\alpha,\beta)} \right) \\
&= - \left(l^{(\alpha,\beta)} \dot{\mathbf{p}}_J^{(\alpha)} - l^{(\beta,\alpha)} \dot{\mathbf{p}}_J^{(\beta)} \right) \cdot \mathbf{n}^{(\alpha,\beta)} - \dot{\gamma} \left(y^{(\alpha)} - y^{(\beta)} \right) n_x^{(\alpha,\beta)}
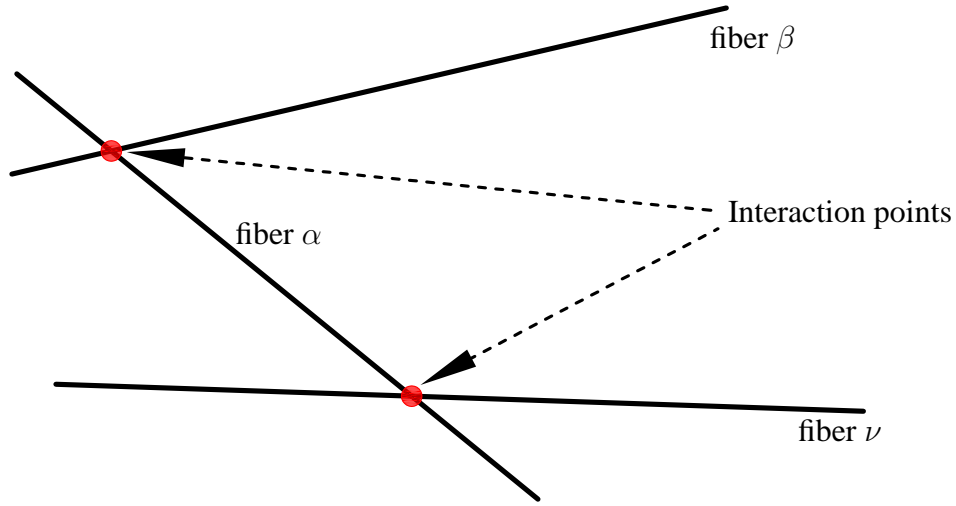\end{aligned}
$$

$$(3.13)$$

Figure 3.7: Simple interaction example

and the second equation corresponding to the couple (α,ν) is written as:

$$
\begin{aligned}
& \frac{1}{K\left(\Theta^{(\alpha,\nu)}\right)} F_2 + \frac{1}{3\pi\eta_0 l^{(\alpha)} Y_A^{(\alpha)}} \left(F_1 \mathbf{n}^{(\alpha,\beta)} \cdot \mathbf{n}^{(\alpha,\nu)} + F_2 \mathbf{n}^{(\alpha,\nu)} \cdot \mathbf{n}^{(\alpha,\nu)} \right) \\
& - \frac{1}{3\pi\eta_0 l^{(\nu)} Y_A^{(\nu)}} \left(F_2 \mathbf{n}^{(\nu,\alpha)} \cdot \mathbf{n}^{(\alpha,\nu)} \right) \\
& + \frac{1}{\pi\eta_0 l^{(\alpha)^3} Y_C^{(\alpha)}} \left(l^{(\alpha,\beta)} F_1 \mathbf{n}^{(\alpha,\beta)} \cdot \mathbf{n}^{(\alpha,\nu)} + l^{(\alpha,\nu)} F_2 \mathbf{n}^{(\alpha,\nu)} \cdot \mathbf{n}^{(\alpha,\nu)} \right) \qquad (3.14) \\
& - \frac{1}{\pi\eta_0 l^{(\nu)^3} Y_C^{(\nu)}} \left(l^{(\nu,\alpha)} F_2 \mathbf{n}^{(\nu,\alpha)} \cdot \mathbf{n}^{(\alpha,\nu)} \right) \\
& = - \left(l^{(\alpha,\nu)} \dot{\mathbf{p}}_J^{(\alpha)} - l^{(\nu,\alpha)} \dot{\mathbf{p}}_J^{(\nu)} \right) \cdot \mathbf{n}^{(\alpha,\nu)} - \dot{\gamma} \left(y^{(\alpha)} - y^{(\nu)} \right) n_x^{(\alpha,\nu)}
\end{aligned}
$$

with $K\left(\Theta^{(\alpha,\nu)}\right) = \dfrac{3\pi\eta_0 d^2}{\Theta^{(\alpha,\nu)} ||\mathbf{p}^{(\alpha)} \times \mathbf{p}^{(\nu)}||}$.

Thus the system to be solved takes the following form: $\mathbf{A} \cdot \mathbf{F} = \mathbf{B}$, where the assembled matrix is:

$$
\mathbf{A}\left(t\right) = \begin{bmatrix} A_{11} & A_{12} \\ A_{21} & A_{22} \end{bmatrix} \qquad (3.15)
$$

with:

$$
\begin{aligned}
A_{11} &= \frac{1}{3\pi\eta_0 l^{(\alpha)} Y_A^{(\alpha)}} \left(\mathbf{n}^{(\alpha,\beta)} \cdot \mathbf{n}^{(\alpha,\beta)}\right) - \frac{1}{3\pi\eta_0 l^{(\beta)} Y_A^{(\beta)}} \left(\mathbf{n}^{(\beta,\alpha)} \cdot \mathbf{n}^{(\alpha,\beta)}\right) \\
&\quad + \frac{1}{\pi\eta_0 l^{(\alpha)3} Y_C^{(\alpha)}} \left(l^{(\alpha,\beta)} \mathbf{n}^{(\alpha,\beta)} \cdot \mathbf{n}^{(\alpha,\beta)}\right) - \frac{1}{\pi\eta_0 l^{(\beta)3} Y_C^{(\beta)}} \left(l^{(\beta,\alpha)} \mathbf{n}^{(\beta,\alpha)} \cdot \mathbf{n}^{(\alpha,\beta)}\right) \\
A_{12} &= \frac{1}{3\pi\eta_0 l^{(\alpha)} Y_A^{(\alpha)}} \left(\mathbf{n}^{(\alpha,\nu)} \cdot \mathbf{n}^{(\alpha,\beta)}\right) + \frac{1}{\pi\eta_0 l^{(\alpha)3} Y_C^{(\alpha)}} \left(l^{(\alpha,\nu)} \mathbf{n}^{(\alpha,\nu)} \cdot \mathbf{n}^{(\alpha,\beta)}\right) \\
A_{21} &= \frac{1}{3\pi\eta_0 l^{(\alpha)} Y_A^{(\alpha)}} \left(\mathbf{n}^{(\alpha,\beta)} \cdot \mathbf{n}^{(\alpha,\nu)}\right) + \frac{1}{\pi\eta_0 l^{(\alpha)3} Y_C^{(\alpha)}} \left(l^{(\alpha,\beta)} \mathbf{n}^{(\alpha,\beta)} \cdot \mathbf{n}^{(\alpha,\nu)}\right) \\
A_{22} &= \frac{1}{K\left(\Theta^{(\alpha,\nu)}\right)} + \frac{1}{3\pi\eta_0 l^{(\alpha)} Y_A^{(\alpha)}} \left(\mathbf{n}^{(\alpha,\nu)} \cdot \mathbf{n}^{(\alpha,\nu)}\right) \\
&\quad - \frac{1}{3\pi\eta_0 l^{(\nu)} Y_A^{(\nu)}} \left(\mathbf{n}^{(\nu,\alpha)} \cdot \mathbf{n}^{(\alpha,\nu)}\right) + \frac{1}{\pi\eta_0 l^{(\alpha)3} Y_C^{(\alpha)}} \left(l^{(\alpha,\nu)} \mathbf{n}^{(\alpha,\nu)} \cdot \mathbf{n}^{(\alpha,\nu)}\right) \\
&\quad - \frac{1}{\pi\eta_0 l^{(\nu)3} Y_C^{(\nu)}} \left(l^{(\nu,\alpha)} \mathbf{n}^{(\nu,\alpha)} \cdot \mathbf{n}^{(\alpha,\nu)}\right)
\end{aligned}
\tag{3.16}
$$

And the second member is:

$$
\mathbf{B}(t) = \begin{bmatrix} B_1 \\ B_2 \end{bmatrix}
\tag{3.17}
$$

with:

$$
\begin{aligned}
B_1 &= -\left(l^{(\alpha,\beta)} \dot{\mathbf{p}}_J^{(\alpha)} - l^{(\beta,\alpha)} \dot{\mathbf{p}}_J^{(\beta)}\right) \cdot \mathbf{n}^{(\alpha,\beta)} - \dot{\gamma}\left(y^{(\alpha)} - y^{(\beta)}\right) n_x^{(\alpha,\beta)} \\
B_2 &= -\left(l^{(\alpha,\nu)} \dot{\mathbf{p}}_J^{(\alpha)} - l^{(\nu,\alpha)} \dot{\mathbf{p}}_J^{(\nu)}\right) \cdot \mathbf{n}^{(\alpha,\nu)} - \dot{\gamma}\left(y^{(\alpha)} - y^{(\nu)}\right) n_x^{(\alpha,\nu)}
\end{aligned}
\tag{3.18}
$$

Therefore one obtains :

$$
\mathbf{F}(t) = \begin{bmatrix} F_1 \\ F_2 \end{bmatrix} = \mathbf{A}^{-1} \cdot \mathbf{B}
\tag{3.19}
$$

Note that $\mathbf{A}$, $\mathbf{B}$, and $\mathbf{F}$ are time dependent because at each time step, a new configuration of interacting fibers is found that could be different from the previous configuration at an earlier time step.

3.2.3   Deriving the kinematic governing equations

Now that the forces have been calculated at an instant t, it is possible to evaluate the time evolution of the kinematics (i.e. orientation and position of center of gravity), using equations (2.33), (2.34) and (2.35).

The numerical scheme used to perform the integration was an explicit finite difference method based on the Taylor series expansion. The purpose of this method is to approximately determine the function $w(t)$ verifying:

$$
\dot{w}(t) = W(t, w(t))
\tag{3.20}
$$

and varying in an interval $[t_0, t_{max}]$. The function $w(t)$ represents either $\mathbf{p}^{(\alpha)}(t)$ or $\mathbf{r}^{(\alpha)}(t)$. t_{max} represents the total evolution time of the function (i.e. the numerical simulation time). At $t = t_0$ s, the initial known condition (given by the initial state) is

$w_0 = w(t = t_0)$. To determine the discrete values w_1, w_2, ... w_P, the interval $[t_0, t_{max}]$ is divided into P sub-intervals:

$$t_p = t_0 + (\Delta t)\, p \qquad p = 0, ..., P \tag{3.21}$$

where Δt is the time step used for the discretization of the interval. Then, the Taylor series expansion of the exact solution $w(t_p + \Delta t) = w(t_{p+1})$ around the point t_p writes:

$$w(t_{p+1}) = w(t_p) + \Delta t \dot{w}(t_p) \tag{3.22}$$

This method is called a single-step method, where the result $w(t_p)$ relative to point t_p suffices to calculate the new approximation $w(t_{p+1})$. In this case if the applied forces at each fiber α at time t are known then $\dot{\mathbf{q}}^{(\alpha)}(t)$ is updated as:

$$\dot{\mathbf{q}}^{(\alpha)}(t) = \frac{1}{3\pi\eta_0 l^{(\alpha)} Y_A^{(\alpha)}} \sum_{i=1}^{N_I} \mathbf{F}_i(t) \tag{3.23}$$

where the forces $\mathbf{F}_i$ are supposed to be both lubrication and contact. Then $\mathbf{p}^{(\alpha)}(t)$ and $\mathbf{r}^{(\alpha)}(t)$ are updated at time $t + \Delta t$ for each fiber as:

$$\mathbf{p}^{(\alpha)}(t + \Delta t) = \mathbf{p}^{(\alpha)}(t) + \Delta t \left(\dot{\mathbf{p}}_J^{(\alpha)}(t) + \sum_{i=1}^{N_I} l^i(t) \mathbf{F}_i(t) \right) \tag{3.24}$$

$$\mathbf{r}^{(\alpha)}(t + \Delta t) = \mathbf{r}^{(\alpha)}(t) + \Delta t \left(\dot{\gamma} y^{(\alpha)}(t)\, \mathbf{e_1} + \dot{\mathbf{q}}^{(\alpha)}(t) \right)$$

where the distances $l^{(\alpha,\beta)}$ and $l^{(\alpha,\mu)}$ are replaced by l^i for the sake of simplicity. The choice of the time step governs the accuracy of the obtained solution. The smaller Δt is, the more accurate are the approximated derivatives. The derivatives are stable, as long as the numerical errors do not increase in time.

3.2.4 Treating the fibers near the REV boundaries

Another important aspect to consider while updating the kinematics, are the 26 cells surrounding the original one (Figure 3.5). Since initially, the n fibers in the simulation lie within a cubic box of side H, with the origin at its center, then all the coordinates lie in the range $\left(-\dfrac{H}{2}, \dfrac{H}{2} \right)$. As the simulation proceeds and the kinematics are updated with respect to (3.23) and (3.24), these fibers will move and probably exit the reference cell. When a fiber leaves the REV by crossing one of the boundaries, it is usual to switch attention to the image fiber entering the box, by simply adding H to, or subtracting H from the appropriate coordinate. One simple way to do this in the frame of molecular dynamics uses the following condition for $\mathbf{r}^{(\alpha)}$ [93]:

$$\begin{cases} \text{if } x^{(\alpha)}(t + \Delta t) > \dfrac{H}{2} & \text{then } x^{(\alpha)}(t + \Delta t) = x^{(\alpha)}(t + \Delta t) - H \\ \text{if } x^{(\alpha)}(t + \Delta t) < -\dfrac{H}{2} & \text{then } x^{(\alpha)}(t + \Delta t) = x^{(\alpha)}(t + \Delta t) + H \end{cases} \tag{3.25}$$

Similar conditions are applied to the y and z coordinates. Note that the positions and orientations of the fibers are updated at each time step only in the original cell that is then replicated. Figure 3.8 summaries the total algorithm used to derive the kinematics.

Once the whole data on the suspensions time evolution is obtained, it will be possible to calculate the evolution of the orientation and interaction tensors. Also the macroscopic properties (i.e. equations (2.54), (2.55),(2.56), (2.57), (2.58) and (2.59)) are then directly computed.

Remark:
In the performed simulations (for deriving the kinematics) the numerical computations were carried out on a 4×AMD Opteron 6204 3.3 GHz Quadcore using a Red Hat Enterprise Linux Server release 6.3 operating system with a 5 GB RAM. The time step used was $\Delta t = 0.01$ s for an interval size of $P = 2.10^4$ (i.e. $t_0 = 0$ s and $t_{max} = 200$ s). The average time for each simulation was approximately 192 hours.

3.3   Computing the macroscopic descriptors and properties

3.3.1   Macroscopic descriptors

Once the kinetic simulation is finished and all the necessary microscopic properties have been stored (orientations, positions and forces) throughout the simulation time, then it is possible to directly calculate the time evolution of the orientation tensor from equation (2.46) and the time evolution of the interaction tensor from equation (2.51).

3.3.2   Macroscopic properties

Similarly, the time evolution of the shear stress growth coefficient, the normal stress growth function, and the total elastic energy are computed with respect to equations (2.59), (2.58) and (2.66).
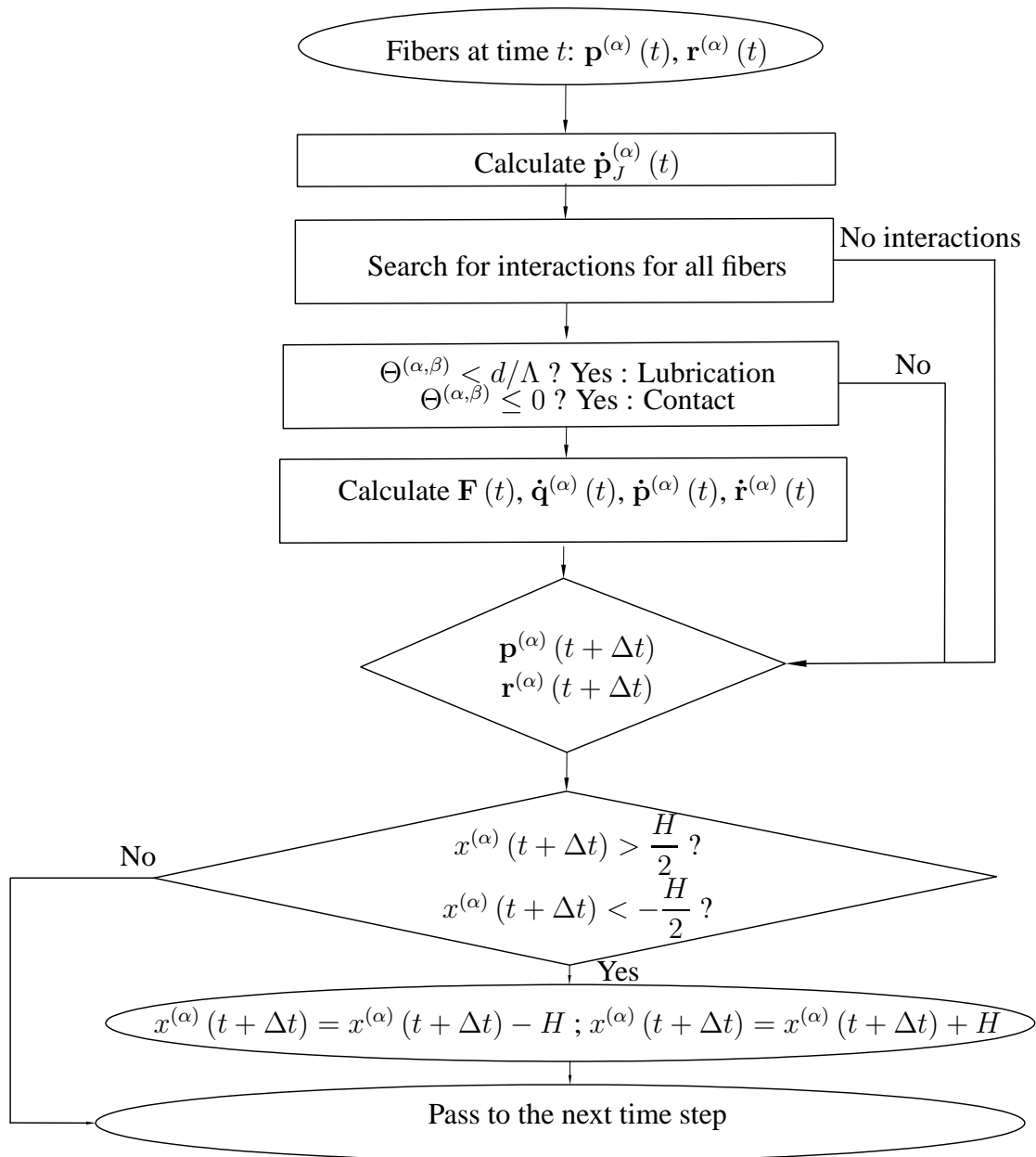
Figure 3.8: Algorithm chart performed at each time step to update fiber position and orientation

3.4 Résumé du chapitre

Dans ce chapitre, l'implémentation numérique du modèle micro-mécanique (présenté dans le chapitre 2) a été détaillée. Ensuite on explique les algorithmes utilisés (résumés sous forme d'organigrammes) pour lancer les simulations. On génère l'état initial des fibres dans un volume repésentatif cubique. Les fibres sont supposées de longueurs différentes; les longueurs suivent une loi de distribution normale avec un écart type et une longueur moyenne spécifiques. Initialement les fibres sont uniformément distribuées dans le volume, orientées de manière isotrope et sont, sans aucune interaction. Une distance de coupure est définie pour juger si une fibre est susceptible d'être en interaction avec sa voisine. Ainsi, si la distance entre les centres de gravités de deux fibres voisines est moins que cette distance critique, donc c'est probable que les fibres entrent en interaction. Les fibres s'interagissent, si la distance qui les sépare (définie dans le chapitre 2) est inférieure à une fraction du diamètre des fibres.

Le calcul détaillé de la cinématique des fibres est ensuite donné. Pour cela le système contenant les forces d'interactions a été résolu par l'intermédiaire d'un exemple simple illustratif où deux fibres seulement sont considérées en interactions. Une méthode explicite issue du développement de Taylor au premier terme est utilisée pour intégrer numériquement les différentes équations cinématiques.

Le calcul des grandeurs macroscopiques se fait directement à partir des équations (2.46), (2.51), (2.59), (2.58) et (2.66) respectivement. Les spécifications du serveur de calcul adpoté pour le lancement des simulations sont annexées à la fin du chapitre (type du calculateur, mémoire utilisée, temps réel de calcul et le nombre du pas de temps).

DNS Simulation results

Contents

The present chapter illustrates the results of the numerical simulations that have been performed with respect to the algorithms described in chapter 3 (throughout this chapter the mean length of the fibers will be denoted by $\langle L \rangle$).

4.1 Monodisperse dilute suspensions

Before studying the kinematic evolution of the polydisperse concentrated suspensions, this section will discuss the case of monodisperse diluted suspensions, where fibers have the same length and each fiber can be traced independently from the other fibers (since no interactions are involved). When the concentration is low enough fiber-fiber interactions do not occur, because the system is not dense enough to allow contact or lubrication. Thus, the orientation evolution will be given by the Jeffery orientation evolution (equation 2.24). A simple shear flow, with a shear rate $\dot{\gamma} = 1\,\mathrm{s}^{-1}$ was applied in the diluted suspensions

having a concentration $\phi = 0.1\% \leq \dfrac{1}{r^2}$ (where r is the average aspect ratio of the fibers); the fibers had a length of 20 mm with $n = 512$ (n is the total number of fibers) and a diameter of $d = 1$ mm. Their initial isotropic state was verified by applying equations (2.46) and (2.51), thus initially it was found: $\mathbf{a_2} \simeq \dfrac{1}{3}\mathbf{I}$ and $\mathbf{b_2} \simeq \dfrac{\pi}{12}\mathbf{I}$.

The orientation will change in a repeating cyclic orbit commonly called the Jeffery Orbit [59]. Thus, the orientation will exhibit a periodic rotation and at each period the fiber flips and is aligned with the first direction of the velocity field ($\mathbf{x}$ axis). The period of this rotation is given by:

$$D = \frac{2\pi}{\dot{\gamma}}\left(r + \frac{1}{r}\right) \tag{4.1}$$

By selecting a random fiber, the evolution of the 3 components of $\mathbf{p}$ (i.e. p_1, p_2 and p_3) is depicted in Figure 4.1 where the period was checked to be equal to equation (4.1). The evolution of the orientation tensor (i.e. a_{11}, a_{22} and a_{33} components), was found to
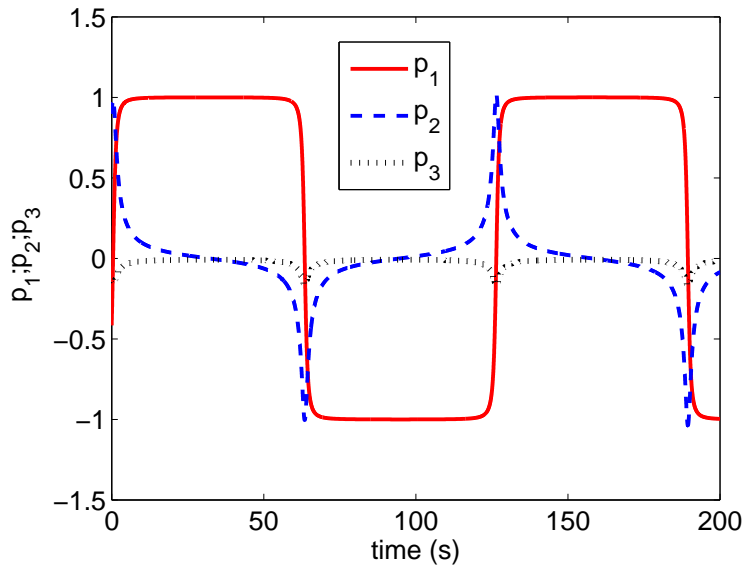

Figure 4.1: Time evolution of the p_1, p_2 and p_3 components

give the periodic behavior associated with the orientation evolution. Figure 4.2 shows this evolution, and this time the period is checked to be equal to half of the period D. The following section will discuss the effects of having different fiber lengths, in the concentrated regime inducing fiber-fiber interactions.

4.2 Polydisperse concentrated suspensions

A volume fraction of fibers of $\phi = 11.5\%$ was used to create the initial microstructure. Note that this concentration falls in the concentrated regime (assumption 4 from section 2.1). A total number of $n = 512$ prolate spheroids were placed into a cubic volume (Figure 4.3). Using less than 500 fibers does not allow a representative description
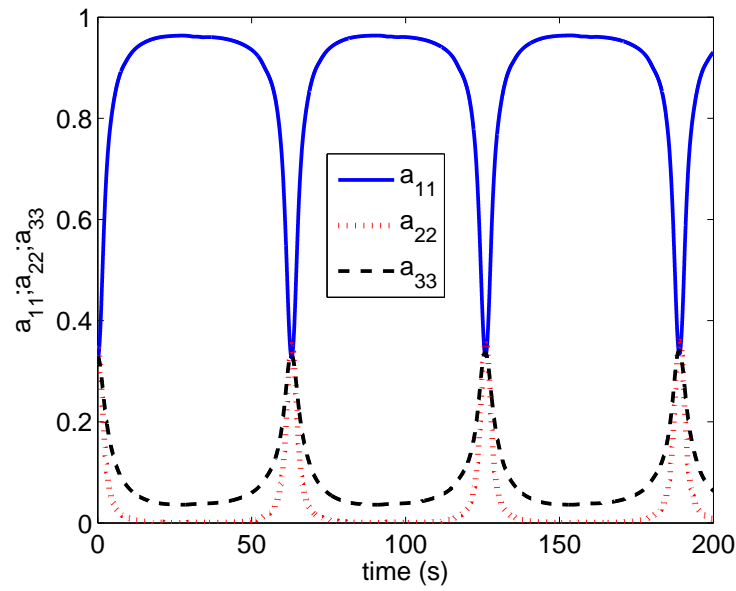
Figure 4.2: Time evolution of the a_{11}, a_{22} and a_{33} components
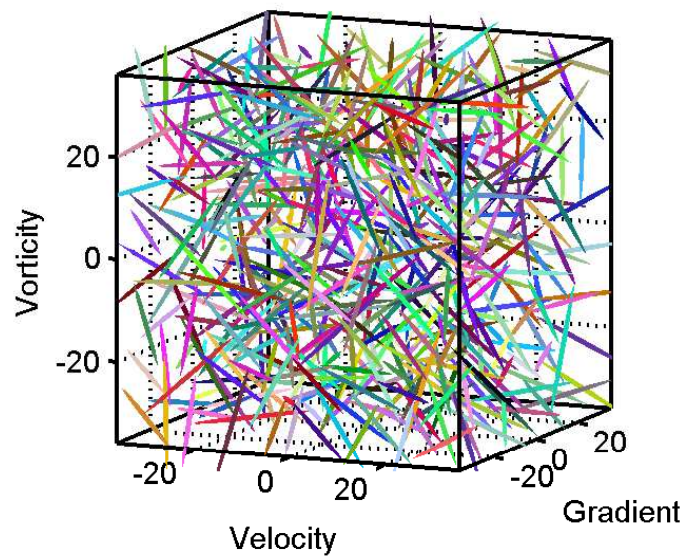

Figure 4.3: Initial state of the fibers (unit of length: mm)

of fiber population [71]. Their isotropic state was verified by applying equations (2.46) and (2.51), thus initially it was found: $\mathbf{a_2} \simeq \frac{1}{3}\mathbf{I}$ and $\mathbf{b_2} \simeq \frac{\pi}{12}\mathbf{I}$.

The mean length of the fibers was set to $\langle L \rangle = 20$ mm with a standard deviation of 3

mm, and the diameter of each fiber is $d = 1$ mm. These values are consistent with the type of glass fibers used in GFP (with $E = 75$ GPa).

4.2.1   Macroscopic descriptors evolution

The same simple shear flow, was applied in the suspensions depicted in Figure 4.3 with the parameters described in section 4.2 (i.e. concentration, length and diameter). Figure 4.4 shows the time evolution of the a_{11}, a_{22} and a_{33} components with time. From Figure 4.4 it is possible to determine the transient phase and an almost steady phase in the region between 100 and 200 seconds where the a_{11}, a_{22} and a_{33} components no longer change. For the a_{11} component, the width of the first peak and the fluctuations that occur in the steady state, are due to the amount of interactions taking place between fibers (contact and lubrification forces). In the almost steady state regime most fibers align in the first direction of the velocity field (Figure 4.4 i.e. $a_{11} \approx 0.9$) but the interactions and the finite aspect ratio produce quick sporadic rotations.

In order to study the interactions involved, the time evolution of the b_{11}, b_{22} and b_{33} components with time, of the interaction tensor has been depicted in Figure 4.4. When fibers almost align with the first direction of the velocity field (maximum value of a_{11}), b_{11}, b_{22} and b_{33} reach a minimun in roughly the same time interval than a_{11} reaches a maximum. This is due to fibers being close to being parallel with the first direction of the velocity field ($\|\mathbf{p}^{(\alpha)} \times \mathbf{p}^{(\beta)}\| \to 0$ in equation (2.51)). Figures 4.4 and 4.5, confirm the fact that the interactions become stable when fibers are almost aligned in this direction.

In the following paragraph the shear stress growth coefficient and the normal stress growth functions deduced from the components of $\mathbf{a_2}$ are discussed and compared with experimental results found in the litterature.

4.2.2   Macroscopic properties evolution

Shear stress growth coefficient and normal stress growth functions

Using equations (2.54) to (2.58), the time evolution of the stress in the suspensions has been calculated. The normalized shear stress growth coefficient is plotted versus time in Figure 4.6. The viscosity has a maximum value at the beginning, when the fiber orientation is isotropic and then it reaches an almost steady value lower than the intial one, when fibers are almost aligned in the first direction of the velocity field for a time $t > 100$ s. This evolution is in agreement with experimental studies found in the litterature for polydisperse suspensions [97, 98, 99, 23].

The evolutions of the normalized normal stress growth functions $N_1^+ = \dfrac{N_1}{\eta_0 \dot{\gamma}}$ and $N_2^+ = \dfrac{N_2}{\eta_0 \dot{\gamma}}$ (equation (2.59)) have been depicted in Figure 4.7. The component N_1^+ exhibits an overshoot in the transient regime and N_2^+ produces an undershoot. Then they become sta-
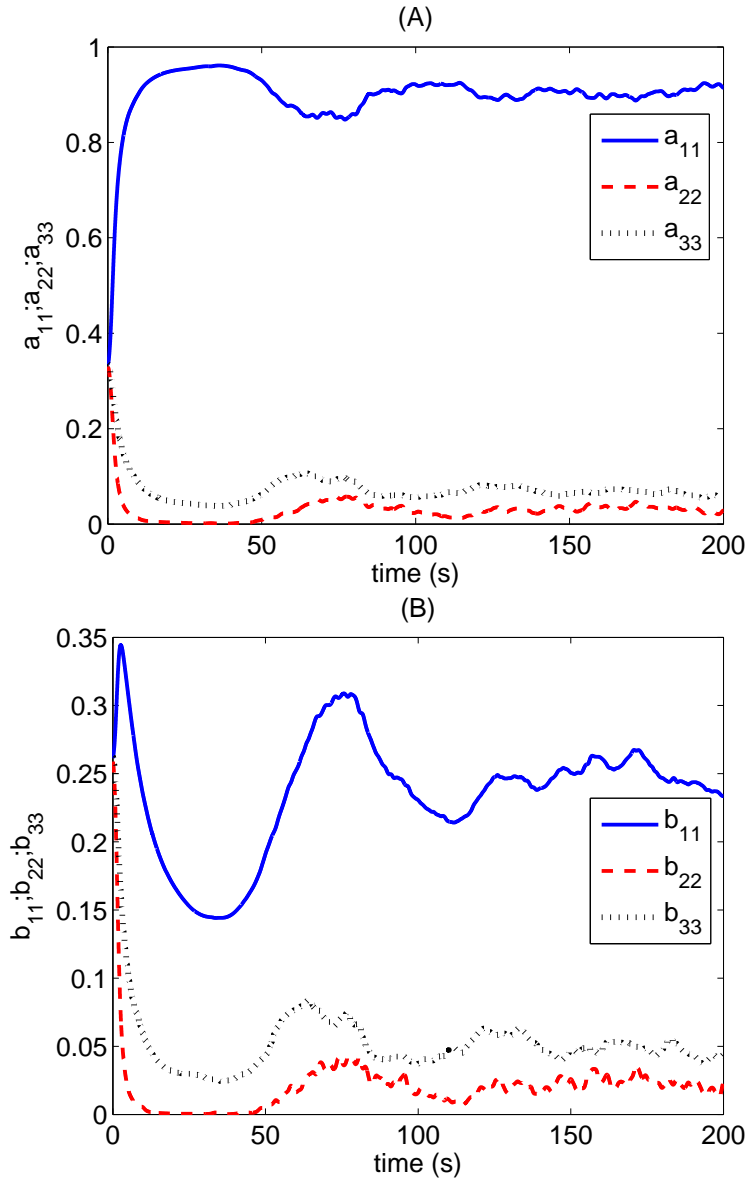
Figure 4.4: (A) Time evolution of the a_{11}, a_{22} and a_{33} components (B) Time evolution of the b_{11}, b_{22} and b_{33} components

ble in the almost steady regime. The phenomena of stress overshoot/undershoot in fiber suspensions in a Newtonian fluid is observed experimentally [97] and it depends on the length of the fibers [99]. The sudden change of fiber orientation in an incipient shear flow gives rise to this overshoot/undershoot at the beginning of the simulation [99].

In what concerns the relationship between N_1^+ and N_2^+, many researchers have assumed that N_2^+ is negligible compared to N_1^+ from either experimental results or numerical simulations [34]. But these stress predictions ignored the interactions between fibers. However, when interactions are considered the qualitative relationship of $N_1^+ \approx -2N_2^+$ is almost obtained. It is more accurate when the microstructure reaches an almost steady state. Moreover $N_1^+ \geq 0$ most of the time, which is consistent with previous works [100].
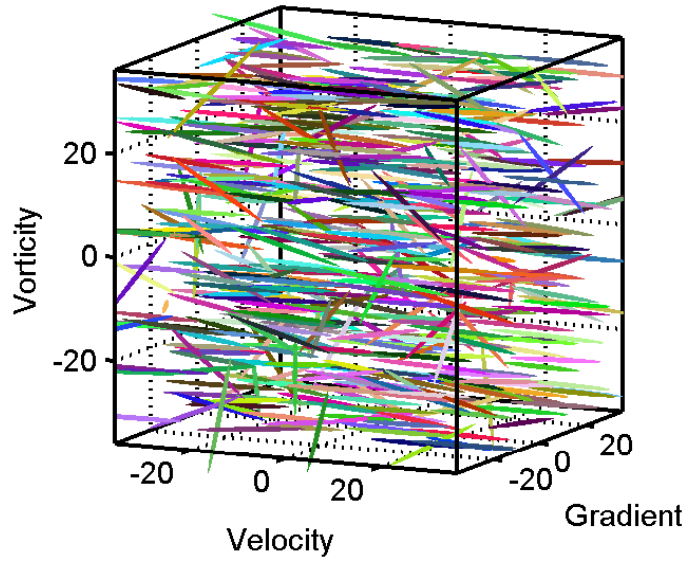
Figure 4.5: Microstructure at $t = 200$ s (unit of length: mm)

Figure 4.6: Normalized shear stress growth coefficient

This is due to the interactions being weak in the flow direction relative to the interactions in the gradient direction [100] . But it is mostly the result of fibers being strongly aligned in the first direction of the velocity field, because the non-hydrodynamic forces (i.e. contact and lubrication forces) make a small contribution to the total stress. In fact, N_1 can

be rewritten as:

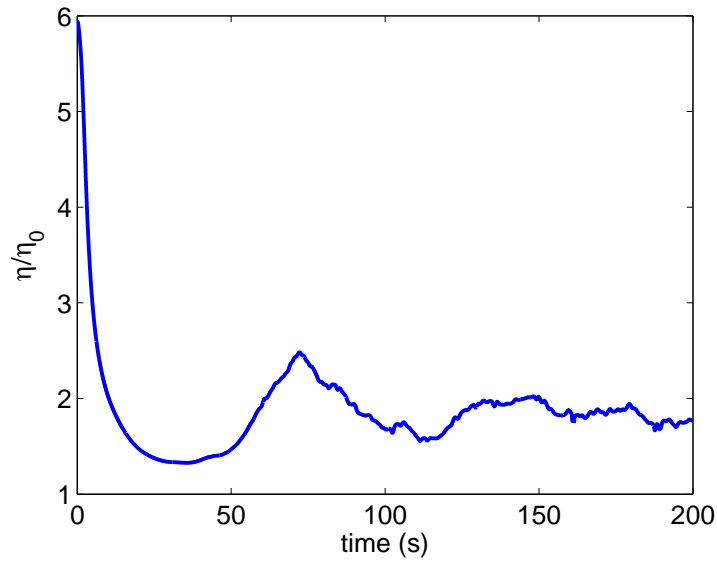$$N_1 = \left(\sigma_{11}^h - \sigma_{11}^{nh}\right) - \left(\sigma_{22}^h - \sigma_{22}^{nh}\right) = \left(\sigma_{11}^h - \sigma_{22}^h\right) + \left(\sigma_{22}^{nh} - \sigma_{11}^{nh}\right) \tag{4.2}$$

(the term $\left(\sigma_{22}^{nh} - \sigma_{11}^{nh}\right)$ is a weak contribution) where in the literature [100] the average value of $\left(\sigma_{11}^h - \sigma_{22}^h\right)$ is :

$$\left\langle \sigma_{11}^h - \sigma_{22}^h \right\rangle \approx \left[\left\langle p_1^3 p_2 \right\rangle - \left\langle p_1 p_2^3 \right\rangle \right] > 0 \tag{4.3}$$

since $\langle p_1^2 \rangle > \langle p_3^2 \rangle > \langle p_2^2 \rangle$ (i.e. $a_{11} > a_{33} > a_{22}$).
A similar interpretation is done for $N_2^+ < 0$; this time with:

$$N_2 = \left(\sigma_{22}^h - \sigma_{22}^{nh}\right) - \left(\sigma_{33}^h - \sigma_{33}^{nh}\right) = \left(\sigma_{22}^h - \sigma_{33}^h\right) + \left(\sigma_{33}^{nh} - \sigma_{22}^{nh}\right) \tag{4.4}$$

(this time the term $\left(\sigma_{33}^{nh} - \sigma_{22}^{nh}\right)$ is a weak contribution) and :

$$\left\langle \sigma_{22}^h - \sigma_{33}^h \right\rangle \approx \left[\left\langle p_x p_y^3 \right\rangle - \left\langle p_x p_y p_z^2 \right\rangle \right] < 0 \tag{4.5}$$

With the interactions having higher amplitude in the gradient direction relative to the vorticity direction [100], this will yield $N_2^+ < 0$ most of the time.
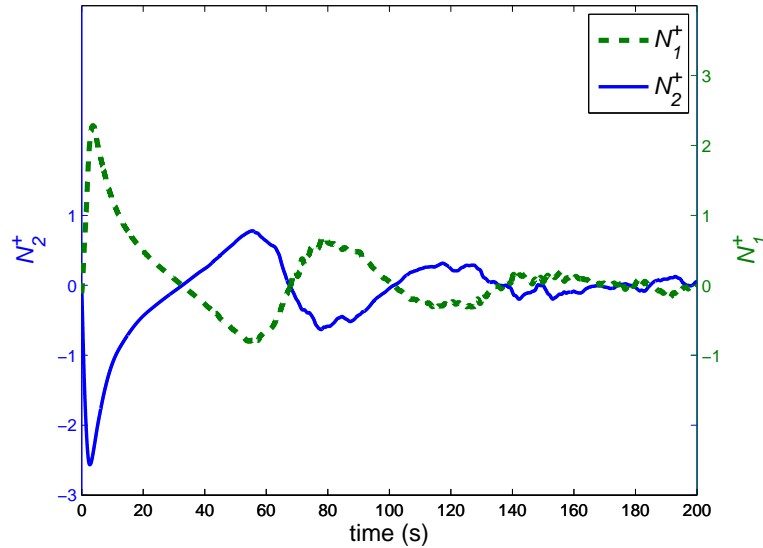
Figure 4.7: Time evolution of the normalized normal stress growth functions

Elastic energy

The statistical evolution of the fiber suspensions with the parameters described in section 4.2 has been analyzed. Figure 4.8 depicts the evolution of the elastic energy. Note that the energy's unit here is the mJ. At the beginning of the simulation, the fibers suddenly change their orientation in the transient state, and peaks of energy are observed.

This indicates, that as expected strong interactions occur in the transient phase, the contribution of the forces to the bending of the fibers become more and more considerable and the elasticity of the suspensions is activated. Then the amplitude of the energy peaks decreases when fibers remain almost aligned in the first direction of the velocity field. In this configuration both the interactions frequency and their intensity decrease, and the elastic energy relaxes. In the almost steady state peaks of energy are again observed. They are due to the sporadic rotation of fibers produced by the interactions and to the finite aspect ratio that prevents a full alignment.
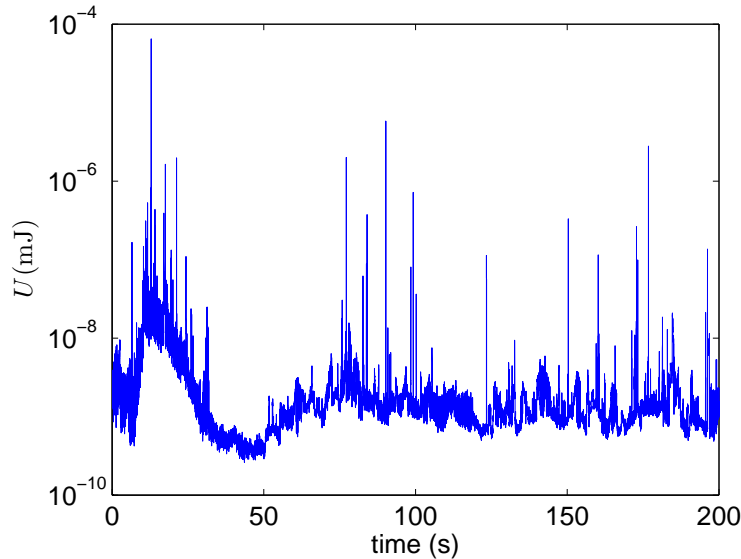

Figure 4.8: Time evolution of the elastic energy

The total number of interactions N_I in the system has been computed (Figure 4.9) and it evolves from $N_I = 0$ at the begining of the simulation ($t = 0$) to an average number of 247 and the maximun being $N_I = 350$. This implies that there are less than one interaction per fiber. In simple beam theory, the fiber would require at least three interactions to bend and to store a significant elastic energy. Figure 4.10 depicts the time evolution of the number of fibers N_f having at least three interactions. However, the hydrodynamic force and torque also apply at the fiber's center of gravity (Figure 2.9). Thus, one interaction per fiber would be enough to activate fiber bending.
Even if the number of interactions per fiber seems low, the system is considered concentrated because the concentration exceeds the inverse of the average aspect ratio (equation 2.3).

4.3   Reversing the flow

Another interesting study is the response of the suspensions viscosity when the flow is reversed, where the number of interactions can help in explaining the results. Reversing
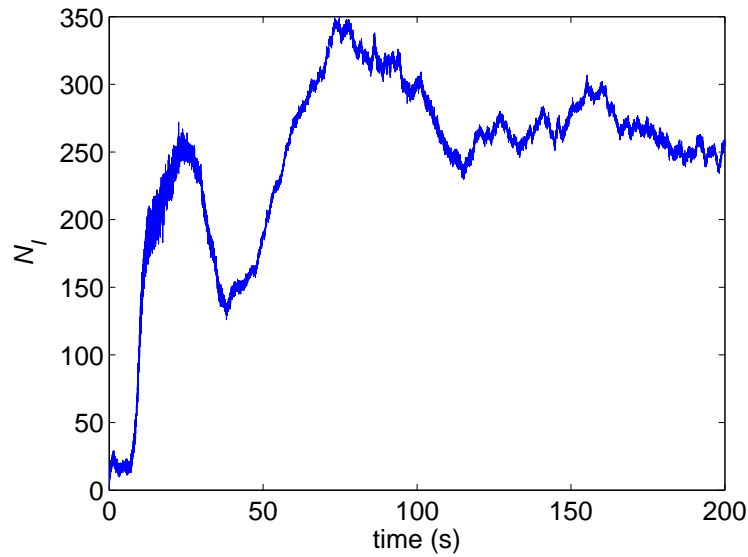
Figure 4.9: Time evolution of the number of interactions
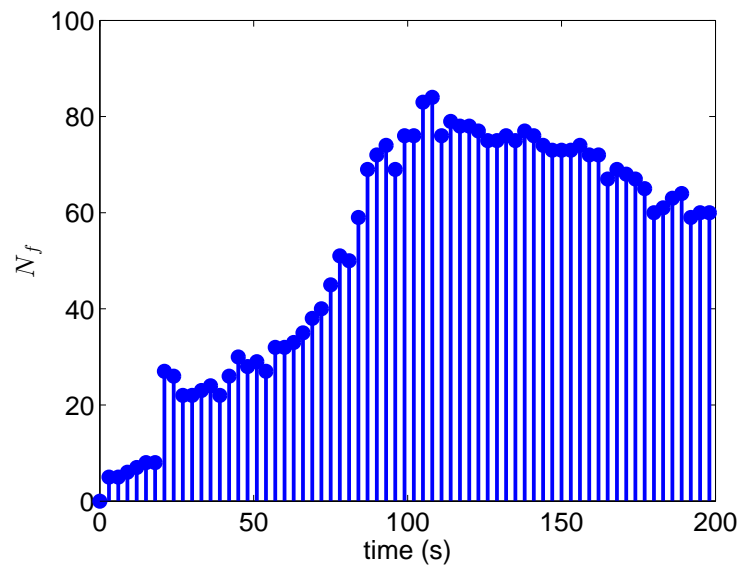
Figure 4.10: Time evolution of the number of fibers having at least three interactions

the flow implies $\dot{\gamma}_r = -\dot{\gamma}_i$ where $\dot{\gamma}_r$ is the shear rate's value for the reversed flow and $\dot{\gamma}_i$ is the value of the shear rate when the flow was initially imposed in the **x** direction. Figure 4.11 shows the response of the system when the microstructure's evolution in the flow stops at $t = 100$ s. Since the interactions are unilateral, the reversibility is broken. Fibers that were in contact during a long period can detach instantaneously when reversing the flow. When the flow is suddenly reversed, while the microstructure is not in an almost steady state, the number of interactions will diminish because fibers will tend to detach (Figure 4.12). Moreover, the loss in the number of interactions results in less entangled

fibers. Thus fibers will tend to rotate, which explains the second peak of viscosity observed after the viscosity increased. The increase in viscosity is due to the fibers tendance to make sporadic rotations and not being close to the first direction of the velocity field characterized by $\dot{\gamma}_r$. In the region between 60 s and 100 s the viscosity is almost the same as for $\dot{\gamma}_i = 1$ s^{-1} because the fibers just began to lose their interactions and do not have enough time to detach considerably.
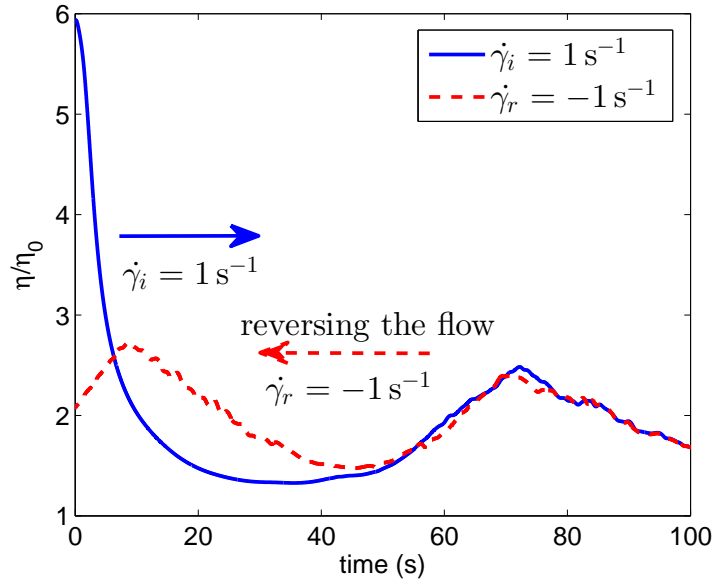

Figure 4.11: Time evolution of the normalized shear stress growth coefficient when the flow is reversed at $t = 100$ s

To compare N_I with the average number of interactions per fiber N_C, the time evolution of nN_C has been plotted (Figure 4.13) (n is again, the total number of fibers). The numbers N_I and nN_C (N_C has been calculated from equation (2.53)) are plotted in logarithmic scale, because nN_C exceeds N_I and it is not possible to notice the same shapes of the curves in a linear representation. There is a shift between the two evolutions because the theory describing N_C considers that the gap Λ allowed between two fibers before entering into contact or lubrication is of the same order of magnitude of d [89]. Since at the beginning fibers are not interacting (i.e. $N_I = 0$), N_I will increase in the first seconds. However for N_C, the theoretical equation gives a maximum value at the beginning of the simulation (i.e. fibers are oriented isotropically in the flow yielding the maximum of interactions) and then N_C will decrease in the first seconds.

Another simulation was carried out, and this time Λ was considered of the same order of magnitude of d ($\Lambda \approx 2d$). The same evolution is again observed but this time the predicted N_I was close to the theoretical number N_C (Figure 4.14).

To report the effect of the fiber dimensions on the statistical evolution of the suspensions, other simulations were carried out. First the mean length of the fibers was changed while maintaining the same diameter ($d = 1$ mm) ; then the diameter of the fibers was
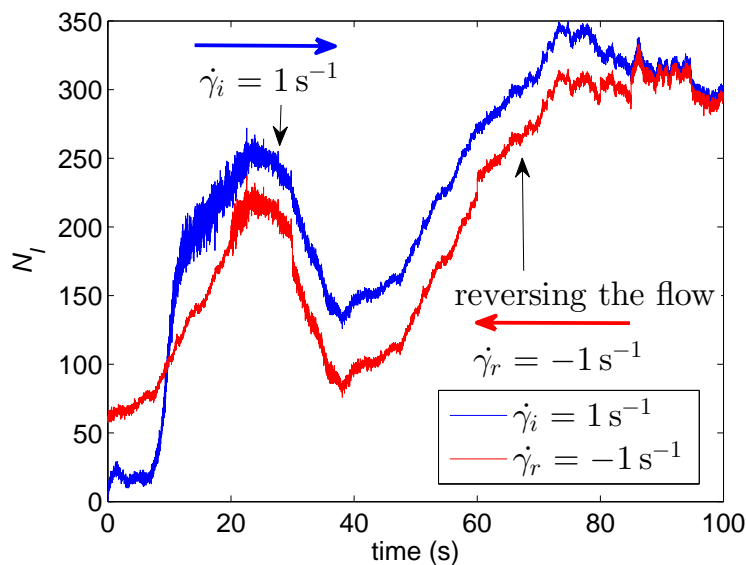
Figure 4.12: Time evolution of the total number of interactions when the flow is reversed at $t = 100$ s

changed while maintaining the same lengths ($\langle L \rangle = 20$ mm). Finally another simulation was carried out by changing the shear rate while maintaining the same other parameters ($\langle L \rangle = 20$ mm and $d = 1$ mm) to conclude on the effect of the shear flow on the magnitude of the interactions involved, i.e. on the elastic energy. Note that in all these simulations, the standard deviation for the distribution lengths was fixed to 3 mm.

Figure 4.13: Time evolution of N_I and nN_C

Figure 4.14: Time evolution of N_I and nN_C with $\Lambda \approx 2d$

4.4   Sensitivity to the dimension and the shear rate effects

4.4.1   Fiber length

Simulations were performed for different mean lengths of fibers. Table 4.1 gives the parameters for the simulations. Figure 4.15 depicts the elastic energy for the three cases.

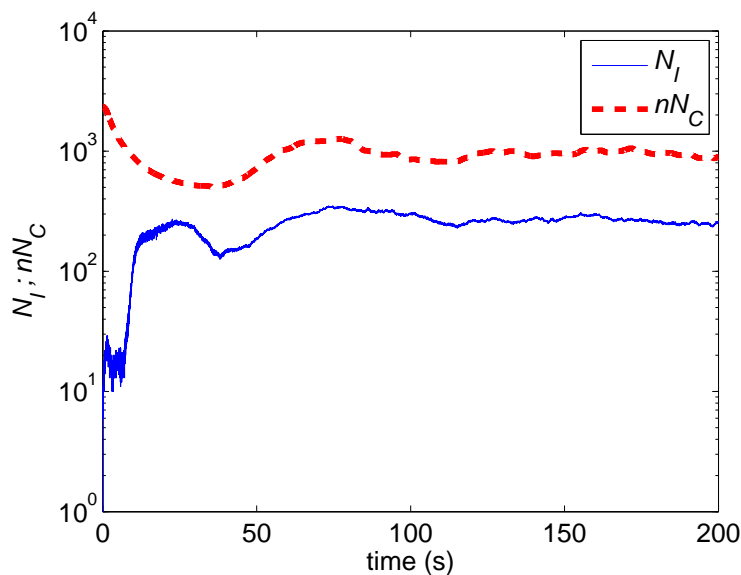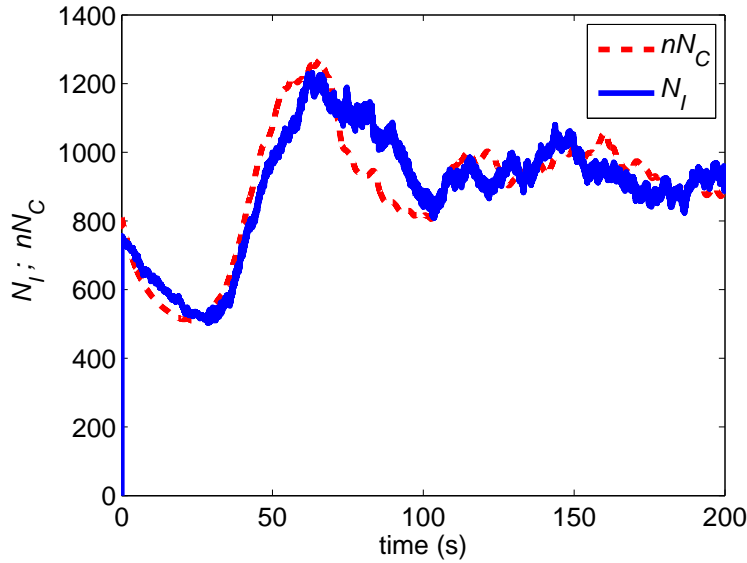| Case	mean length $\langle L \rangle$ (mm)	diameter d (mm)	shear rate $\dot{\gamma}$ (s^{-1})
Case 1	$\langle L_1 \rangle = 10$	1	1
Case 2	$\langle L_2 \rangle = 20$	1	1
Case 3	$\langle L_3 \rangle = 30$	1	1

Table 4.1: Parameters for the simulations

From Table 4.2 it can be noticed that the energy increases when the lengths of the fibers increase. When fibers are longer the bending torques are higher and with them the elastic

Cases	mean length $\langle L \rangle$ (mm)	Average energy $< U >$ (mJ)
Case 1	$\langle L_1 \rangle = 10$	$< U_1 >= 3.57\,10^{-9}$
Case 2	$\langle L_2 \rangle = 20$	$< U_2 >= 6.76\,10^{-9}$
Case 3	$\langle L_3 \rangle = 30$	$< U_3 >= 5.7\,10^{-8}$

Table 4.2: Energy time average

energy. Another noticeable behavior, is the almost absence of peaks of energy in the almost steady state regime for the highest mean length ($\langle L_3 \rangle = 30$ mm). This is due to fibers being the most close to the first direction of the velocity field, with a greater aspect ratio. Hence fibers tend to be more aligned (i.e. $\|\mathbf{p}^{(\alpha)} \times \mathbf{p}^{(\beta)}\| \to 0$). Being the

aspect ratio very high the alignement is more stable. Moreover the sporadic rotation due to fiber-fiber interactions is lower because the higher is the length the more intense are the entanglements that prevent fiber rotations. Even if the number of interactions increases, their intensity (when fibers are almost aligned) decreases. The evolution of N_I has been
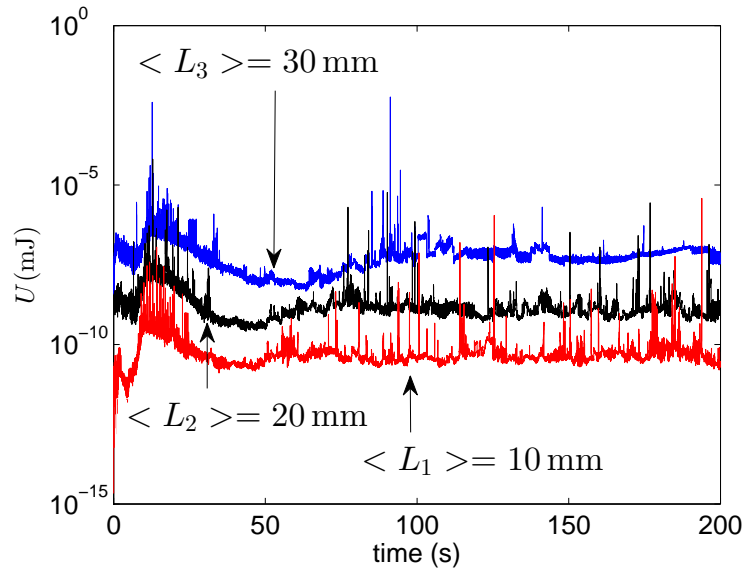

Figure 4.15: Time evolution of the elastic energy for three different lengths (average lengths are given in mm)
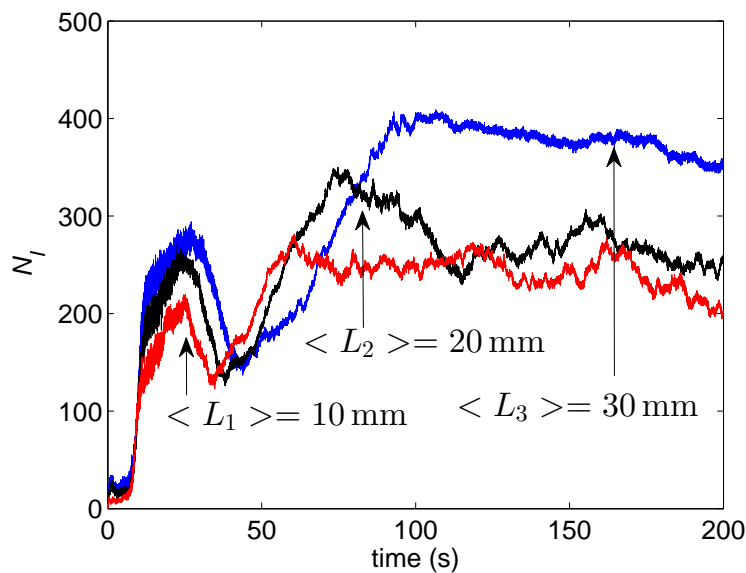

Figure 4.16: Time evolution of the total number of interactions (average lengths are given in mm)

also reported in Figure 4.16. It is clear that in average, the number N_I increases when the

aspect ratio increases.

4.4.2 Fiber diameter

Another set of simulations was carried out, by only varying this time the diameter of the fibers. Table 4.3 gives the parameters that were considered. Figure 4.17 compares

Parameters	mean length $\langle L \rangle$ (mm)	diameter d (mm)	shear rate $\dot{\gamma}$ (s^{-1})
Case 1	$\langle L \rangle = 20$	$d_1 = 1$	1
Case 2	$\langle L \rangle = 20$	$d_2 = 1.5$	1

Table 4.3: Parameters for the simulations

the evolution of the elastic energy for two different fiber diameters. Table 4.4 proves that as expected the elastic energy decreases with the fiber diameter, because the area torques appear in the denominator of the elastic energy expression (equation (2.65)). The number

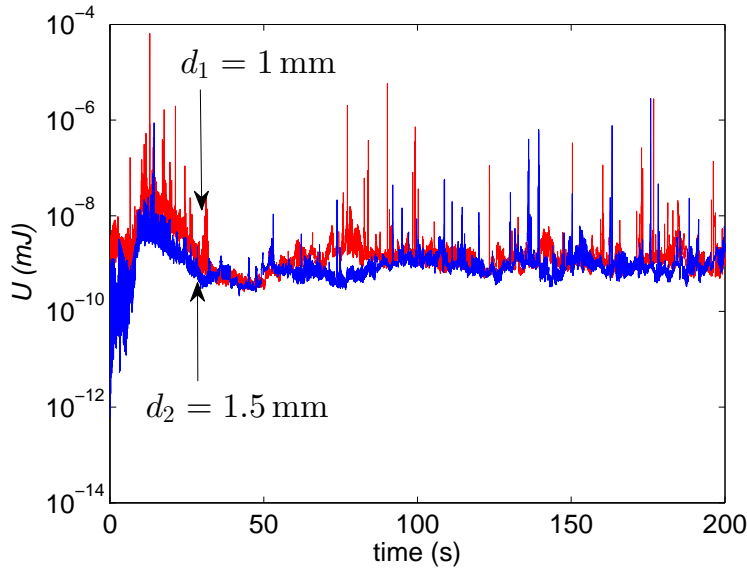| Cases	diameter d (mm)	Average energy $< U >$ (mJ)
Case 1	$d_1 = 1$	$< U_1 >= 6.76 \, 10^{-9}$
Case 2	$d_2 = 1.5$	$< U_2 >= 1.5 \, 10^{-9}$

Table 4.4: Energy time average

Figure 4.17: Time evolution of the elastic energy for different diameters

N_I is in average lower for case 2 because of the lower aspect ratio.

4.4.3 Shear rate effect

To investigate the effect of the shear rate on the elastic energy, simulations were carried out by varying the shear rate. Table 4.5 shows the parameters involved. Figure 4.19
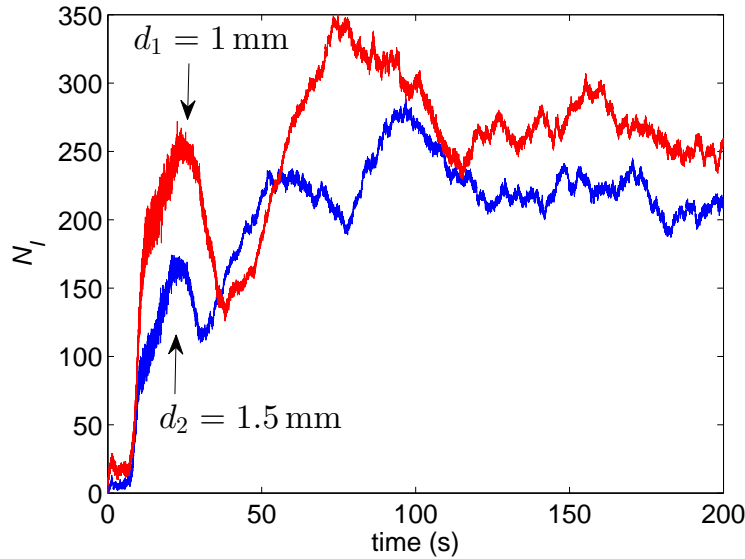
Figure 4.18: Time evolution of the number of interactions

compares the energy for the different cases. Note that the representations are now func-

Cases	mean length $\langle L \rangle$ (mm)	diameter d (mm)	shear rate $\dot{\gamma}$ (s^{-1})
Case 1	20	1	$\dot{\gamma}_1 = 1$
Case 2	20	1	$\dot{\gamma}_2 = 10$
Case 3	20	1	$\dot{\gamma}_3 = 20$

Table 4.5: Parameters for the simulations

tions of the shear rate multiplied by the time (i.e. $\dot{\gamma}t$; Figures 4.19 and 4.21). As expected it can be noticed that the energy increases with the applied shear rate. The interactions intensity increases with the shear rate and consequently fibers will experience much more bending and store more elasticity. Table 4.6 shows the increase of the average energy according to time from 0 to 200 s.

Figure 4.20 depicts the averaged energy versus the applied shear rate where a linear evo-

Cases	shear rate $\dot{\gamma}$ (s^{-1})	Average energy $< U >$ (mJ)
Case 1	$\dot{\gamma}_1 = 1$	$< U_1 >= 6.76\,10^{-9}$
Case 2	$\dot{\gamma}_2 = 10$	$< U_2 >= 1.75\,10^{-6}$
Case 2	$\dot{\gamma}_3 = 20$	$< U_3 >= 3.5\,10^{-6}$

Table 4.6: Energy time average

lution can be noticed. This linear dependence of $< U >$ with $\dot{\gamma}$ gives $< U(\dot{\gamma} = 0) >= 0$: no elastic energy is stored when the flow stops. In fact, stopping the flow in the simulation imposes that $\dot{\gamma} = 0$ in equations (2.5), (2.7) and (2.8) resulting in no interaction forces at all. This means no bending will occur and $U = 0$. Moreover, the scaling of $< U >$
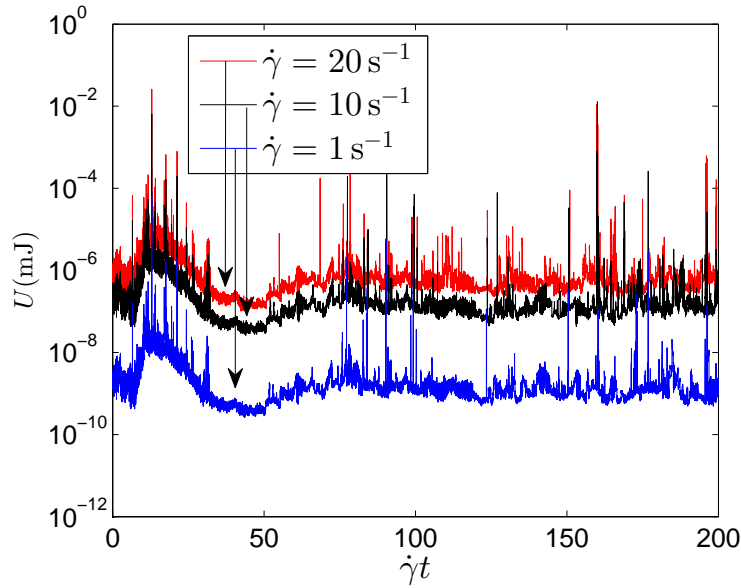
Figure 4.19: Time evolution of the elastic energy for different applied shear rates

as a function of $\dot{\gamma}$ can be related to studies where the difference between the normalized normal stress growth functions $N_1^+ - N_2^+$ increased linearly with $\dot{\gamma}$ for fiber suspensions in Newtonian fluids [101]. These studies also showed that $N_1^+ - N_2^+$ can increase with the flexibility of the fibers (i.e. when the bending torques increase with $\dot{\gamma}$ and the fibers exhibit more bending).

In average, the number of interactions is independent of the shear rate which is in agree-
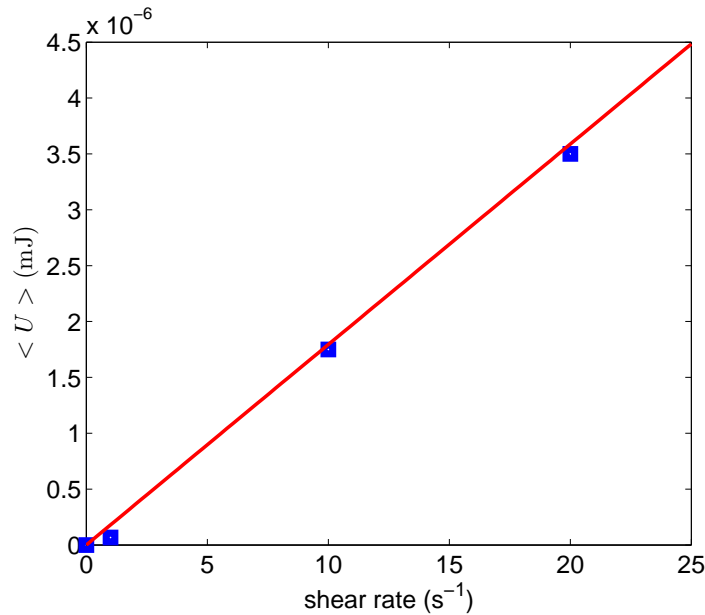
Figure 4.20: Evolution of the average energy with the shear rate
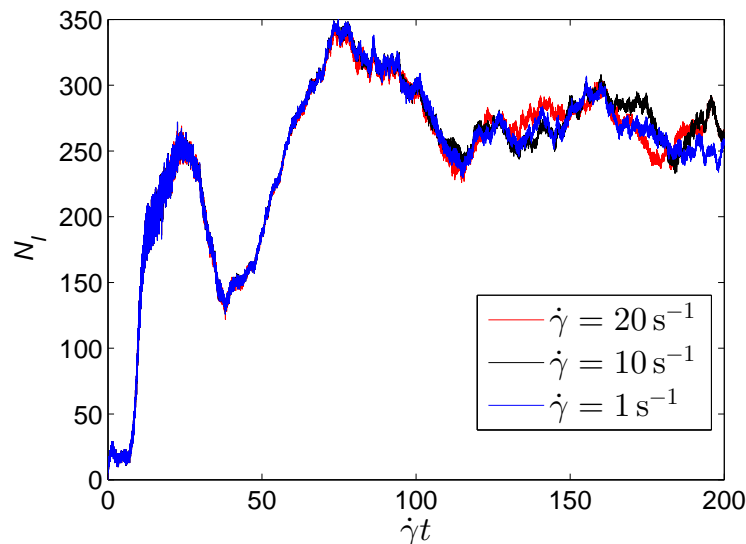
Figure 4.21: Time evolution of the total number of interactions

ment with other studies [41]. Although it may seem that higher shear rates induce more frequent interactions but as fibers become more aligned, the interactions decrease. This is why, here, N_I was found insensible to the applied shear rate as depicted in Figure 4.21. The interactions between fibers depend on the distance between them: in concentrated systems that distance is of the order of a fraction of the fibers diameter.

4.5 Conclusion

A DNS of concentrated fiber suspensions immersed in a Newtonian fluid was conducted. The contribution of this work concerns the treatment of the suspensions elasticity associated with the mechanism of fibers bending. Ingredients came from a micromechanical model describing the kinematic evolution as well as an accurate description of the interactions involved in the systems.

For a given concentration volume with fixed diameter and mean length, the evolution of the kinematics associated with the interactions were studied. From the time evolution of the orientation tensor two regimes were distinguished: a transient phase where the orientation state evolves from an isotropic state to a state where most of the fibers are aligned in the velocity field, that constitutes the almost steady state regime.
For the macroscopic properties, the normal stress growth functions N_1^+ and N_2^+ showed a shoot in the transient phase then a stable value in the steady state in agreement with previous experimental results. The normalized normal stress growth functions, underwent an overshoot and an undershoot respectively in the transient phase due to fibers suddenly changing their orientation in the transient state. The signs of N_1^+ and N_2^+ were discussed and it was found that assuming N_2^+ negligible compared to N_1^+ is inaccurate for the study done here for concentrated suspensions with interactions.
Then the statistical evolutions were reported, including the elastic energy and the number

of interactions. When the flow was reversed, the number of interactions decreased and as a result fibers lost their tendency to be aligned, and that was shown by the evolution of the viscosity in the reverse direction. For the energy it was found that peaks appear at the beginning of the simulation when fibers suddenly changed their orientation and the elasticity of the suspensions is activated. When fibers were close to being parallel to the first direction of the velocity field, the elasticity diminished and the suspensions relaxed with relatively weak interactions.

Comparing the total number of interactions N_I with the theoretical average number of interactions per fiber N_C, it was found that it depends on the gap allowed between two fibers when they are not interacting. The same curve shape was obtained but with a shift between nN_C (where n is the total number of fibers) and N_I. Then by changing this gap, the number of interactions predicted by the simulation was close to the one given by the theory.

The effects of the fiber length, diameter and the shear rate on the elastic energy were also analyzed and interpreted from the number and intensity of the interactions. The higher are the shear rate or the ratio length/diameter, greater is the elastic energy.

The simulations were repeated many times in order to conclude that in average, the evolution of the different computed physical variables are representative in a statistical sense.

4.6   Résumé du chapitre

Des simulations numériques directes de suspensions concentrées de fibres immergées dans un fluide newtonien ont été effectuées. La contribution de ce travail concerne le traitement de l'élasticité des suspensions associée au mécanisme de flexion des fibres. Les ingrédients principaux provenaient d'un modèle micromécanique décrivant l'évolution cinématique avec une description précise des interactions impliquées dans le système. Pour une concentration volumique donnée avec un diamètre fixe une longueur moyenne des fibres, l'évolution de la cinématique associés aux interactions a été étudiée. D'après l'évolution du tenseur d'orientation, deux régimes ont été distingués: une phase transitoire où l'orientation évolue d'un état isotrope à un état où la plupart des fibres sont alignées, ce qui constitue le régime stationnaire.

En ce qui concerne les propriétés macroscopiques, les différences de contraintes normales N_1^+ et N_2^+ présentaient un "overshoot/undershoot" dans la phase transitoire avant de devenir stables à l'état stationnaire. Ce comportement était en accord avec des mesures expérimentales. Les caractères "overshoot" et "undershoot" respectivement pour N_1^+ et N_2^+ sont dues au changement brusque de l'orientation des fibres dans la phase transitoire. Les signes de N_1^+ et N_2^+ ont été discutés et c'était trouvé que N_2^+ ne peut pas être considérée négligeable devant N_1^+ dans le cas de suspensions concentrées avec la présence d'interactions entre les fibres. Ensuite, les évolutions statistiques ont été signalés: l'énergie élastique et le nombre des interactions. Lorsque l'écoulement a été inversé, le nombre d'interactions a diminué et par conséquent les fibres ont perdu leur tendance à être alignées, et cela a été démontré par l'évolution de la viscosité dans le sens inverse. Pour l'énergie élastique, des pics apparaissent au début de la simulation lorsque les fibres ont brusquement changé leur orientation où l'élasticité des suspensions est activée. Lorsque les fibres étaient presque alignées, l'élasticité diminuait et les suspensions subissaient une relaxation avec des interactions relativement faibles.

Il a été constaté que la différence entre N_I (nombre total d'interactions) et N_C (nombre moyen théorique d'interactions par fibre) dépend de la distance critique autorisée entre deux fibres (la distance critique permise entre deux fibres est la distance limite au-dessous de laquelle on considère une interaction entre elles). La même allure de courbe pour N_I que pour N_C a été obtenue mais avec un décalage de nN_C (n étant le nombre total des fibres). Puis en variant cet espacement, le nombre d'interactions prédit par la simulation était proche de celui donné par la théorie.

Les effets du changement des longueurs des fibres, leur diamètre et le taux de cisaillement sur l'évolution de l'énergie élastique ont été également analysés et interprétés.

III

Conclusion

Throughout this part, microscopic based simulations have been described at three stages. In the first stage the micro-mechanical model based on DNS was explained in its theoretical background along with the main assumptions. In this model, concentrated fiber suspensions were considered and the governing equations of motion were thus constructed in the presence of interactions between fibers. After that, the macroscopic properties were defined and in particular the elasticity was introduced. The forces were supposed to cause the bending of the fibers, which exhibited small deformations leading to the storage of an elastic energy.

In the second stage the numerical implementation and the main algorithms were discussed. In this section it was very important to demonstrate how the initial state of the fiber suspensions was created in the REV, because the time evolution of all the different physics depends on it. It was shown how the search for interactions between fibers was carried out and later under which distance criteria was a lubrication or contact considered respectively. Then the process of deriving the interaction forces was written by the means of a simple example that assumed only two interaction points. Thus the system to be solved was written explicitly in order to illustrate how the forces were obtained at each time step. Finally the numerical method used to update the kinematics at each time step was detailed as well as the algorithm summarizing all the process.

In the third and final stage, the main numerical results were shown. A number of $n = 512$ fibers were considered in the REV. The effect of having different lengths of the fibers on the kinematics was evidenced. Then the time evolution of the macroscopic properties was discussed from the point of view of the numerical model and the previous experimental and numerical results found in the literature. Following that, the flow was reversed and this left the conclusion of the non reversibility of the system due to unilateral interactions. Changing the minimum gap allowed between two fibers (i.e. Λ) had an effect on the the time evolution of the number of interactions: N_I became close to the theoretical number nN_C. After that the size and shear rate effects on the time evolution of the number of interactions and the elastic energy was proven. Finally the linear evolution of the elastic energy with the shear rate was indeed true and compatible with other studies.

The perspective of this part is to develop more sophisticated models for a deeper physical study of the interactions. Further studies will focus on generating an initial state consisting of more and more entangled fibers (thousands instead of hundreds) in order to ensure higher interactions where the formation of clusters of fibers rather than a population of fibers is possible. This future study is important from an industrial point of view, where lots of flow based processes (such as compression of Sheet Molding Compounds (SMC)) involve the interactions of thousands of entangled fibers. The effect of increasing the interactions on the evolution of the different physical variables (orientation, macroscopic properties, energy, etc....) will be then investigated.

IV

An introduction to kinetic theory

Short fiber suspensions present different morphologies depending on their concentrations. When the concentration is dilute enough one can describe the microstructure by tracking a population of rods that move with the suspending fluid and orient depending on the velocity gradient according to the Jeffery's equation [22] that relates the orientation evolution with the flow velocity field. In that case the motion and orientation of each fiber is assumed decoupled from the others. The representative population can involve too many fibers, and in that case the computational efforts to track the population is unaffordable. Thus, the simple and well-defined physics must be sacrificed in order to derive coarser descriptions. The main objective remains the modeling and simulation of very concentrated suspensions, where the formation of clusters (i.e. aggregates) of fibers is possible (chapter 1, section 1.3.2). Kinetic theory descriptions are a reasonable compromise between (fine) micro and (fast) macro descriptions.

Kinetic theory approaches [5, 6, 102] describe such systems at the mesoscopic scale. Their main advantage is their capability to address macroscopic systems, while keeping the fine physics through a number of conformational coordinates introduced for describing the microstructure and its time evolution. At this mesoscopic scale, the microstructure is defined from a distribution function that depends on the physical space, the time and a number of conformational coordinates - the rods orientation in the case of slender bodies suspensions. The moments of this distribution constitutes a coarser description in general used in macroscopic modeling [17].

The main issue in kinetic theory approaches lies in the fact that it must define the appropriate conformational coordinates. Then, the most correct approximations have to be used to better determine the time evolution of these conformational coordinates (time evolution governing equations of the moments usually involve closure approximations). After that, one has to consider and derive the interaction mechanisms.

In the following chapters, theoretical models are proposed. First a model detailing the kinematics of a single fiber (dilute suspensions) is explained. Then, the proposed mechanical model for describing the kinematics of rigid and deformable aggregates is discussed. Following that, a general enough multi-scale kinetic theory description is established, taking into account interaction, diffusion and elastic effects.

<div style="text-align: right; font-size: 3em; color: red;">5</div>

Theoretical models

Contents

In this chapter the theoretical used models based on kinetic theory approaches are addressed. These models concern dilute, semi-dilute and concentrated suspensions (for the sake of clarity, the analysis in this chapter is restricted to the 2D case; the important calculations are detailed in Appendix B).
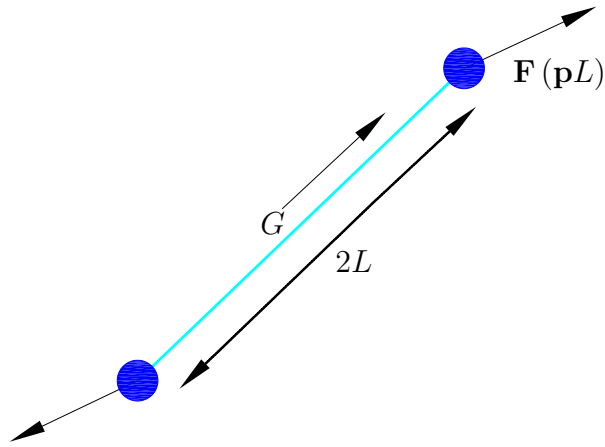
Figure 5.1: Hydrodynamic forces applied on a rod immersed in a Newtonian fluid

5.1   Dilute suspensions of non-Brownian rods

5.1.1   Description of one rod in the suspensions

A suspending medium consisting of a Newtonian fluid of viscosity η is considered, in which there are suspended rigid and non-Brownian rods. It is assumed that that their presence and orientation do not affect the flow kinematics that is defined by the velocity field $\mathbf{v}\left(\mathbf{x}, t\right)$. The conformation of each rod $\mathcal{R}$ of length $2L$ can be described from its orientation given by the unit vector $\mathbf{p}$ located at the rod center of gravity G and aligned along the rod axis. Inertial effects are neglected in the sequel.

The orientation evolution of an ellipsoidal particle is described by Jeffery's equation [22]; this equation can be derived in a very simple way. In Figure 5.1, the fiber is modeled by a rod and two beads located at both rod ends. The hydrodynamic forces (Stokes drag) are presumed to apply at these ends. It is further postulated that forces that apply on each bead $\mathbf{F}$ depend on the difference of velocities between the fluid and the bead, the first one given by $\mathbf{v}_0 + \nabla \mathbf{v} \cdot \mathbf{p}L$ and the second one by $\mathbf{v}_G + \dot{\mathbf{p}}L$. Thus, the force $\mathbf{F}\left(\mathbf{p}L\right)$ reads:

$$\mathbf{F}\left(\mathbf{p}L\right) = \xi\left(\mathbf{v}_0 + \nabla \mathbf{v} \cdot \mathbf{p}L - \mathbf{v}_G - \dot{\mathbf{p}}L\right) \tag{5.1}$$

where ξ is the friction coefficient, $\mathbf{v}_0$ the fluid velocity at the rod center of gravity, and $\mathbf{v}_G$ the velocity of the center of gravity. If $\mathbf{F}$ applies on the bead at $\mathbf{p}L$, then the force on the opposite bead at $-\mathbf{p}L$ reads:

$$\mathbf{F}\left(-\mathbf{p}L\right) = \xi\left(\mathbf{v}_0 - \nabla \mathbf{v} \cdot \mathbf{p}L - \mathbf{v}_G + \dot{\mathbf{p}}L\right) \tag{5.2}$$

By adding equations (5.1) and (5.2), the force balance results in:

$$\mathbf{F}\left(\mathbf{p}L\right) + \mathbf{F}\left(-\mathbf{p}L\right) = 2\xi\left(\mathbf{v}_0 - \mathbf{v}_G\right) = \mathbf{0} \tag{5.3}$$

which implies $\mathbf{v}_0 = \mathbf{v}_G$. This simply means that the rod's center of gravity is moving with the fluid velocity. For the sake of simplicity the forces are rewritten as: $\mathbf{F}\left(\mathbf{p}L\right) = \mathbf{F}$ and $\mathbf{F}\left(-\mathbf{p}L\right) = -\mathbf{F}$.

Since inertia effects are neglected, then the resulting torque must also vanish; there is only one possibility for this: the force have to act along $\mathbf{p}$. Thus it is possible to write:

$$\lambda \mathbf{p} = \xi L \left(\nabla \mathbf{v} \cdot \mathbf{p} - \dot{\mathbf{p}} \right) \tag{5.4}$$

Multiplying equation (5.4) by $\mathbf{p}$ and taking into account that $\mathbf{p} \cdot \mathbf{p} = 1$ and $\mathbf{p} \cdot \dot{\mathbf{p}} = 0$, the following is obtained:

$$\lambda = \xi L \left(\nabla \mathbf{v} : (\mathbf{p} \otimes \mathbf{p}) \right) \tag{5.5}$$

Replacing equation (5.5) in equation (5.1) gives:

$$\xi L \left(\nabla \mathbf{v} : (\mathbf{p} \otimes \mathbf{p}) \right) \mathbf{p} = \xi L \left(\nabla \mathbf{v} \cdot \mathbf{p} - \dot{\mathbf{p}} \right) \tag{5.6}$$

Finally this can be easily rearranged to :

$$\dot{\mathbf{p}} = \nabla \mathbf{v} \cdot \mathbf{p} - \left(\nabla \mathbf{v} : (\mathbf{p} \otimes \mathbf{p}) \right) \mathbf{p} \tag{5.7}$$

which is the Jeffery's equation for fibers with infinite aspect ratios (equation (2.26)).

5.1.2 Description of a population of rods

There are two methods to describe a population of $\mathcal{N}$ rods:
the first one consists in specifying each rod orientation by considering the unit vector aligned along its axis, that is, by considering $\mathbf{p}_i$, $i = 1, ..., \mathcal{N}$. The main drawback of this method lies in the necessity of tracking the evolution of each "computational" rod by solving the corresponding Jeffery equation, and even if conceptually there is no major difficulty, the computing cost could be excessive in most practical applications [4];
the second method uses a probability distribution function (PDF) $\psi(\mathbf{x}, t, \mathbf{p})$ that gives the fraction of rods that at position $\mathbf{x}$ and time t are oriented along direction $\mathbf{p}$. This PDF satisfies the normalization condition:

$$\int_{\mathcal{S}} \psi(\mathbf{x}, t, \mathbf{p}) \, d\mathbf{p} = 1, \quad \forall \mathbf{x}, \ \forall t \tag{5.8}$$

with $\mathcal{S}$ is the surface of the unit sphere, where $\mathbf{p}$ is defined.
Conservation of probability yields

$$\frac{\partial \psi}{\partial t} + \nabla_x \cdot (\dot{\mathbf{x}} \, \psi) + \nabla_p \cdot (\dot{\mathbf{p}} \, \psi) = 0 \tag{5.9}$$

where, $\nabla_x = \dfrac{\partial}{\partial \mathbf{x}}$, $\nabla_p = \dfrac{\partial}{\partial \mathbf{p}}$ and for inertialess rods, $\dot{\mathbf{x}} = \mathbf{v}(\mathbf{x}, t)$, and the rod rotary velocity is given by Jeffery's equation (equation (5.7)). The price to pay is an impressive model dimensionality, as the orientation distribution $\psi(\mathbf{x}, t, \mathbf{p})$ is defined in a 6-dimensional domain.

5.1.3 Macroscopic description

The PDF described in section 5.1.2 can be rarely solved, when models are defined in such a high dimension domain. Thus, mesoscopic models are often coarsened to derive

macroscopic models. At the macroscopic scale, the orientation distribution function is replaced by its moments for describing the microstructure [17]. The macroscopic descriptions usually use the first two main non-zero moments: the second and the fourth-order moments (previously defined in section 2.4.1, equations (2.44) and (2.45)). For the sake of notation simplicity, the second and fourth order moments are now denoted by $\mathbf{a}$ and $\mathbf{A}$ respectively.

5.1.4   Microstructural macroscopic evolution

At the microscopic scale the microstructure's evolution is given by the time evolution of the PDF moments. For $\mathbf{a}$ this evolution is written as:

$$
\begin{aligned}
\dot{\mathbf{a}} &= \int_{\mathcal{S}} (\dot{\mathbf{p}} \otimes \mathbf{p} + \mathbf{p} \otimes \dot{\mathbf{p}}) \, \psi \, d\mathbf{p} \\
&= \int_{\mathcal{S}} (\nabla \mathbf{v} \cdot \mathbf{p} - (\nabla \mathbf{v} : (\mathbf{p} \otimes \mathbf{p})) \, \mathbf{p}) \otimes \mathbf{p} \, \psi d\mathbf{p} \\
&\quad + \int_{\mathcal{S}} \mathbf{p} \otimes (\nabla \mathbf{v} \cdot \mathbf{p} - (\nabla \mathbf{v} : (\mathbf{p} \otimes \mathbf{p})) \, \mathbf{p}) \, \psi d\mathbf{p} \\
&= \nabla \mathbf{v} \cdot \mathbf{a} + \mathbf{a} \cdot (\nabla \mathbf{v})^{T} - 2 \, \mathbf{A} : \nabla \mathbf{v}
\end{aligned}
\tag{5.10}
$$

(Note that ψ is assumed to be only a function of $\mathbf{p}$ here, thus the time derivative of ψ vanishes). This equation involves the fourth-order moment $\mathbf{A}$. The time derivative of $\mathbf{A}$, will involve the sixth order moment, and so on.

This is where closure approximations interfere. $\mathbf{A}$ can be expressed as a function of $\mathbf{a}$, using these approximations. There are different closure relations in the literature [19, 37, 103, 104]. $\mathbf{A}$ can be approximated with the quadratic closure relation (only valid when all rods are locally aligned in the same direction) as follows:

$$
\mathbf{A} \approx \mathbf{a} \otimes \mathbf{a}
\tag{5.11}
$$

This gives :

$$
\dot{\mathbf{a}} \approx \nabla \mathbf{v} \cdot \mathbf{a} + \mathbf{a} \cdot (\nabla \mathbf{v})^{T} - 2 \, (\nabla \mathbf{v} : \mathbf{a}) \, \mathbf{a}
\tag{5.12}
$$

and invoking again symmetry considerations,

$$
\dot{\mathbf{a}} \approx \nabla \mathbf{v} \cdot \mathbf{a} + \mathbf{a} \cdot (\nabla \mathbf{v})^{T} - 2 \, (\mathbf{D} : \mathbf{a}) \, \mathbf{a}
\tag{5.13}
$$

5.2   Dilute suspensions of Brownian rods

In the previous sections, dilute suspensions of rods were considered free from Brownian effects and hydrodynamic interactions. The Brownian effects are the result of the fluid's molecular bombardment acting on the beads. These effects were widely analyzed in [11, 104, 105] when focusing on a microscopic description.

5.2.1   Microscopic description

Beads are now subjected to hydrodynamic forces given by:

$$
\mathbf{F}^{H} = \xi \, (\nabla \mathbf{v} \cdot \mathbf{p} L - \dot{\mathbf{p}} L)
\tag{5.14}
$$

where the superscript "H" refers to the hydrodynamic nature.

The Brownian forces are assumed to be acting in the rod direction and perpendicular to the rod axis. The components applying in the rod direction are presumed equilibrated. The ones being perpendicular to the rod axis contribute to the rotation of the rod, and they affect the rod rotary velocity. Again, the rod inertia is neglected thus the resultant torque must vanish leading to:

$$\mathbf{F}^H \cdot \mathbf{t} + \mathbf{F}^B \cdot \mathbf{t} = 0 \tag{5.15}$$

where $\mathbf{F}^B$ denotes the Brownian force and $\mathbf{t}$ is the unit vector tangent to the unit circle. Introducing the expression of $\mathbf{F}^H$ in (5.15) the following is obtained:

$$\mathbf{t}^T \cdot \nabla \mathbf{v} \cdot \mathbf{p} - \|\dot{\mathbf{p}}\| = -\frac{\mathbf{F}^B \cdot \mathbf{t}}{\xi L} \tag{5.16}$$

where $\dot{\mathbf{p}} = \|\dot{\mathbf{p}}\|\mathbf{t}$ was used. Equation (5.16) can be rewritten as:

$$\dot{\mathbf{p}} = \left(\mathbf{t}^T \cdot \nabla \mathbf{v} \cdot \mathbf{p}\right)\mathbf{t} + \frac{\mathbf{F}^B \cdot \mathbf{t}}{\xi L}\mathbf{t} \tag{5.17}$$

The vectorial equivalence $\left(\mathbf{t}^T \cdot \nabla \mathbf{v} \cdot \mathbf{p}\right)\mathbf{t} = \nabla \mathbf{v} \cdot \mathbf{p} - \left(\mathbf{p}^T \cdot \nabla \mathbf{v} \cdot \mathbf{p}\right)\mathbf{p}$ and equation (5.7) allow writing:

$$\begin{aligned}
\dot{\mathbf{p}} &= \nabla \mathbf{v} \cdot \mathbf{p} - \left(\mathbf{p}^T \cdot \nabla \mathbf{v} \cdot \mathbf{p}\right)\mathbf{p} + \frac{\mathbf{F}^B \cdot \mathbf{t}}{\xi L}\mathbf{t} \\
&= \nabla \mathbf{v} \cdot \mathbf{p} - \left(\mathbf{p}^T \cdot \nabla \mathbf{v} \cdot \mathbf{p}\right)\mathbf{p} + \frac{\mathbf{F}^B - \left(\mathbf{F}^B \cdot \mathbf{p}\right)\mathbf{p}}{\xi L}
\end{aligned} \tag{5.18}$$

where the contribution of the Brownian effects to the time evolution of the rotary velocity is :

$$\dot{\mathbf{p}}^B = \frac{\mathbf{F}^B - \left(\mathbf{F}^B \cdot \mathbf{p}\right)\mathbf{p}}{\xi L} \tag{5.19}$$

5.2.2 Mesoscopic description

At the mesoscopic scale, Brownian effects try to randomize the rod orientation distribution. This mechanism can be modeled by assuming a diffusion term in the Fokker-Planck equation:

$$\frac{\partial \psi}{\partial t} + \nabla_x \cdot (\mathbf{v}\psi) + \nabla_p \cdot (\dot{\mathbf{p}}\psi) = \nabla_p \cdot (D_r \nabla_p \psi) \tag{5.20}$$

where $\dot{\mathbf{p}}$ is given by equation (5.7), and D_r is the rotary diffusion.

To introduce the Brownian contribution $\dot{\mathbf{p}}^B$ in equation (5.20), the Fokker-Planck equation can be rewritten in the form:

$$\begin{aligned}
&\frac{\partial \psi}{\partial t} + \nabla_x \cdot (\mathbf{v}\psi) + \nabla_p \cdot (\dot{\mathbf{p}}\psi) - \nabla_p \cdot (D_r \nabla_p \psi) \\
&= \frac{\partial \psi}{\partial t} + \nabla_x \cdot (\mathbf{v}\psi) + \nabla_p \cdot (\check{\dot{\mathbf{p}}}\psi)
\end{aligned} \tag{5.21}$$

where the effective rotary velocity is given by:

$$\dot{\mathbf{p}} = \nabla\mathbf{v} \cdot \mathbf{p} - \left(\mathbf{p}^T \cdot \nabla\mathbf{v} \cdot \mathbf{p}\right)\mathbf{p} - D_r\frac{\nabla_p\psi}{\psi} \tag{5.22}$$

which now contains the flow-induced Jeffery contribution and the Brownian one, with:

$$\dot{\mathbf{p}}^B = -D_r\frac{\nabla_p\psi}{\psi} \tag{5.23}$$

5.2.3   Macroscopic description

At the microscopic scale, the problem is simplified by considering the moments of the orientation distribution function. In what follows, the Brownian contribution to the time evolution of the second-order moment is derived in a very simple approach. The process starts by considering equation (2.44), whose time derivative involves now the effective rotational velocity $\dot{\mathbf{p}}$:

$$\dot{\mathbf{a}} = \int_{\mathcal{S}} \left(\dot{\mathbf{p}} \otimes \mathbf{p} + \mathbf{p} \otimes \dot{\mathbf{p}}\right)\psi\,d\mathbf{p} \tag{5.24}$$

which is easily developed to:

$$
\begin{aligned}
\dot{\mathbf{a}} &= \int_{\mathcal{S}} \left(\nabla\mathbf{v} \cdot \mathbf{p} - (\nabla\mathbf{v} : (\mathbf{p} \otimes \mathbf{p}))\,\mathbf{p} + \dot{\mathbf{p}}^B\right) \otimes \mathbf{p}\,\psi\,d\mathbf{p} \\
&+ \int_{\mathcal{S}} \mathbf{p} \otimes \left(\nabla\mathbf{v} \cdot \mathbf{p} - (\nabla\mathbf{v} : (\mathbf{p} \otimes \mathbf{p}))\,\mathbf{p} + \dot{\mathbf{p}}^B\right)\psi\,d\mathbf{p} \\
&= \int_{\mathcal{S}} \left(\nabla\mathbf{v} \cdot \mathbf{p} - (\nabla\mathbf{v} : (\mathbf{p} \otimes \mathbf{p}))\,\mathbf{p}\right) \otimes \mathbf{p}\,\psi\,d\mathbf{p} \\
&+ \int_{\mathcal{S}} \mathbf{p} \otimes \left(\nabla\mathbf{v} \cdot \mathbf{p} - (\nabla\mathbf{v} : (\mathbf{p} \otimes \mathbf{p}))\,\mathbf{p}\right)\psi\,d\mathbf{p} \\
&+ \int_{\mathcal{S}} \left(\dot{\mathbf{p}}^B \otimes \mathbf{p} + \mathbf{p} \otimes \dot{\mathbf{p}}^B\right)\psi\,d\mathbf{p} \\
&= \dot{\mathbf{a}}^J + \dot{\mathbf{a}}^B
\end{aligned} \tag{5.25}
$$

where $\dot{\mathbf{a}}^J$ is the flow-induced microstructure evolution given by equation (5.10) and $\dot{\mathbf{a}}^B$ is the Brownian contribution:

$$\dot{\mathbf{a}}^B = \int_{\mathcal{S}} \left(\dot{\mathbf{p}}^B \otimes \mathbf{p} + \mathbf{p} \otimes \dot{\mathbf{p}}^B\right)\psi\,d\mathbf{p} \tag{5.26}$$

Equation (5.23) can be rewritten as:

$$\dot{\mathbf{p}}^B = -D_r\frac{\nabla_\theta\psi}{\psi} = -D_r\frac{\frac{\partial\psi}{\partial\theta}}{\psi} \tag{5.27}$$

where $\mathbf{p}$ has been substituted by the angle θ (this angle gives the orientation of the rod), since $\mathbf{p}$ can be written as:

$$\mathbf{p} = cos\,(\theta)\,\mathbf{x} + sin\,(\theta)\,\mathbf{y} \tag{5.28}$$

($\mathbf{x}$ and $\mathbf{y}$ are the unit vectors along the two dimensions). Then using the development: $\frac{\partial \psi}{\partial \theta} = \frac{\partial \psi}{\partial \mathbf{p}} \frac{\partial \mathbf{p}}{\partial \theta} = \frac{\partial \psi}{\partial \mathbf{p}} \mathbf{t}$ and taking into account:

$$\begin{aligned} \frac{\partial \mathbf{p}}{\partial \theta} &= \mathbf{t} \\ \frac{\partial \mathbf{t}}{\partial \theta} &= -\mathbf{p} \end{aligned} \qquad (5.29)$$

$\dot{\mathbf{p}}^B$ becomes:

$$\dot{\mathbf{p}}^B = -D_r \frac{\frac{\partial \psi}{\partial \theta}}{\psi} \mathbf{t} \qquad (5.30)$$

where $\mathbf{p}$ was again replaced by θ (a change of variable took place). Therefore equation (5.26) reduces to:

$$\dot{\mathbf{a}}^B = -D_r \int_{\mathcal{S}} (\mathbf{t} \otimes \mathbf{p} + \mathbf{p} \otimes \mathbf{t}) \frac{\partial \psi}{\partial \theta} d\theta \qquad (5.31)$$

Performing a simple part integration on equation (5.31) yields:

$$\dot{\mathbf{a}}^B = -2D_r \int_{\mathcal{S}} (\mathbf{p} \otimes \mathbf{p} - \mathbf{t} \otimes \mathbf{t}) \psi(\theta) d\theta \qquad (5.32)$$

where the following easy proved relationship was used:

$$\begin{aligned} \mathbf{p} \otimes \mathbf{p} + \mathbf{t} \otimes \mathbf{t} &= \mathbf{I} \\ \mathbf{t} \otimes \mathbf{t} &= \mathbf{I} - \mathbf{p} \otimes \mathbf{p} \end{aligned} \qquad (5.33)$$

Equation (5.33) allows one to put equation (5.32) is the form:

$$\begin{aligned} \dot{\mathbf{a}}^B &= -2D_r \int_{\mathcal{S}} (2\mathbf{p} \otimes \mathbf{p} - \mathbf{I}) \psi(\theta) d\theta = -2D_r (2\mathbf{a} - \mathbf{I}) \\ &= -4D_r \left(\mathbf{a} - \frac{\mathbf{I}}{2} \right) \end{aligned} \qquad (5.34)$$

In the absence of flow, $\dot{\mathbf{a}}^J = 0$; in this case this leads to an isotropic steady state, i.e. $\mathbf{a}(t \to \infty) = \frac{\mathbf{I}}{2}$.

Finally the generalized macroscopic governing orientation evolution equation is:

$$\dot{\mathbf{a}} = \nabla \mathbf{v} \cdot \mathbf{a} + \mathbf{a} \cdot (\nabla \mathbf{v})^T - 2 (\mathbf{A} : \mathbf{D}) - 2 d_m D_r \left(\mathbf{a} - \frac{\mathbf{I}}{d_m} \right) \qquad (5.35)$$

where d_m represents the space dimension ($d_m = 2$ in the 2D case and 3 in the 3D case)

5.3   Semi-dilute suspensions

There are many approaches used to model semi-dilute (or semi-concentrated) suspensions. The most used one considers that rod-rod interactions tend to randomize the orientation distribution. An additional diffusion coefficient is introduced for accounting

for these interactions. In the absence of flow, the microstructure must not evolve artificially. This is why the added diffusion coefficient must scale with the flow intensity (i.e. with the shear rate intensity $\dot{\gamma}$). The interaction-diffusion coefficient D_I is assumed to be of the form:

$$D_I = C_I \cdot f\left(D^{eq}\right), \tag{5.36}$$

where D^{eq} is related to the second invariant of the rate of strain tensor, i.e. $D^{eq} = \sqrt{2\mathbf{D} : \mathbf{D}}$. The simplest choice consists in considering the dependence $f(D^{eq}) = D^{eq}$ [49]. Thus, the so-called Folgar-Tucker model reads

$$\dot{\mathbf{a}} = \nabla\mathbf{v} \cdot \mathbf{a} + \mathbf{a} \cdot (\nabla\mathbf{v})^T - 2\,(\mathbf{A} : \mathbf{D}) - 2d_m D_I \left(\mathbf{a} - \frac{\mathbf{I}}{d_m}\right), \tag{5.37}$$

with D_I given by Eq. (5.36).

It is clear that the previous approaches based on direct simulations (in chapters 2, 3, and 4) are finer and more precise when considering rod-rod interactions explicitly [67, 76, 70]. In the works given by [62], interactions were explicitly described at the macroscopic scale by means of so-called interaction tensors that can be obtained from the moments of the orientation distribution function [88].

5.4 Concentrated suspensions

The emphasis will now be turned to the most interesting case from an industrial point of view: concentrated suspensions. When the concentration is high enough, the configuration of rods is much more complex. Clusters/aggregates of rods (i.e. fibers) are formed when having many entangled rods immersed in a flow. These aggregates exhibit an almost rigid motion when a shear flow is applied. An example commonly encountered in the industry are carbon nanotube suspensions. These cases were sufficiently examined in [55, 66, 106]. Two types of clusters are defined and studied in the following proposed models: rigid and deformable clusters. Note that, the suspending fluid is considered to be always Newtonian and a simple shear flow is applied. Another remark is that, concentrated suspensions are considered to form a cluster when fibers get entangled. However dilute cluster suspensions are considered (i.e. in the following descriptions the governing equations are valid for each cluster in the suspensions, but only one cluster is studied).

5.4.1 Micro-mechanical description of the kinematics of rigid clusters

Each rod composing a cluster, is assumed to have the same shape as that of one single rod (rod with two beads as described before in 5.1.1).

The representation of a cluster is depicted in Figure 5.2, again in the 2D case. This configuration does not involve size effects, but it incorporates the orientation distribution; it constitutes the most simple version of the model, which could be later enriched with more complex assumptions. This cluster is considered to be composed of N rods of length $2L$ oriented in the directions $\mathbf{p}_i$, $i = 1, ..., N$, as shown in Figure 5.3 (index i denotes the number of each rod). When Brownian effects are neglected, then only flow induced hydrodynamic forces are considered (the rod-rod hydrodynamic interactions are
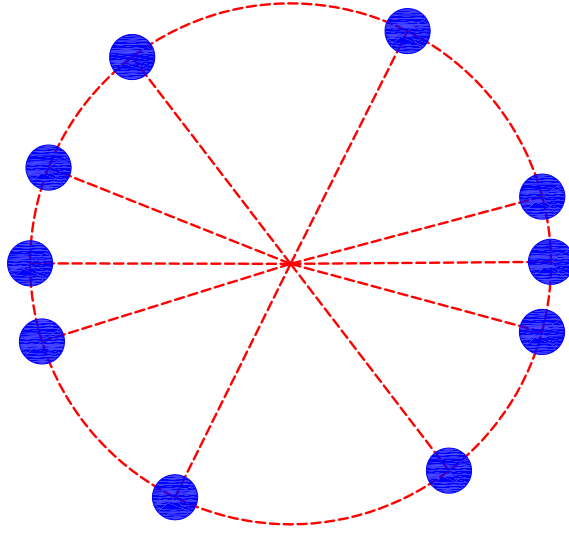
Figure 5.2: Star representation of a cluster composed of rigid rods

not considered in this work). For each bead, a force $\mathbf{F}_i$ apply at position $L\mathbf{p}_i$ (Figure 5.3). And the same analysis is made for the expression of the force as in section 5.1.1. Thus is it written as:

$$\mathbf{F}_i = \xi \ (\nabla \mathbf{v} \cdot \mathbf{p}_i L - \dot{\mathbf{p}}_i L) \tag{5.38}$$

where now the flow velocity $\mathbf{v}$ is unperturbed by the presence of the cluster. From the construction of Figure 5.3 it is clear that the forces are self-equilibrated. The moment induced by forces applying on rod i is given by

$$\mathbf{M}_i = 2 \ L \ \mathbf{p}_i \times \mathbf{F}_i \tag{5.39}$$

Since inertia effects are neglected, then the resulting moment for the cluster must vanish:

$$\sum_{i=1}^{i=N} \mathbf{M}_i = \mathbf{0} \tag{5.40}$$

then taking into account equations (5.38) and (5.39) results in:

$$\sum_{i=1}^{i=N} \mathbf{p}_i \times (\nabla \mathbf{v} \cdot \mathbf{p}_i) = \sum_{i=1}^{i=N} \mathbf{p}_i \times \dot{\mathbf{p}}_i \tag{5.41}$$

The cluster angular velocity $\boldsymbol{\omega}$ can be defined such that:

$$\dot{\mathbf{p}}_i = \boldsymbol{\omega} \times \mathbf{p}_i \tag{5.42}$$

where $\boldsymbol{\omega}$ and $\mathbf{p}_i$ are orthogonal in the 2D case, thus: $\mathbf{p}_i \times \dot{\mathbf{p}}_i = \boldsymbol{\omega}, \ \forall i$, and then it results:

$$\sum_{i=1}^{i=N} \mathbf{p}_i \times (\nabla \mathbf{v} \cdot \mathbf{p}_i) = \sum_{i=1}^{i=N} \mathbf{p}_i \times \dot{\mathbf{p}}_i = N \ \boldsymbol{\omega} \tag{5.43}$$
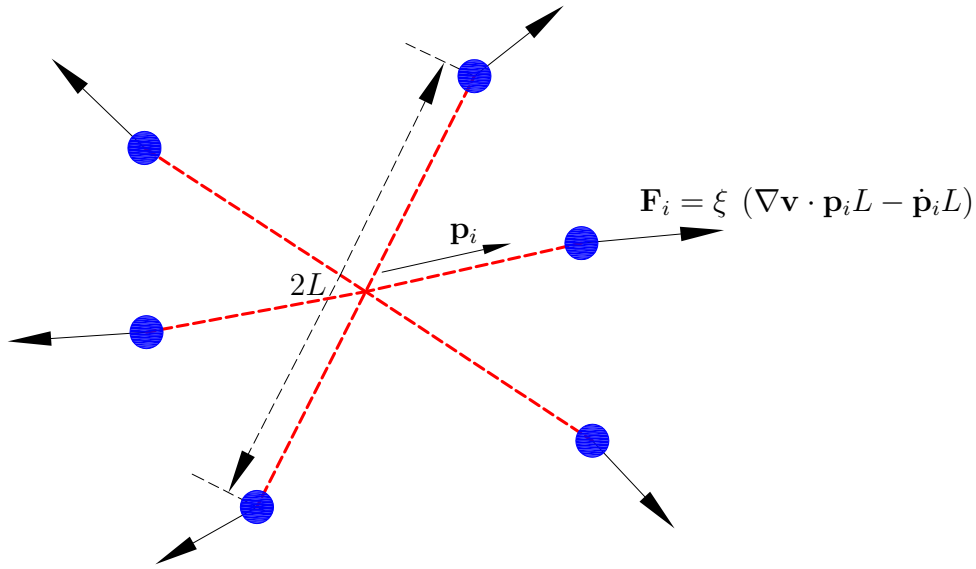
Figure 5.3: Hydrodynamic forces applying on a rigid cluster composed of rods

Hence, the kinematics of the rigid cluster can be defined from:

$$\boldsymbol{\omega} = \frac{\sum\limits_{i=1}^{i=N} \mathbf{p}_i \times (\nabla \mathbf{v} \cdot \mathbf{p}_i)}{N} \tag{5.44}$$

where for each rod j the evolution of the orientation is given by:

$$\dot{\mathbf{p}}_j = \boldsymbol{\omega} \times \mathbf{p}_j = \frac{\left(\sum\limits_{i=1}^{i=N} \mathbf{p}_i \times (\nabla \mathbf{v} \cdot \mathbf{p}_i)\right) \times \mathbf{p}_j}{N} \tag{5.45}$$

When there are many rods composing the cluster, the orientation distribution $\psi(\mathbf{p})$ is defined. Then all the sums in the previous expressions are substituted by the corresponding integrals weighted with ψ. Then equation (5.44) becomes:

$$\boldsymbol{\omega} = \int_{\mathcal{S}} (\mathbf{p} \times (\nabla \mathbf{v} \cdot \mathbf{p})) \ \psi(\mathbf{p}) \, d\mathbf{p} \tag{5.46}$$

Then $\dot{\mathbf{p}}$ for any rod reads:

$$\dot{\mathbf{p}} = \boldsymbol{\omega} \times \mathbf{p} = \int_{\mathcal{S}} ((\mathbf{p} \times (\nabla \mathbf{v} \cdot \mathbf{p})) \times \mathbf{p}) \ \psi(\mathbf{p}) \, d\mathbf{p} \tag{5.47}$$

Cross products can be written in a more compact form by using the third order Levi-Civita permutation tensor $\boldsymbol{\varepsilon}$ (see Appendix A).This allows equation (5.46) to be written as:

$$\boldsymbol{\omega} = \boldsymbol{\varepsilon} : (\nabla \mathbf{v} \cdot \mathbf{a}) \tag{5.48}$$

Note that, for the sake of notation simplicity the time dependence of the distribution function ψ is not shown explicitly.

The rotation tensor $\mathbf{W}$ is defined such that:

$$\boldsymbol{\omega} \times \mathbf{p} = \mathbf{W} \cdot \mathbf{p} \tag{5.49}$$

that allows writing:

$$\dot{\mathbf{p}} = \mathbf{W} \cdot \mathbf{p} \tag{5.50}$$

It is easy to prove from equations (5.48)-(5.50) [107] that:

$$\mathbf{W} = \mathbf{\Omega} + \mathbf{D} \cdot \mathbf{a} - \mathbf{a} \cdot \mathbf{D} \tag{5.51}$$

where $\mathbf{D}$ and $\mathbf{\Omega}$ are respectively the symmetric and skew-symmetric components of the velocity gradient $\nabla \mathbf{v}$.

Thus, a rigid cluster rotates with a velocity that only depends on the second moment of its orientation distribution, $\mathbf{a}$. Any rigid cluster having the same orientation tensor $\mathbf{a}$ will have the same angular velocity. Finally an expression giving the time evolution of $\mathbf{a}$, $\dot{\mathbf{a}}$ can be derived. The derivative of $\mathbf{a}$ is:

$$\dot{\mathbf{a}} = \int_{\mathcal{S}} (\dot{\mathbf{p}} \otimes \mathbf{p} + \mathbf{p} \otimes \dot{\mathbf{p}}) \ \psi(\mathbf{p}) \, d\mathbf{p} \tag{5.52}$$

(Note that ψ is assumed to be only a function of $\mathbf{p}$ here, thus the time derivative of ψ vanishes). Now, taking into account equation (5.50) it results:

$$\dot{\mathbf{a}} = \int_{\mathcal{S}} ((\mathbf{W} \cdot \mathbf{p}) \otimes \mathbf{p} + \mathbf{p} \otimes (\mathbf{W} \cdot \mathbf{p})) \ \psi(\mathbf{p}) \, d\mathbf{p} = \mathbf{W} \cdot \mathbf{a} + \mathbf{a} \cdot \mathbf{W}^T \tag{5.53}$$

It is easy to prove the objectivity of expression (5.53) that corresponds to the Jauman's convective derivative as well as its null trace, i.e. $\text{trace}(\dot{\mathbf{a}}) = 0$ [107].

5.4.2 Micro-mechanical description of the kinematics of deformable clusters

In this section the most complex and realistic case is considered: deformable clusters. This time two types of forces are applying on each bead, one due to the fluid-rod friction once more modeled from equation (5.38), and the other $\mathbf{F}_i^C$ due to the rods entanglements. This last force is assumed scaling with the difference between the rigid motion velocity (the one that the bead would have if the cluster would be rigid) and the real one:

$$\mathbf{F}_i^C = \mu \left(\mathbf{W} \cdot \mathbf{p}_i \, L - \dot{\mathbf{p}}_i \, L \right) \tag{5.54}$$

When μ is large enough forces $\mathbf{F}_i^C$ dominate the momentum balances enforcing the cluster rotary velocity $\mathbf{W}$ to each rod composing it (rigid behavior). By adding both forces it results:

$$\mathbf{F}_i = \mathbf{F}_i^H + \mathbf{F}_i^C = L \left((\mu \, \mathbf{W} + \xi \, \nabla \mathbf{v}) \cdot \mathbf{p}_i - (\xi + \mu) \, \dot{\mathbf{p}}_i \right) \tag{5.55}$$

that can be rewritten as:

$$\mathbf{F}_i = L \, (\xi + \mu) \, \left(\frac{\mu \, \mathbf{W} + \xi \, \nabla \mathbf{v}}{\xi + \mu} \cdot \mathbf{p}_i - \dot{\mathbf{p}}_i \right) \tag{5.56}$$

where $\xi + \mu$ is the equivalent friction coefficient. Similarly, the equivalent traceless gradient $\mathbf{G}$ is defined as:

$$\mathbf{G} = \frac{\mu \, \mathbf{W} + \xi \, \nabla \mathbf{v}}{\xi + \mu} \tag{5.57}$$

Then $\dot{\mathbf{p}}_i$ is just:

$$\dot{\mathbf{p}}_i = \mathbf{G} \cdot \mathbf{p}_i - (\mathbf{G} : (\mathbf{p}_i \otimes \mathbf{p}_i)) \ \mathbf{p}_i \tag{5.58}$$

Since both $\mathbf{W}$ and $\mathbf{\Omega}$ are skew-symmetric it results: $\mathbf{W} : (\mathbf{p}_i \otimes \mathbf{p}_i) = 0$ and the same in the case of considering $\mathbf{\Omega}$, implying $\mathbf{G} : (\mathbf{p}_i \otimes \mathbf{p}_i) = \dfrac{\xi}{\xi + \mu} \ \mathbf{D} : (\mathbf{p}_i \otimes \mathbf{p}_i)$ and then:

$$\dot{\mathbf{p}}_i = \mathbf{G} \cdot \mathbf{p}_i - \frac{\xi}{\xi + \mu} \ (\mathbf{D} : (\mathbf{p}_i \otimes \mathbf{p}_i)) \ \mathbf{p}_i \tag{5.59}$$

that can be rewritten as:

$$\begin{aligned}
\dot{\mathbf{p}}_i &= \frac{\mu}{\xi + \mu} \ \mathbf{W} \cdot \mathbf{p}_i + \frac{\xi}{\xi + \mu} \ \nabla \mathbf{v} \cdot \mathbf{p}_i - \frac{\xi}{\xi + \mu} \ (\mathbf{D} : (\mathbf{p}_i \otimes \mathbf{p}_i)) \ \mathbf{p}_i \\
&= \frac{\xi}{\xi + \mu} \ \dot{\mathbf{p}}_i^J + \frac{\mu}{\xi + \mu} \ \mathbf{W} \cdot \mathbf{p}_i \\
&= \frac{\xi}{\xi + \mu} \ \dot{\mathbf{p}}_i^J + \frac{\mu}{\xi + \mu} \ \dot{\mathbf{p}}_i^R
\end{aligned} \tag{5.60}$$

where $\dot{\mathbf{p}}_i^J$ represents the hydrodynamic contribution in absence of rod-rod interactions (dilute regime described by the Jeffery's equation) and $\dot{\mathbf{p}}_i^R$ the one coming from the rods entanglements that results in a rigid-like cluster kinematics.

The two limit cases are when: $\xi \gg \mu$ and here hydrodynamic effects are preponderant/the rod kinematics is governed by the Jeffery's equation, i.e. $\dot{\mathbf{p}}_i \approx \dot{\mathbf{p}}_i^J$; $\mu \gg \xi$ and here the cluster is too rigid and the rods adopt the velocity dictated by the rigid cluster kinematics $\dot{\mathbf{p}}_i \approx \dot{\mathbf{p}}_i^R$.

Again if the orientation of the rods of a deformable cluster is given by the orientation distribution $\psi(\mathbf{p})$, the time derivative of its second order moment $\dot{\mathbf{a}}$ results in:

$$\dot{\mathbf{a}} = \int_{\mathcal{S}} (\dot{\mathbf{p}} \otimes \mathbf{p} + \mathbf{p} \otimes \dot{\mathbf{p}}) \ \psi(\mathbf{p}) \, d\mathbf{p} \tag{5.61}$$

By considering the expression of the microscopic velocity $\dot{\mathbf{p}}$

$$\dot{\mathbf{p}} = \frac{\xi}{\xi + \mu} \ \dot{\mathbf{p}}^J + \frac{\mu}{\xi + \mu} \ \dot{\mathbf{p}}^R \tag{5.62}$$

it results:

$$\dot{\mathbf{a}} = \frac{\xi}{\xi + \mu} \ \dot{\mathbf{a}}^J + \frac{\mu}{\xi + \mu} \ \dot{\mathbf{a}}^R \tag{5.63}$$

with $\dot{\mathbf{a}}^J$ and $\dot{\mathbf{a}}^R$ the resulting expressions when equation (5.62) is introduced into equation (5.61):

$$\begin{cases} \dot{\mathbf{a}}^J = \mathbf{\Omega} \cdot \mathbf{a} - \mathbf{a} \cdot \mathbf{\Omega} + \mathbf{D} \cdot \mathbf{a} + \mathbf{a} \cdot \mathbf{D} - 2 \, \mathbf{A} : \mathbf{D} \\ \dot{\mathbf{a}}^R = \mathbf{W} \cdot \mathbf{a} + \mathbf{a} \cdot \mathbf{W}^T \end{cases} \tag{5.64}$$

The objectivity of the resulting evolution equation of $\dot{\mathbf{a}}$ was proved in [107]. Usually the fourth order moment $\mathbf{A}$ is expressed from the second order one by considering any of the numerous closure relations proposed in the literature [19, 37, 103, 104].

Until now the deformation mechanisms neglected that a cluster can experience an elastic deformation with a fading-memory. That is, the reference configuration is a combination of the recent experienced deformations.

5.4.3 Elasticity of the aggregates

So far, both rigid and deformable clusters was considered to exhibit only translations and rotations when a simple shear flow is applied; this means that the models are still purely viscous. Therefore, these models cannot account for the elastic component evidenced during classical rheological experiments on suspensions involving clusters [66]. To account for this elasticity, an elastic mechanism is introduced in the model at the aggregates scale.

At the microscale, observations show that, during a simple shear flow, the deformable aggregates rotate with the flow and stretch. When the flow stops, stretching relaxes and a reference configuration is recovered. This relaxation mechanism depends on the stretching duration. Indeed, if the aggregate has undergone a short-time deformation, it will come back to its initial conformation (i.e. to its initial moment descriptor $\mathbf{a}$). However, if the deformation state has been prolonged, the cluster will experience internal reconfigurations and will not come back to its initial conformation but to one close to the deformed state. To introduce this "aggregate" elasticity in the model, an additional term is added in the evolution equation of $\mathbf{a}$:

$$\dot{\mathbf{a}} = \frac{1}{1+\mathcal{E}} \dot{\mathbf{a}}^J + \frac{\mathcal{E}}{\mathcal{E}+1} \dot{\mathbf{a}}^R - \beta^e \left(\mathbf{a} - \mathbf{a}^r\right) \tag{5.65}$$

where β^e is the elasticity coefficient and $\mathcal{E} = \dfrac{\mu}{\xi}$. One can notice that the last term in equation (5.65) is similar to the last term in equation (5.37). The reference conformation $\mathbf{a}^r$ is built by considering a fading memory function that takes into account the deformation history experienced by the cluster. In the model, the cluster conformation is described by the tensor $\mathbf{a}$ whose eigenvalues can be used to evaluate the cluster stretching. Assuming $\mathbf{a}_\tau$ known at times $\tau \leq t$, the previous stretching states of the cluster can be estimated by:

$$\mathbf{a}_\tau = \mathbf{R}_\tau^T \cdot \mathbf{\Lambda}_\tau \cdot \mathbf{R}_\tau \tag{5.66}$$

where $\mathbf{R}_\tau$ is the matrix containing the main eigenvectors of $\mathbf{a}$. The equilibrium stretching state $\mathbf{\Lambda}_t^r$ that the cluster tries to recover at time t reads:

$$\mathbf{\Lambda}_t^r = \int_0^t m\left(t-\tau\right) \mathbf{\Lambda}_\tau \, d\tau \tag{5.67}$$

where $m\left(t-\tau\right)$ is a memory function [108] which decreases as $t-\tau$ increases. Finally, the equilibrium configuration at time t, $\mathbf{a}_t^r$ is obtained by applying:

$$\mathbf{a}_t^r = \mathbf{R}_t^T \cdot \mathbf{\Lambda}_t^r \cdot \mathbf{R}_t \tag{5.68}$$

5.4.4 Deformable clusters with Brownian motions

In all the previous descriptions, the clusters were supposed free from Brownian effects. However, in concentrated regimes clusters interact hydrodynamically and tend to randomize the orientation distribution. To mimic this randomizing effect, a fourth term

is added in the right hand side of equation (5.65) which is simply similar to the one in equation (5.37):

$$\dot{\mathbf{a}} = \frac{1}{1+\mathcal{E}} \, \dot{\mathbf{a}}^J + \frac{\mathcal{E}}{\mathcal{E}+1} \, \dot{\mathbf{a}}^R - \frac{1}{1+\mathcal{E}} \left[\beta^e \left(\mathbf{a} - \mathbf{a}^r \right) - \beta^r \left(\mathbf{a} - \frac{\mathbf{I}}{2} \right) \right] \qquad (5.69)$$

where $d_m = 2$ in the 2D case and β^r accounts for these randomizing effects. This time the terms characterizing the elasticity and the Brownian effects are weighted by $\dfrac{1}{1+\mathcal{E}}$, because they cannot apply on the rigid components of the orientation tensor: only the deformable part related to $\dot{\mathbf{a}}^J$ can be assumed to recover a reference configuration $\mathbf{a}^r$ or the isotropic state.

5.4.5 Numerical example

In this example a simple shear flow with a shear rate of $\dot{\gamma} = 1$, is applied to fiber suspensions immersed in a Newtonian fluid. The velocity field is given by:

$$\mathbf{v}^T = [\dot{\gamma} y, 0] \qquad (5.70)$$

The evolution of the kinematic of the cluster is now given by equation (5.69). The cluster is initially in an isotropic state $\left(\mathbf{a}_{t=0} = \dfrac{\mathbf{I}}{2} \right)$. From Figure 5.4, one can notice the evolution of the a_{11} component of $\mathbf{a}$ for $\mathcal{E} = 5$, $\beta^e = 10$ and $\beta^r = 1$. It is clear that, the microstructure reaches a steady state at the end of the simulation. This is mostly due to the last term in equation (5.69), containing the diffusion effects. The first effect is related
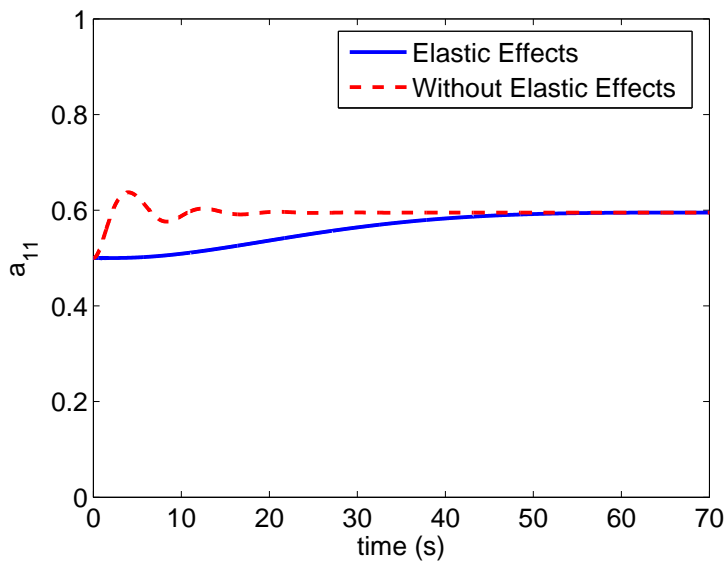

Figure 5.4: Time evolution of the a_{11} in both cases: with elastic effects (in continuous line) and without elastic effects (in dashed line)

to a reference memory configuration that the cluster tries to recover when it is stretching.

The second one is related to the Brownian diffusion, that tries to randomize the configuration and orient the fibers in the isotropic state. The elasticity vanishes in the steady shear flow (Figure 5.4), because at long time, the reference orientation coincides with the actual one (i.e. at the steady state $\dot{\mathbf{a}} = \mathbf{0}$ and $\mathbf{a}\,(t \to \infty) = \mathbf{a}^r$). This implies the following conclusion: the elasticity is ineffective in steady shear flows. In fact, plotting the evolution of a_{11} without elastic effects (i.e. equation (5.69) without the term $\beta^e\,(\mathbf{a} - \mathbf{a}^r)$), shows that at the steady state the two time evolution are superimposed one another confirming again the complete loss of memory elastic effects due to stretching.

5.5   Conclusion

The study of concentrated suspensions using the models of rigid and deformable clusters at the mesoscopic scale allows the following conclusion. The most realistic model of deformable clusters, associated with the elastic memory effects and the Brownian diffusion showed that the elasticity was inactive in simple shear flows. This raises the question of where this elasticity could play an active role in terms of memory effects. In flows that exhibit oscillations, like small amplitude oscillatory flows, the steady steady is never reached and the cluster will be stretching continuously. Thus, this could be a case where the elasticity mechanisms are well activated.

5.6   Résumé du chapitre

L'objectif de ce chapitre était de présenter les éléments et les différents modèles de suspensions de fibres en utilisant des méthodes basées sur la théorie cinétique. La théorie cinétique est une approche micro-macro qui permet de considérer le système à l'échelle mésoscopique tout en conservant la physique fine nécessaire à la description de la microstructure et de son évolution. Cela est possible grâce à l'introduction d'un certain nombre de coordonées de conformation. L'approche proposée pour construire les modèles peut être résumé en trois points : (i) la microstructure est définie à l'échelle micro, via l'introduction de différents paramètres de conformation, et son évolution est obtenue à partir de l'écriture de l'équilibre ; (ii) une fonction de distribution est introduite à l'échelle méso, représentant la fraction de particules présentant une certaine conformation à un certain temps et en un certain point de l'espace, cette fonction contient par définition toute les informations sur la microstructure ; (iii) les propriétés macroscopiques de la suspension sont ensuite calculées à partir des différents moments de la distribution. Après avoir montrée que cette approche permet de retrouver l'équation de Jeffery pour les suspensions diluées, elle est appliquée aux suspensions concentrées présentant des agrégats de fibres, agrégats dans un premier temps rigides puis déformables. Ensuite, afin de rendre compte de toutes les physiques mises en jeu dans le cas de ces suspensions concentrées, l'élasticité des agrégats ainsi que les effets aléatoires dus aux interactions hydrodynamiques entre agrégats sont introduits dans le modèle.

L'étude de suspensions concentrées de fibres en utilisant les modèles des agrégats rigides et déformables à l'échelle mésoscopique permet la conclusion suivante. Le modèle le plus réaliste (agrégats déformables) associé aux effets de mémoire (élasticité avec la diffusion Brownienne), a montré que l'élasticité était inactive dans le cas d'un écoulement de cisaillement simple. Dans ce type d'écoulement, l'état stationnaire est atteint et donc la configuration de référence $\mathbf{a}^r$ coïncidait avec la configuration actuelle $\mathbf{a}$.

V

Conclusion

Throughout this part, an alternative suggestion for treating and studying concentrated fiber suspensions was presented: kinetic theory approaches. Then, the models based on the mesoscopic scale were detailed. A fiber was modeled by a rod with two beads at its ends, and that was the description done at first for dilute suspensions of fibers/rods. Then, when the suspending fluid's molecules came in interaction with the rod, Brownian effects were considered along with the resulting forces that were added to the purely hydrodynamic ones.

After that, semi-dilute/semi-concentrated suspensions were described by considering rod-rod interactions illustrated by a diffusion term scaling with the intensity of the applied shear shear rate.

Consequently concentrated suspensions were thoroughly investigated. The proposed models assumed the most complex configurations. Aggregates of fibers are formed when the suspensions are very concentrated. When the cluster is purely rigid and the Brownian effects are neglected, then it would rotate freely in the flow under the one effect of the hydrodynamic forces. When it is deformable, an additional force was taken into account. This force is responsible for the rod-rod interaction and entanglements. More real phenomena were developed with the possibility of cluster stretching (memory and elastic effects) with Brownian effects.

In what concerns the overall presented cluster models here (both rigid and deformable), it is true that they are a good compromise between accuracy and computational efficiency. They seem to represent the physics quite well through the kinetic theory approaches. However, they rely mostly on very particular physics associated with many phenomenological assumptions and considerations (rigidity and deformability of clusters, Brownian diffusion, elasticity and memory effects). All of these previous hypothesis have been considered in an attempt to explain the experimental observations of aggregates of fibers. Due to these hypothesis, it is important to validate the model of aggregates. DNS could be a natural candidate for this mission. In future works, aggregates of fibers will be created at the microscopic scale (DNS). Then the results of the DNS study will be compared with the kinetic theory aggregate model, in order to conclude on their validity and their credibility.

6

General Conclusion and Perspectives

Throughout this thesis, the main objective was to study the rheology of concentrated fiber suspensions. The importance of such a study, lies in the fact that concentrated fiber suspensions are now raising interesting questions both scientifically and technologically. In the presented work here, concentrated fiber suspensions were carefully addressed at the three known scales: microscopic scale (direct numerical simulations or DNS), mesoscopic and macroscopic scale (kinetic theory approaches).

The DNS model allowed the precise and fine analysis of the physics that were involved at the microscopic scale for hundreds of fibers: orientation, position, and the interaction forces. Then it was directly possible to evaluate macroscopic rheological properties, validated with experimental measurements. The great efficiency of DNS approaches is the capacity to precisely model the detailed kinematic evolution of the microstructure. Another positive point for DNS is their capability to validate other models that exist on a higher scale (i.e. mesoscopic and macroscopic). However, the main drawback of such intensive calculations is the computational cost, where the processed calculation time is sacrificed in favor of the precision of the final solution. The perspectives of the DNS approach is to attempt the simulation of real industrial processes, in real time. In the SMC (Sheet Molding Compounds) process, thousands of fibers are confined in a mold. And the DNS is a natural candidate to simulate such confinement in a compact enough volume, since they mainly simulate fiber suspensions in volumes. Another interesting application is considering flexible fibers that exhibit large deformations (instead of small deformations that were assumed in this work), and the ability to model the dry glass projection on a wall in real time. Such a project, could permit the precise analysis of fiber bending and choose which fibers are suitable to reinforce concrete structures and withstand the highest mechanical impacts (for example).

The kinetic theory approaches are a significant simplification of the complex physics involved in rheology. The price to be paid in such approaches is the lack of precision in favor of the simulation time. This is clear, since all the necessary information of the mi-

crostructure are contained in one function. However, the simplicity of the methods here is that they can grant one the simulation of endless possibilities of complex and real scenarios (deformable clusters, elasticity, Brownian effects, etc,...) without any considerable difficulties at the computational level. The presented models here could be extended to more than the ones that have been presented. But without an effective validation, their physics will be considered doubtful. The future and most important works in the kinetic theory frame, has to be both the numerical and experimental verification of these models. Once again the natural candidate for a numerical recognition of these models is DNS. DNS is a true testimony for proving once and for all that a compromise between accuracy and very in-depth analysis is possible. Moreover, the continuous search and development of experimental work is crucial for a far more solid support of the kinetic theory.

6.1 Résumé du chapitre

Dans cette thèse, l'objectif principal était l'étude de la rhéologie de suspensions concentrées de fibres. L'importance d'une telle étude, réside dans le fait que les suspensions concentrées de fibres soulèvent aujourd'hui des questions intéressantes à la fois scientifiquement et technologiquement. Dans le travail présenté ici, des suspensions de fibres concentrées ont été traitées à trois échelles connues: l'échelle microscopique (de simulations numériques directes ou DNS), mésoscopique et macroscopique (approches de la théorie cinétique).

Le modèle de la DNS a permis l'analyse précise et fine de la physique impliquée à l'échelle microscopique pour des centaines de fibres: l'orientation, la position et les forces d'interaction. Ensuite, il était possible d'évaluer directement les propriétés rhéologiques macroscopiques, validées avec des mesures expérimentales. La DNS modélise précisément l'évolution de la cinématique détaillée de la miscrostructure. Un autre point positif pour la DNS, c'est qu'elle permet de valider d'autres modèles existants sur une plus grande échelle (c'est à dire les échelles mésoscopique et macroscopique). Toutefois, l'inconvénient principal de tels calculs intensifs est le coût de calcul, où le temps de calcul est sacrifié au profit de la précision de la solution finale. Les perspectives de l'approche de DNS est d'essayer de simuler des procédés industriels en temps réel. Dans le processus SMC (Sheet Molding Compounds), des milliers de fibres sont confinées dans un moule. Et la DNS est un candidat naturel pour simuler ce type de confinement dans un volume assez compact. Une autre application intéressante et envisageable par la DNS concerne les fibres flexibles sous grandes déformations (au lieu de petites déformations qui ont été considérées dans ce travail), et la possibilité de modéliser la projection de fibres de verre sur un mur en temps réel. Un tel projet, pourrait permettre l'analyse précise de la flexion de chaque fibre et de choisir lesquelles des fibres sont susceptibles de renforcer les structures de béton et de résister aux impacts mécaniques (par exemple).

Les approches de la théorie cinétique représentent une simplification significative de la physique complexe impliquée dans la rhéologie. Le prix à payer dans ces approches est le manque de précision en faveur du temps de simulation. Cela est clair, puisque toutes les informations nécessaires à la description de la microstructure sont contenues dans une fonction unique. Toutefois, la simplicité des méthodes ici est qu'elles peuvent permettre de considérer des possibilités infinies de physiques complexes et réels (agrégats déformables, élasticité, effets Browniens, etc, ...) sans aucune difficulté considérable au niveau de calcul. Malgré cela, une vraie validation des modèles présentés dans ce chapitre est nécessaire. Les travaux à venir et les perspectives seront la vérification numérique et expérimentale de ces modèles. Aussi, la DNS peut servir comme outil de validation de ces modèles. Mais, l'optimal sera de faire concorder ces modèles avec des études expérimentales.

DNS Appendix

Contents

A.1   Vector and Tensor notation

Throughout the previous chapters the following tensor products are considered according to the Einstein notation convention [71]:

- if $\mathbf{C}$ and $\mathbf{B}$ are first rank tensors, then the single contraction "·", reads $(\mathbf{C} \cdot \mathbf{B}) = C_j B_j$
- if $\mathbf{C}$ and $\mathbf{B}$ are first rank tensors, then the dyadic product "$\otimes$" reads $(\mathbf{C} \otimes \mathbf{B})_{jk} = C_j B_k$;
- if $\mathbf{C}$ and $\mathbf{B}$ are respectively second and first rank tensors, then the single contraction "·" reads: $(\mathbf{C} \cdot \mathbf{B})_j = C_{jm} B_m$;
- if $\mathbf{C}$ and $\mathbf{B}$ are second rank tensors, then the single contraction "·" reads: $(\mathbf{C} \cdot \mathbf{B})_{jk} = C_{jm} B_{mk}$;

The permutation tensor (Levi-Civita tensor) is defined as [83]:

$$\begin{cases} \varepsilon_{ijk} = +1, & \text{if } ijk = 123, \text{ 231 or 312} \\ \varepsilon_{ijk} = -1, & \text{if } ijk = 321, \text{ 132 or 213} \\ \varepsilon_{ijk} = 0, & \text{if any two indices are alike} \end{cases} \qquad \text{(A.1)}$$

Note also that [83]:

$$\varepsilon_{ijk} = \frac{1}{2}\left(i-j\right)\left(j-k\right)\left(k-i\right) \qquad \text{(A.2)}$$

And:

$$\sum_{j=1}^{3}\varepsilon_{jkl}\varepsilon_{mij} = \sum_{j=1}^{3}\varepsilon_{klj}\varepsilon_{mij} = \delta_{km}\delta_{li} - \delta_{ki}\delta_{lm} \qquad \text{(A.3)}$$

which in the Einstein notation becomes

$$\varepsilon_{klj}\varepsilon_{mij} = \delta_{km}\delta_{li} - \delta_{ki}\delta_{lm} \qquad \text{(A.4)}$$

In this appendix, let $\boldsymbol{\delta}_1$, $\boldsymbol{\delta}_2$ and $\boldsymbol{\delta}_3$ will be the unit vectors in the direction of the **x**, **y** and **z** axes.

A.2   Vector product (or Cross product) of Two Vectors

The vector product of two vectors **v** and **w** is defined as [83]:

$$\begin{aligned} [\mathbf{v} \times \mathbf{w}] &= \left[\left\{\sum_{j=1}^{3}\boldsymbol{\delta}_j v_j\right\} \times \left\{\sum_{k=1}^{3}\boldsymbol{\delta}_k w_k\right\}\right] \\ &= \sum_{j=1}^{3}\sum_{k=1}^{3}\left[\boldsymbol{\delta}_j \times \boldsymbol{\delta}_k\right] v_j w_k \\ &= \sum_{i=1}^{3}\sum_{j=1}^{3}\sum_{k=1}^{3}\varepsilon_{ijk}\boldsymbol{\delta}_i v_j w_k \\ &= \varepsilon_{ijk} v_j w_k \quad \text{(In the Einstein notation)} \end{aligned} \qquad \text{(A.5)}$$

A.3 The double contraction of two tensors

Two second rank tensors (or higher order rank tensors) $\mathbf{v}$ and $\mathbf{w}$ may be multiplied to the double dot operation as follows:

$$
\begin{aligned}
(\mathbf{v}:\mathbf{w}) &= \left[\left\{\sum_{i=1}^{3}\sum_{j=1}^{3}\boldsymbol{\delta}_i\boldsymbol{\delta}_j v_{ij}\right\}:\left\{\sum_{k=1}^{3}\sum_{l=1}^{3}\boldsymbol{\delta}_k\boldsymbol{\delta}_l w_{kl}\right\}\right] \\
&= \sum_{i=1}^{3}\sum_{j=1}^{3}\sum_{k=1}^{3}\sum_{l=1}^{3}\left(\boldsymbol{\delta}_i\boldsymbol{\delta}_j:\boldsymbol{\delta}_k\boldsymbol{\delta}_l\right) v_{ij}w_{kl} \\
&= \sum_{i=1}^{3}\sum_{j=1}^{3}\sum_{k=1}^{3}\sum_{l=1}^{3}\delta_{il}\delta_{jk} v_{ij}w_{kl} \\
&= \sum_{i=1}^{3}\sum_{j=1}^{3} v_{ij}w_{ji} \\
&= v_{ij}w_{ji} \quad \text{(In the Einstein notation)}
\end{aligned}
\tag{A.6}
$$

A.4 Detailed calculation

In this part the index α is sometimes removed for the sake of simplicity.

A.4.1 Detailed calculation of $\dot{\mathbf{p}}^{(\alpha)} = -\mathbf{p}^{(\alpha)} \times \left(\omega^{(\alpha)} - \boldsymbol{\Omega}\right)$

Using equation (A.5):

$$
\boldsymbol{\Omega} = \frac{1}{2}\left(\nabla \times \mathbf{V}\right) = \frac{1}{2}\varepsilon_{ijk}\frac{\partial}{\partial x_j}V_k
\tag{A.7}
$$

$$
\begin{aligned}
\Omega_1 &= \sum_{j=1}^{3}\sum_{k=1}^{3}\frac{1}{2}\varepsilon_{1jk}\frac{\partial}{\partial x_j}V_k = 0 \\
\Omega_2 &= \sum_{j=1}^{3}\sum_{k=1}^{3}\frac{1}{2}\varepsilon_{2jk}\frac{\partial}{\partial x_j}V_k = 0 \\
\Omega_3 &= \sum_{j=1}^{3}\sum_{k=1}^{3}\frac{1}{2}\varepsilon_{3jk}\frac{\partial}{\partial x_j}V_k = -\frac{\dot{\gamma}}{2}
\end{aligned}
\tag{A.8}
$$

Hence:

$$
\boldsymbol{\Omega}^T = \left[0;0;-\frac{\dot{\gamma}}{2}\right]
\tag{A.9}
$$

Thus:

$$
\dot{\mathbf{p}} = \mathbf{p} \times \boldsymbol{\Omega} - \mathbf{p} \times \omega
\tag{A.10}
$$

$$
\begin{aligned}
\mathbf{p} \times \boldsymbol{\Omega} &= (\boldsymbol{\delta}_i p_i) \times (\boldsymbol{\delta}_j \Omega_j) \\
&= (\boldsymbol{\delta}_i p_i) \times \left(\frac{1}{2}\varepsilon_{jkl}\frac{\partial}{\partial x_k}V_l\boldsymbol{\delta}_j\right) \\
&= \frac{1}{2}p_i\frac{\partial V_l}{\partial x_k}\varepsilon_{jkl}\varepsilon_{mij}\boldsymbol{\delta}_m
\end{aligned}
\tag{A.11}
$$

Using equation ([A.4](#)):

$$
\begin{aligned}
\Rightarrow \mathbf{p} \times \boldsymbol{\Omega} &= \frac{1}{2} p_i \frac{\partial V_l}{\partial x_k} \left(\delta_{km}\delta_{li} - \delta_{ki}\delta_{lm} \right) \boldsymbol{\delta}_m \\
&= \frac{1}{2} p_l \frac{\partial V_l}{\partial x_k} \boldsymbol{\delta}_k - \frac{1}{2} p_k \frac{\partial V_l}{\partial x_k} \boldsymbol{\delta}_l \\
&= \frac{1}{2} \left(\sum_{l=1}^{3} \sum_{k=1}^{3} p_l \frac{\partial V_l}{\partial x_k} \boldsymbol{\delta}_k \right) - \frac{1}{2} \left(\sum_{l=1}^{3} \sum_{k=1}^{3} p_k \frac{\partial V_l}{\partial x_k} \boldsymbol{\delta}_l \right) \\
&= \frac{1}{2} \left[\nabla \mathbf{V} - (\nabla \mathbf{V})^T \right] \cdot \mathbf{p} \\
&= \mathbf{W} \cdot \mathbf{p}
\end{aligned}
\tag{A.12}
$$

With : $k = m$, $l = i$, in $\delta_{km}\delta_{li}$ and $k = i$, $l = m$, in $\delta_{ki}\delta_{lm}$ and:

$$
\nabla \mathbf{V} =
\begin{bmatrix}
\dfrac{\partial V_1}{\partial x_1} & \dfrac{\partial V_1}{\partial x_2} & \dfrac{\partial V_1}{\partial x_3} \\[2ex]
\dfrac{\partial V_2}{\partial x_1} & \dfrac{\partial V_2}{\partial x_2} & \dfrac{\partial V_2}{\partial x_3} \\[2ex]
\dfrac{\partial V_3}{\partial x_1} & \dfrac{\partial V_3}{\partial x_2} & \dfrac{\partial V_3}{\partial x_3}
\end{bmatrix}
\tag{A.13}
$$

Then:

$$
\begin{aligned}
\boldsymbol{\omega}^{(\alpha)} &= -\boldsymbol{\xi}^{(\alpha)^{-1}} \cdot \left(\mathbf{T}^{(\alpha)} + \boldsymbol{\mathcal{H}}^{(\alpha)} : \mathbf{D} \right) \\
&= \boldsymbol{\omega}_1^{(\alpha)} + \boldsymbol{\omega}_2^{(\alpha)}
\end{aligned}
\tag{A.14}
$$

where:

$$
\boldsymbol{\omega}_1^{(\alpha)} = -\boldsymbol{\xi}^{(\alpha)^{-1}} \cdot \mathbf{T}^{(\alpha)}
\tag{A.15}
$$

with :

$$
\begin{aligned}
\xi_{jk}^{(\alpha)^{-1}} &= -\frac{1}{\pi \eta_0 l^{(\alpha)3}} \left[\frac{1}{Y_C^{(\alpha)}} \delta_{jk} + \left(\frac{1}{X_C^{(\alpha)}} - \frac{1}{Y_C^{(\alpha)}} \right) p_j^{(\alpha)} p_k^{(\alpha)} \right] \Leftrightarrow \\
\boldsymbol{\xi}^{(\alpha)^{-1}} &= -\frac{1}{\pi \eta_0 l^{(\alpha)3}} \left[\frac{1}{Y_C^{(\alpha)}} \mathbf{I} + \left(\frac{1}{X_C^{(\alpha)}} - \frac{1}{Y_C^{(\alpha)}} \right) \mathbf{p}^{(\alpha)} \otimes \mathbf{p}^{(\alpha)} \right]
\end{aligned}
\tag{A.16}
$$

and:

$$
\mathbf{T}^{(\alpha)} = \mathbf{p}^{(\alpha)} \times \left(\sum_{\beta \neq \alpha} l^{(\alpha,\beta)} F_c^{(\alpha,\beta)} \mathbf{n}^{(\alpha,\beta)} + \sum_{\mu \neq \alpha} l^{(\alpha,\mu)} F_{lb}^{(\alpha,\mu)} \mathbf{n}^{(\alpha,\mu)} \right)
\tag{A.17}
$$

$$
\begin{aligned}
\boldsymbol{\omega}_1^{(\alpha)} &= -\boldsymbol{\xi}^{(\alpha)^{-1}} \cdot \mathbf{T}^{(\alpha)} \\
&= \frac{1}{\pi \eta_0 l^{(\alpha)3}} \left[\frac{1}{Y_C^{(\alpha)}} \mathbf{I} + \left(\frac{1}{X_C^{(\alpha)}} - \frac{1}{Y_C^{(\alpha)}} \right) \mathbf{p}^{(\alpha)} \otimes \mathbf{p}^{(\alpha)} \right] \mathbf{T}^{(\alpha)}
\end{aligned}
\tag{A.18}
$$

$$\mathbf{p}^{(\alpha)} \otimes \mathbf{p}^{(\alpha)} \cdot \mathbf{T}^{(\alpha)} = \mathbf{p}^{(\alpha)} \otimes \mathbf{p}^{(\alpha)} \cdot \mathbf{p}^{(\alpha)}$$

$$\times \left(\sum_{\beta \neq \alpha} l^{(\alpha,\beta)} F_c^{(\alpha,\beta)} \mathbf{n}^{(\alpha,\beta)} + \sum_{\mu \neq \alpha} l^{(\alpha,\mu)} F_{lb}^{(\alpha,\mu)} \mathbf{n}^{(\alpha,\mu)} \right)$$

$$= \mathbf{p}^{(\alpha)} \otimes \mathbf{p}^{(\alpha)} \cdot \mathbf{p}^{(\alpha)} \times \left(\sum_{\beta \neq \alpha} l^{(\alpha,\beta)} F_c^{(\alpha,\beta)} \mathbf{n}^{(\alpha,\beta)} \right) \qquad (A.19)$$

$$+ \mathbf{p}^{(\alpha)} \otimes \mathbf{p}^{(\alpha)} \cdot \mathbf{p}^{(\alpha)} \times \left(\sum_{\mu \neq \alpha} l^{(\alpha,\mu)} F_{lb}^{(\alpha,\mu)} \mathbf{n}^{(\alpha,\mu)} \right)$$

Let:

$$\mathbf{p}^{(\alpha)} \times \mathbf{n}^{(\alpha,\beta)} = \begin{bmatrix} p_2 n_3 - p_3 n_2 \\ p_3 n_1 - p_1 n_3 \\ p_1 n_2 - p_2 n_1 \end{bmatrix} = \mathbf{P}^\beta \qquad (A.20)$$

(the same is applied for $\mathbf{p}^{(\alpha)} \times \mathbf{n}^{(\alpha,\mu)}$, i.e. $\mathbf{p}^{(\alpha)} \times \mathbf{n}^{(\alpha,\mu)} = \mathbf{P}^\mu$)
Then:

$$\Rightarrow \mathbf{p}^{(\alpha)} \otimes \mathbf{p}^{(\alpha)} \cdot \mathbf{T}^{(\alpha)} = \mathbf{p}^{(\alpha)} \otimes \mathbf{p}^{(\alpha)} \left[\left(\sum_{\beta \neq \alpha} l^{(\alpha,\beta)} F_c^{(\alpha,\beta)} \mathbf{P}^\beta \right) \right]$$

$$+ \mathbf{p}^{(\alpha)} \otimes \mathbf{p}^{(\alpha)} \left[\left(\sum_{\mu \neq \alpha} l^{(\alpha,\mu)} F_{lb}^{(\alpha,\mu)} \mathbf{P}^\mu \right) \right] \qquad (A.21)$$

$$\mathbf{p}^{(\alpha)} \otimes \mathbf{p}^{(\alpha)} \cdot \mathbf{P}^\beta = \begin{bmatrix} p_1^2 & p_1 p_2 & p_1 p_3 \\ p_1 p_2 & p_2^2 & p_2 p_3 \\ p_1 p_3 & p_2 p_3 & p_3^2 \end{bmatrix} \begin{bmatrix} p_2 n_3 - p_3 n_2 \\ p_3 n_1 - p_1 n_3 \\ p_1 n_2 - p_2 n_1 \end{bmatrix}$$

$$= \begin{bmatrix} p_1^2 (p_2 n_3 - p_3 n_2) + p_1 p_2 (p_3 n_1 - p_1 n_3) + p_1 p_3 (p_1 n_2 - p_2 n_1) \\ p_1 p_2 (p_2 n_3 - p_3 n_2) + p_2^2 (p_3 n_1 - p_1 n_3) + p_2 p_3 (p_1 n_2 - p_2 n_1) \\ p_1 p_3 (p_2 n_3 - p_3 n_2) + p_2 p_3 (p_3 n_1 - p_1 n_3) + p_3^2 (p_1 n_2 - p_2 n_1) \end{bmatrix}$$

$$= \begin{bmatrix} 0 \\ 0 \\ 0 \end{bmatrix}$$

$$(A.22)$$

the same is applied for $\mathbf{p}^{(\alpha)} \otimes \mathbf{p}^{(\alpha)} \cdot \mathbf{P}^\mu$.

$$\Rightarrow \mathbf{p}^{(\alpha)} \otimes \mathbf{p}^{(\alpha)} \cdot \mathbf{T}^{(\alpha)} = \begin{bmatrix} 0 \\ 0 \\ 0 \end{bmatrix} \qquad (A.23)$$

$$\Rightarrow \boldsymbol{\omega}_1^{(\alpha)} = \frac{1}{\pi \eta_0 l^{(\alpha)3}} \frac{1}{Y_C^{(\alpha)}} \mathbf{T}^{(\alpha)} \qquad (A.24)$$

$$-\mathbf{p}^{(\alpha)} \times \boldsymbol{\omega}_1^{(\alpha)} = -\frac{1}{\pi\eta_0 l^{(\alpha)3}} \frac{1}{Y_C^{(\alpha)}} \mathbf{p}^{(\alpha)} \times$$

$$\left[\mathbf{p}^{(\alpha)} \times \left(\sum_{\beta \neq \alpha} l^{(\alpha,\beta)} F_c^{(\alpha,\beta)} \mathbf{n}^{(\alpha,\beta)} + \sum_{\mu \neq \alpha} l^{(\alpha,\mu)} F_{lb}^{(\alpha,\mu)} \mathbf{n}^{(\alpha,\mu)} \right) \right] \quad \text{(A.25)}$$

$$= \frac{1}{\pi\eta_0 l^{(\alpha)3}} \frac{1}{Y_C^{(\alpha)}} \left(\sum_{\beta \neq \alpha} l^{(\alpha,\beta)} F_c^{(\alpha,\beta)} \mathbf{n}^{(\alpha,\beta)} + \sum_{\mu \neq \alpha} l^{(\alpha,\mu)} F_{lb}^{(\alpha,\mu)} \mathbf{n}^{(\alpha,\mu)} \right)$$

with :

$$\mathbf{p}^{(\alpha)} \times \left(\mathbf{p}^{(\alpha)} \times \mathbf{n}^{(\alpha,\beta)} \right) = -\mathbf{n}^{(\alpha,\beta)} \left(\text{i.e. } \mathbf{p}^{(\alpha)} \times \left(\mathbf{p}^{(\alpha)} \times \mathbf{n}^{(\alpha,\mu)} \right) = -\mathbf{n}^{(\alpha,\mu)} \right) \quad \text{(A.26)}$$

Using equation (A.6):

$$\begin{aligned}
\boldsymbol{\mathcal{H}} : \mathbf{D} &= \left[-\pi\eta_0 l^3 Y_H \left(\varepsilon_{ikl} p_j p_l D_{mn} + \varepsilon_{jkl} p_i p_l D_{mn} \right) \right] \left[\boldsymbol{\delta}_i \boldsymbol{\delta}_j \boldsymbol{\delta}_k : \boldsymbol{\delta}_m \boldsymbol{\delta}_n \right] \\
&= \left[-\pi\eta_0 l^3 Y_H \left(\varepsilon_{ikl} p_j p_l D_{mn} + \varepsilon_{jkl} p_i p_l D_{mn} \right) \right] \left[\boldsymbol{\delta}_i \delta_{jn} \delta_{km} \right] \quad \text{(A.27)} \\
&= -\pi\eta_0 l^3 Y_H \left(\varepsilon_{ikl} p_j p_l D_{kj} + \varepsilon_{jkl} p_i p_l D_{kj} \right) \boldsymbol{\delta}_i
\end{aligned}$$

with $\boldsymbol{\delta}_i \boldsymbol{\delta}_j \boldsymbol{\delta}_k : \boldsymbol{\delta}_m \boldsymbol{\delta}_n = \boldsymbol{\delta}_i \delta_{jn} \delta_{km} = \boldsymbol{\delta}_i$ (i.e. $j = n$ and $k = m$)

$$\begin{aligned}
\boldsymbol{\omega}_2^{(\alpha)} &= -\boldsymbol{\xi}^{(\alpha)^{-1}} \cdot \left(\boldsymbol{\mathcal{H}}^{(\alpha)} : \mathbf{D} \right) \\
&= +\frac{1}{\pi\eta_0 l^3} \left[\frac{1}{Y_C} \delta_{jk} + \left(\frac{1}{X_C} - \frac{1}{Y_C} \right) p_j p_k \right] \boldsymbol{\delta}_j \boldsymbol{\delta}_k \quad \text{(A.28)} \\
&\quad \cdot \left[-\pi\eta_0 l^3 Y_H \left(\varepsilon_{ikl} p_j p_l D_{kj} + \varepsilon_{jkl} p_i p_l D_{kj} \right) \boldsymbol{\delta}_i \right]
\end{aligned}$$

Let: $\mathbf{C} = \boldsymbol{\mathcal{H}} : \mathbf{D} = -\pi\eta_0 l^3 Y_H \left(\varepsilon_{ikl} p_j p_l D_{kj} + \varepsilon_{jkl} p_i p_l D_{kj} \right) \boldsymbol{\delta}_i = \text{a vector}$

$$\begin{aligned}
C_i &= -\pi\eta_0 l^3 Y_H \left(\varepsilon_{ikl} p_j p_l D_{kj} + \varepsilon_{jkl} p_i p_l D_{kj} \right) \\
C_k &= -\pi\eta_0 l^3 Y_H \left(\varepsilon_{kil} p_j p_l D_{ij} + \varepsilon_{jil} p_k p_l D_{ij} \right)
\end{aligned} \quad \text{(A.29)}$$

$$\begin{aligned}
-\boldsymbol{\xi}^{(\alpha)^{-1}} \cdot \mathbf{C} &= \left(\boldsymbol{\delta}_j \boldsymbol{\delta}_k \xi_{jk} \right) \left(\boldsymbol{\delta}_i A_i \right) \\
&= \delta_{ki} \boldsymbol{\delta}_j \xi_{jk} A_k \\
&\quad (i = k \Rightarrow \delta_{ki} = 1) \\
&= \boldsymbol{\delta}_j \frac{1}{\pi\eta_0 l^3} \left[\frac{1}{Y_C} \delta_{jk} + \left(\frac{1}{X_C} - \frac{1}{Y_C} \right) p_j p_k \right] \\
&\quad \cdot \left[-\pi\eta_0 l^3 Y_H \left(\varepsilon_{kil} p_j p_l D_{ij} + \varepsilon_{jil} p_k p_l D_{ij} \right) \right] \\
&= \boldsymbol{\delta}_j \left[-\frac{Y_H}{Y_C} \left(\varepsilon_{kil} p_j p_l D_{ij} \delta_{jk} + \varepsilon_{jil} p_k p_l D_{ij} \delta_{jk} \right) \right] \\
&\quad + \boldsymbol{\delta}_j \left[-Y_H \left(\frac{1}{X_C} - \frac{1}{Y_C} \right) \left(\varepsilon_{kil} p_j p_l p_j p_k D_{ij} \delta_{jk} + \varepsilon_{jil} p_k p_l p_j p_k D_{ij} \delta_{jk} \right) \right]
\end{aligned}$$

$$\text{(A.30)}$$

with:

$$\varepsilon_{jil} p_l D_{ij} = \sum_{j=1}^{3} \sum_{k=1}^{3} \sum_{l=1}^{3} \varepsilon_{jil} p_l D_{ij} = 0$$

$$\varepsilon_{kil}p_jp_lp_jp_kD_{ij}\delta_{jk} = \varepsilon_{kil}p_j^2p_lp_kD_{ij}\delta_{jk} = \varepsilon_{kil}p_lp_kD_{ik} = 0$$

$$\varepsilon_{jil}p_kp_lp_jp_kD_{ij}\delta_{jk} = \varepsilon_{jil}p_k^2p_lp_jD_{ij}\delta_{jk} = \varepsilon_{jil}p_lp_jD_{ij}\delta_{jk} = \left(\varepsilon_{jil}p_lD_{ij}\right)p_j\delta_{jk} = 0$$

$$\Rightarrow \boldsymbol{\omega}_2 = -\frac{Y_H}{Y_C}\varepsilon_{kil}p_jp_lD_{ij}\delta_{jk}(j=k) \Leftrightarrow \boldsymbol{\omega}_2 = -\frac{Y_H}{Y_C}\varepsilon_{jil}p_kp_lD_{ik} \Leftrightarrow \boldsymbol{\omega}_2 = -\frac{Y_H}{Y_C}\varepsilon_{ikl}p_jp_lD_{kj}$$

Let $p_m = B_m$ and $(\omega_2)_i = C_i$.

Using equation (A.5):

$$
\begin{aligned}
-\mathbf{p} \times \boldsymbol{\omega}_2 &= \frac{Y_H}{Y_C}\varepsilon_{nmi}\varepsilon_{ikl}p_mp_jp_lD_{kj}\boldsymbol{\delta}_n \\
&= \frac{Y_H}{Y_C}\varepsilon_{nmi}\varepsilon_{kli}p_mp_jp_lD_{kj}\boldsymbol{\delta}_n \\
&= \frac{Y_H}{Y_C}p_mp_jp_lD_{kj}\left(\delta_{nk}\delta_{ml} - \delta_{nl}\delta_{mk}\right)\boldsymbol{\delta}_n \\
&= \left(\frac{Y_H}{Y_C}p_mp_jp_lD_{kj}\delta_{nk}\delta_{ml} - \frac{Y_H}{Y_C}p_mp_jp_lD_{kj}\delta_{nl}\delta_{mk}\right)\boldsymbol{\delta}_n \\
&\quad (n=k\,;\ m=l;\ n=l;\ m=k) \\
&= \left(\frac{Y_H}{Y_C}p_mp_jp_mD_{nj} - \frac{Y_H}{Y_C}p_kp_jp_nD_{kj}\right)\boldsymbol{\delta}_n \\
&= \left(\frac{Y_H}{Y_C}p_m^2p_jD_{nj} - \frac{Y_H}{Y_C}p_kp_jp_nD_{kj}\right)\boldsymbol{\delta}_n \\
&= \left(\frac{Y_H}{Y_C}p_m^2p_jD_{nj} - \frac{Y_H}{Y_C}p_kp_jp_nD_{kj}\right)\boldsymbol{\delta}_n \\
&= \left(\frac{Y_H}{Y_C}p_jD_{nj} - \frac{Y_H}{Y_C}D_{kj}p_kp_jp_n\right)\boldsymbol{\delta}_n \\
&= \lambda\mathbf{D}\cdot\mathbf{p} - \lambda\mathbf{D}:(\mathbf{p}\otimes\mathbf{p})
\end{aligned}
\tag{A.31}
$$

This is obtained by using equation (A.3), with $\lambda = \dfrac{Y_H}{Y_C}$.

Finally:

$$
\begin{aligned}
\dot{\mathbf{p}} &= \frac{1}{\pi\eta_0 l^{(\alpha)3}}\frac{1}{Y_C^{(\alpha)}}\left(\sum_{\beta\neq\alpha}l^{(\alpha,\beta)}F_c^{(\alpha,\beta)}\mathbf{n}^{(\alpha,\beta)} + \sum_{\mu\neq\alpha}l^{(\alpha,\mu)}F_{lb}^{(\alpha,\mu)}\mathbf{n}^{(\alpha,\mu)}\right) \\
&\quad + \lambda^{(\alpha)}\mathbf{D}\cdot\mathbf{p}^{(\alpha)} - \lambda\mathbf{D}:(\mathbf{p}^{(\alpha)}\otimes\mathbf{p}^{(\alpha)}) + \mathbf{W}\cdot\mathbf{p}^{(\alpha)} \\
&= \frac{1}{\pi\eta_0 l^{(\alpha)3}}\frac{1}{Y_C^{(\alpha)}}\left(\sum_{\beta\neq\alpha}l^{(\alpha,\beta)}F_c^{(\alpha,\beta)}\mathbf{n}^{(\alpha,\beta)} + \sum_{\mu\neq\alpha}l^{(\alpha,\mu)}F_{lb}^{(\alpha,\mu)}\mathbf{n}^{(\alpha,\mu)}\right) + \dot{\mathbf{p}}_J^{(\alpha)}
\end{aligned}
\tag{A.32}
$$

A.4.2   Detailed calculation of $\dot{\mathbf{q}}^{(\alpha)}$

$$\dot{\mathbf{q}} = -\boldsymbol{\zeta}^{-1} \cdot \mathbf{F}$$
$$= \frac{1}{3\pi\eta_0 l Y_A}\mathbf{I} \cdot \mathbf{F} + \frac{1}{3\pi\eta_0 l}\left(\frac{1}{X_A} - \frac{1}{Y_A}\right)\mathbf{p} \otimes \mathbf{p} \cdot \mathbf{F} \tag{A.33}$$

with $\mathbf{F} = \displaystyle\sum_{\beta \neq \alpha} F_c^{(\alpha,\beta)}\mathbf{n}^{(\alpha,\beta)} + \sum_{\mu \neq \alpha} F_{lb}^{(\alpha,\mu)}\mathbf{n}^{(\alpha,\mu)}$

and:
$$\boldsymbol{\zeta}^{-1} = -\frac{1}{3\pi\eta_0 l}\left[\frac{1}{Y_A}\mathbf{I} + \left(\frac{1}{X_A} - \frac{1}{Y_A}\right)\mathbf{p}^{(\alpha)} \otimes \mathbf{p}^{(\alpha)}\right] \text{ [82]}.$$

But:

$$
\begin{aligned}
\mathbf{p} \otimes \mathbf{p} \cdot \mathbf{n} &=
\begin{bmatrix}
p_1^2 & p_1 p_2 & p_1 p_3 \\
p_1 p_2 & p_2^2 & p_2 p_3 \\
p_1 p_3 & p_2 p_3 & p_3^2
\end{bmatrix}
\begin{bmatrix}
n_1 \\ n_2 \\ n_3
\end{bmatrix} \\
&=
\begin{bmatrix}
p_1^2 n_1 + p_1 p_2 n_2 + p_1 p_3 n_3 \\
p_1 p_2 n_1 + p_2^2 n_2 + p_2 p_3 n_3 \\
p_1 p_3 n_1 + p_2 p_3 n_2 + p_3^2 n_3
\end{bmatrix} \\
&=
\begin{bmatrix}
p_1 \left(p_1 n_1 + p_2 n_2 + p_3 n_3\right) \\
p_2 \left(p_1 n_1 + p_2 n_2 + p_3 n_3\right) \\
p_3 \left(p_1 n_1 + p_2 n_2 + p_3 n_3\right)
\end{bmatrix} \\
&=
\begin{bmatrix}
0 \\ 0 \\ 0
\end{bmatrix} \\
&= \mathbf{0}
\end{aligned}
\tag{A.34}
$$

Because $\mathbf{n} \perp \mathbf{p}$. Thus:

$$\dot{\mathbf{q}}^{(\alpha)} = \frac{1}{3\pi\eta_0 l^{(\alpha)} Y_A^{(\alpha)}}\left(\sum_{\beta \neq \alpha} F_c^{(\alpha,\beta)}\mathbf{n}^{(\alpha,\beta)} + \sum_{\mu \neq \alpha} F_{lb}^{(\alpha,\mu)}\mathbf{n}^{(\alpha,\mu)}\right) \tag{A.35}$$

A.5   Detailed expressions of $\Gamma_{ijkl}^{(0)}$, $\Gamma_{ijkl}^{(1)}$ and $\Gamma_{ijkl}^{(2)}$

These expressions are given by Kim and Karilla [82] as:

$$
\begin{aligned}
\Gamma_{ijkl}^{(0)} &= \frac{3}{2}\left(p_i p_j - \frac{1}{3}\delta_{ij}\right)\left(p_k p_l - \frac{1}{3}\delta_{kl}\right) \\
\Gamma_{ijkl}^{(1)} &= \frac{1}{2}\left(p_i \delta_{jl} p_k + p_j \delta_{kl} p_k + p_i \delta_{jk} p_l + p_j \delta_{ik} p_l - 4 p_i p_j p_k p_l\right) \\
\Gamma_{ijkl}^{(2)} &= \frac{1}{2}\Big(\delta_{ik}\delta_{jl} + \delta_{jk}\delta_{il} - \delta_{ij}\delta_{kl} + p_i p_j \delta_{kl} + \delta_{ij} p_k p_l - p_i \delta_{jl} p_k \\
&\qquad - p_j \delta_{il} p_k - p_i \delta_{jk} p_l - p_j \delta_{ik} p_l + p_i p_j p_k\Big)
\end{aligned}
\tag{A.36}
$$

A.6 Hydrodynamic coefficients

Let:

$$e = \frac{\sqrt{r^2 - 1}}{r} \tag{A.37}$$

and:

$$L = ln\left(\frac{1 + e}{1 - e}\right) \tag{A.38}$$

then these coefficients are defined as [82]:

$$X_A = \frac{8}{3}e^3\left[-2e + \left(1 + e^2\right)L\right]^{-1} \tag{A.39}$$

$$Y_A = \frac{16}{3}e^3\left[2e + \left(3e^2 - 1\right)L\right]^{-1} \tag{A.40}$$

$$X_C = \frac{4}{3}e^3\left(1 - e^2\right)\left[2e - \left(1 - e^2\right)L\right]^{-1} \tag{A.41}$$

$$Y_C = \frac{4}{3}e^3\left(2 - e^2\right)\left[\left(1 + e^2\right)L - 2e\right]^{-1} \tag{A.42}$$

$$Y_H = \frac{4}{3}e^5\left[\left(1 + e^2\right)L - 2e\right]^{-1} \tag{A.43}$$

$$X_M = \frac{8}{15}e^5\left[\left(3 - e^2\right)L - 6e\right]^{-1} \tag{A.44}$$

$$Y_M = \frac{4}{5}e^5\left[2e\left(1 - 2e^2\right) - \left(1 - e^2\right)L\right] \tag{A.45}$$

$$Z_M = \frac{16}{5}e^5\left(1 - e^2\right)\left[3\left(1 - e^2\right)^2 L - 2e\left(3 - 5e^2\right)\right]^{-1} \tag{A.46}$$

Kinetic theory Appendix

Contents

B.1 Detailed calculation

B.1.1 Detailed calculation of $\left(\mathbf{t}^T \cdot \nabla\mathbf{v} \cdot \mathbf{p}\right)\mathbf{t} = \nabla\mathbf{v}{\cdot}\mathbf{p}{-}\left(\mathbf{p}^T \cdot \nabla\mathbf{v} \cdot \mathbf{p}\right)\mathbf{p}$

In 2D, $\mathbf{p}$ is defined from equation (5.28). Thus, $\mathbf{p}$ can be written as:

$$\mathbf{p}^T = [cos\left(\theta\right),\ sin\left(\theta\right)] \tag{B.1}$$

with:

$$\mathbf{t}^T = \frac{\partial \mathbf{p}^T}{\partial \theta} = [-sin\left(\theta\right),\ cos\left(\theta\right)] \tag{B.2}$$

The velocity gradient is (in a simple shear flow):

$$\nabla\mathbf{v} = \begin{bmatrix} 0 & \dot{\gamma} \\ 0 & 0 \end{bmatrix} \tag{B.3}$$

Thus:

$$
\begin{aligned}
\left(\mathbf{t}^T \cdot \nabla \mathbf{v} \cdot \mathbf{p}\right) \mathbf{t} \\
= \left([-sin\,(\theta)\,,\ cos\,(\theta)] \cdot \begin{bmatrix} 0 & \dot{\gamma} \\ 0 & 0 \end{bmatrix} \cdot [cos\,(\theta)\,,\ sin\,(\theta)] \right) [-sin\,(\theta)\,,\ cos\,(\theta)] \\
= \left([-sin\,(\theta)\,,\ cos\,(\theta)] \cdot \begin{bmatrix} \dot{\gamma}sin\,(\theta) \\ 0 \end{bmatrix} \right) [-sin\,(\theta)\,,\ cos\,(\theta)] \\
= \dot{\gamma}sin^2\,(\theta) \begin{bmatrix} sin\,(\theta) \\ -cos\,(\theta) \end{bmatrix}
\end{aligned}
\tag{B.4}
$$

And:

$$
\begin{aligned}
\nabla \mathbf{v} \cdot \mathbf{p} - \left(\mathbf{p}^T \cdot \nabla \mathbf{v} \cdot \mathbf{p}\right) \mathbf{p} \\
= \begin{bmatrix} \dot{\gamma}sin\,(\theta) \\ 0 \end{bmatrix} - \dot{\gamma}sin\,(\theta)\,cos\,(\theta) \begin{bmatrix} cos\,(\theta) \\ sin\,(\theta) \end{bmatrix} \\
= \dot{\gamma}sin\,(\theta) \begin{bmatrix} 1 - cos^2\,(\theta) \\ -sin\,(\theta)\,cos\,(\theta) \end{bmatrix} \\
= \dot{\gamma}sin\,(\theta) \begin{bmatrix} sin^2\,(\theta) \\ -sin\,(\theta)\,cos\,(\theta) \end{bmatrix} \\
= \dot{\gamma}sin^2\,(\theta) \begin{bmatrix} sin\,(\theta) \\ -cos\,(\theta) \end{bmatrix}
\end{aligned}
\tag{B.5}
$$

Therefore:

$$
\left(\mathbf{t}^T \cdot \nabla \mathbf{v} \cdot \mathbf{p}\right) \mathbf{t} = \nabla \mathbf{v} \cdot \mathbf{p} - \left(\mathbf{p}^T \cdot \nabla \mathbf{v} \cdot \mathbf{p}\right) \mathbf{p}
\tag{B.6}
$$

B.1.2   Detailed calculation of $\boldsymbol{\omega} = \int_{\mathcal{S}} \left(\mathbf{p} \times (\nabla \mathbf{v} \cdot \mathbf{p})\right)\,\psi(\mathbf{p})\,d\mathbf{p}$

Using equation (A.5) from section A.2, one can write:

$$
\begin{aligned}
\boldsymbol{\omega} &= \int_{\mathcal{S}} \left(\mathbf{p} \times (\nabla \mathbf{v} \cdot \mathbf{p})\right)\,\psi(\mathbf{p})\,d\mathbf{p} \\
&= \int_{S} \varepsilon_{ijk} p_j\,(\nabla v)_{kl}\,p_l \psi\,(\mathbf{p}) \\
&= \boldsymbol{\varepsilon} : \left(\mathbf{a} \cdot (\nabla \mathbf{v})^T\right)
\end{aligned}
\tag{B.7}
$$

Then using equation (A.6) from section A.3 it results (with $\mathbf{K} = \mathbf{a} \cdot (\nabla \mathbf{v})^T$)

$$\omega_i = \boldsymbol{\varepsilon} : (\mathbf{K}) = \left[\left\{ \sum_{i=1}^{3} \sum_{j=1}^{3} \sum_{k=1}^{3} \boldsymbol{\delta}_i \boldsymbol{\delta}_j \boldsymbol{\delta}_k \varepsilon_{ijk} \right\} : \left\{ \sum_{l=1}^{3} \sum_{m=1}^{3} \boldsymbol{\delta}_l \boldsymbol{\delta}_m K_{lm} \right\} \right]$$

$$= \sum_{i=1}^{3} \sum_{j=1}^{3} \sum_{k=1}^{3} \sum_{l=1}^{3} \sum_{m=1}^{3} \left(\boldsymbol{\delta}_i \boldsymbol{\delta}_j \boldsymbol{\delta}_k : \boldsymbol{\delta}_l \boldsymbol{\delta}_m \right) \varepsilon_{ijk} K_{lm}$$

$$= \sum_{i=1}^{3} \sum_{j=1}^{3} \sum_{k=1}^{3} \sum_{l=1}^{3} \sum_{m=1}^{3} \left(\boldsymbol{\delta}_i \delta_{jm} \delta_{kl} \right) \varepsilon_{ijk} K_{lm} \qquad \text{(B.8)}$$

$$= \sum_{i=1}^{3} \sum_{j=1}^{3} \sum_{k=1}^{3} \boldsymbol{\delta}_i \varepsilon_{ijk} K_{kj}$$

$$= \varepsilon_{ijk} K_{kj}$$

$$= \varepsilon_{i11} K_{11} + \varepsilon_{i12} K_{21} + \varepsilon_{i21} K_{12} + \varepsilon_{i22} K_{22}$$

Using equations (A.1) this is reduced to:

$$\omega_i = \varepsilon_{i12} K_{21} + \varepsilon_{i21} K_{12} = K_{21} - K_{12} \qquad \text{(B.9)}$$

But,

$$\mathbf{K} = \mathbf{a} \cdot (\mathbf{D} - \mathbf{\Omega})$$

$$= \begin{bmatrix} a_{11} & a_{12} \\ a_{12} & a_{22} \end{bmatrix} \cdot \begin{bmatrix} D_{11} - \Omega_{11} & D_{12} - \Omega_{12} \\ D_{21} - \Omega_{21} & D_{22} - \Omega_{22} \end{bmatrix}$$

$$= \begin{bmatrix} a_{12} \left(D_{21} - \Omega_{21} \right) & a_{11} \left(D_{12} - \Omega_{12} \right) \\ a_{22} \left(D_{21} - \Omega_{21} \right) & a_{12} \left(D_{12} - \Omega_{12} \right) \end{bmatrix} \qquad \text{(B.10)}$$

$$= a_{22} \left(D_{21} - \Omega_{21} \right) - a_{11} \left(D_{12} - \Omega_{12} \right)$$

$$= \left(1 - a_{11} \right) \left(D_{21} - \Omega_{21} \right) - a_{11} \left(D_{12} - \Omega_{12} \right)$$

$$= 2 D_{12} - 2 D_{12} a_{11}$$

with:

$$\mathbf{D} = \begin{bmatrix} 0 & \dfrac{\dot{\gamma}}{2} \\ \dfrac{\dot{\gamma}}{2} & 0 \end{bmatrix} \qquad \text{(B.11)}$$

and:

$$\mathbf{\Omega} = \begin{bmatrix} 0 & \dfrac{\dot{\gamma}}{2} \\ -\dfrac{\dot{\gamma}}{2} & 0 \end{bmatrix} \qquad \text{(B.12)}$$

Then,

$$\omega_3 = 2 D_{12} - 2 D_{12} a_{11} \qquad \text{(B.13)}$$

Thus, in the 2D case when $\mathbf{p}^T = [p_1, p_2, 0]$ and $\boldsymbol{\omega}^T = [0, 0, \omega_3]$:

$$\mathbf{W} = \begin{bmatrix} 0 & \omega_3 \\ -\omega_3 & 0 \end{bmatrix} \qquad \text{(B.14)}$$

It can be shown that $\mathbf{W} = \mathbf{\Omega} + \mathbf{D} \cdot \mathbf{a} - \mathbf{a} \cdot \mathbf{D}$. In fact:

$$\mathbf{D} \cdot \mathbf{a} = \left[\begin{array}{cc} a_{12}D_{12} & a_{22}D_{12} \\ a_{11}D_{12} & a_{12}D_{12} \end{array} \right] \tag{B.15}$$

and

$$\mathbf{a} \cdot \mathbf{D} = \left[\begin{array}{cc} a_{12}D_{12} & a_{11}D_{12} \\ a_{22}D_{12} & a_{12}D_{12} \end{array} \right] \tag{B.16}$$

Thus,

$$\begin{aligned} \mathbf{\Omega} + \mathbf{D} \cdot \mathbf{a} - \mathbf{a} \cdot \mathbf{D} &= \left[\begin{array}{cc} 0 & \left(1 - a_{11}\right) D_{12} - a_{11}D_{12} + \Omega_{12} \\ a_{11}D_{12} - \left(1 - a_{11}\right) D_{12} + \Omega_{21} & 0 \end{array} \right] \\ &= \left[\begin{array}{cc} 0 & 2D_{12} - 2D_{12}a_{11} \\ -\left(2D_{12} - 2D_{12}a_{11}\right) & 0 \end{array} \right] \\ &= \left[\begin{array}{cc} 0 & \omega_3 \\ -\omega_3 & 0 \end{array} \right] \\ &= \mathbf{W} \end{aligned} \tag{B.17}$$

B.1.3 Detailed calculation of $\dot{\mathbf{p}}_i = \mathbf{G} \cdot \mathbf{p}_i - \left(\mathbf{G} : \left(\mathbf{p}_i \otimes \mathbf{p}_i\right)\right) \mathbf{p}_i$

Having:

$$\mathbf{G} = \frac{\mu\,\mathbf{W} + \xi\,\nabla\mathbf{v}}{\xi + \mu} \tag{B.18}$$

Then:

$$\mathbf{G} : \left(\mathbf{p} \otimes \mathbf{p}\right) = \left(\frac{\mu\,\mathbf{W} + \xi\,\nabla\mathbf{v}}{\xi + \mu}\right) : \mathbf{P} \tag{B.19}$$

Using equation (A.6) from section A.3 it results (with $\mathbf{P} = \mathbf{p} \otimes \mathbf{p}$):

$$\mathbf{W} : \mathbf{P} = W_{ij}P_{ji} = 0 \tag{B.20}$$

with $W_{12} = -W_{21}$. Then:

$$\nabla\mathbf{v} : \mathbf{P} = \left(\mathbf{D} + \mathbf{\Omega}\right) : \mathbf{P} \tag{B.21}$$

with

$$\mathbf{\Omega} : \mathbf{P} = \Omega_{ij}P_{ji} = 0 \tag{B.22}$$

and $\Omega_{12} = -\Omega_{21}$. Finally:

$$\mathbf{G} : \left(\mathbf{p} \otimes \mathbf{p}\right) = \mathbf{D} : \left(\mathbf{p} \otimes \mathbf{p}\right) \tag{B.23}$$

and:

$$\dot{\mathbf{p}}_i = \mathbf{G} \cdot \mathbf{p}_i - \frac{\xi}{\xi + \mu} \left(\mathbf{D} : \left(\mathbf{p}_i \otimes \mathbf{p}_i\right)\right) \mathbf{p}_i \tag{B.24}$$

List of Tables

List of Figures

Bibliography

[1] S. G. Advani. *Flow and Rheology in Polymer Composites Manufacturing*. Elsevier Publishers, Amsterdam 1994. 21

[2] L.A. Berglund and M. L. Ericson. *Polypropylene: Structure, Blends and Composites*. (Chapman and Hall, London), 1995. 21

[3] K. A. Ericsson, S. Toll, and J. A. E. Manson. Sliding plate rheometry of planar oriented concentrated fiber suspension. *Rheologica Acta*, 36:397–405, 1997. 21, 26

[4] C. Binetruy, F. Chinesta, and R. Keunings. *Flows in polymers, reinforced polymers and composites. A multiscale approach.* Springer, 2015. 24, 97

[5] R.B. Bird, C.F. Curtiss, R.C. Armstrong, and O. Hassager. *Dynamics of polymeric liquids, Volume 2, Kinetic Theory*. John Wiley and Sons, 1987. 24, 93

[6] M. Doi and S.F. Edwards. *The Theory of Polymer Dynamics*. Clarendon Press, Oxford, 1987. 24, 93

[7] A. Ammar and F. Chinesta. A particle strategy for solving the fokker-planck equation governing the fibre orientation distribution in steady recirculating flows involving short fibre suspensions. *In Lectures Notes on Computational Science and Engineering, Springer*, 43:1–16, 2005. 24

[8] C.V. Chaubal, A. Srinivasan, O. Egecioglu, and L.G. Leal. Smoothed particle hydrodynamics techniques for the solution of kinetic theory problems. *Journal of Non Newtonian Fluid Mechanics*, 70:125–154, 1997. 24

[9] F. Chinesta, G. Chaidron, and A. Poitou. On the solution of the fokker- planck equation in steady recirculating flows involving short fibre suspensions. *Journal of Non Newtonian Fluid Mechanics*, 113:97–125, 2003. 24

[10] C. Cruz, L. Illoul, F. Chinesta, and G. Regnier. Effects of a bent structure on the linear viscoelastic response of carbon nanotube diluted suspensions. *Rheologica Acta*, 49:1141–1155, 2010. 24, 26, 27

[11] C. Cruz, F. Chinesta, and G. Regnier. Review on the brownian dynamics simulation of bead-rod-spring models encountered in computational rheology. *Archives of Computational Methods in Engineering*, 19/2:227–259, 2012. 24, 27, 98

[12] H.C. Ottinger, M. Laso, P. Moldenaers, and R. Keunings. Smart polymers in finite-element calculations in theoretical and applied rheology. *Proceedings on the XIth International Congress on Rheology, Elsevier, Amsterdam*, 1:286–288, 1992. 24

[13] P. Wapperom, R. Keunings, and V. Legat. The backward-tracking lagrangian particle method for transient viscoelastic fows. *Journal of Non Newtonian Fluid Mechanics*, 91:273–295, 2000. 24

[14] P. Wapperom and R. Keunings. Numerical simulation of branched polymer melts in transient complex fows using pom-pom models. *Journal of Non Newtonian Fluid Mechanics*, 97:267–281, 2001. 24

[15] C. Chauviere and A. Lozinski. Simulation of dilute polymer solutions using a fokker-planck equation. *Computer and Fluids*, 33:687–696, 2004. 24

[16] A. Lozinski and C. Chauviere. A fast solver for fokker-planck equation applied to viscoelastic fows calculations: 2d fene model. *Journal of Computational Physics*, 189:607–625, 2003. 24

[17] S. G. Advani and C. L. Tucker. The use of tensors to describe and predict fiber orientation in short fiber composites. *Journal of Rheology*, 31(8):751–784, 1987. 24, 25, 45, 93, 98

[18] S. Advani. Flow and rheology in polymer composites manufacturing. *Composite Materials Series, Elsevier New York*, 10, 1994. 24, 25

[19] S. Advani and C. Tucker. Closure approximations for three-dimensional structure tensors. *Journal of Rheology*, 34:367–386, 1990. 24, 98, 106

[20] K. Chiba, A. Ammar, and F. Chinesta. On the fiber orientation in steady recirculating fows involving short fibers suspensions. *Rheologica Acta*, 44:406–417, 2005. 24

[21] R. Keunings. On the peterlin approximation for finitely extensible dumbbells. *Journal of Non Newtonian Fluid Mechanics*, 68:85–100, 1997. 24

[22] G. B. Jeffery. The motion of ellipsoidal particles immersed in a viscous fluid. *Proceedings Royal Society*, A102(161), 1922. 25, 49, 93, 96

[23] G. Ausias, J. F. Agassant, M. Vincent, P. G. Lafleur, P. A. Lavoie, and P. J. Carreau. Rheology of short glass fiber reinforced polypropylene. *Journal of Rheology*, 36 (4):525–542, 1992. 25, 70

[24] G. G. Lipscomb, M. M. Denn, D. H. Hur, and D. V. Boger. The flow of fiber suspensions in complex geometries. *Journal of Non-Newtonian Fluid Mechanics*, 26:297–325, 1988. 25

[25] N. Phan-Thien and A. L. Graham. A new constitutive model for fibre suspensions: Flow past a sphere. *Rheologica Acta*, 30:44–57, 1991. 25

[26] G. Batchelor. The stress system in a suspension of force-free particles. *Journal of Fluid Mechanics*, 41:545–570, 1970a. 25

[27] G. Batchelor. Transport properties of two-phase materials with random structure. *Annual Review of Fluid Mechanics*, 6:227–255, 1974. 25

[28] G. Batchelor. Slender-body theory for particles of arbitrary cross-section in stokes flow. *Journal of Fluid Mechanics*, 44:419–440, 1970b. 25

[29] G. Batchelor. The stress generated in a non-dilute suspension of elongated particles by pure straining motion. *Journal of Non Newtonian Fluid Mechanics*, 46(4):813–829, 1971. 25

[30] S. M. Dinh and R. C. Armstrong. A rheological equation of the state for semiconcentrated fiber suspensions. *Journal of Rheology*, 28:207–227, 1984. 25

[31] D. L. Koch. A model for orientational diffusion in fiber suspensions. *Physics of Fluids*, 7:2086–2088, 1995. 25

[32] D. L. Koch and E. S. G. Shaqfeh. The average rotation rate of a fiber in the linear flow of a semidilute suspension. *Physics of Fluids*, 2:2093–2102, 1990. 25

[33] E. S. G. Shaqfeh and D. Koch. Orientational dispersion of fibers in extensional flows. *Physics of Fluids*, 2:1077–1093, 1990. 25

[34] M. P. Petrich, D. L. Koch, and C. Cohen. An experimental determination of the stress microstructure relationship in semi-concentrated fiber suspensions. *Journal of Non Newtonian Fluid Mechanics*, 95:101–133, 2000. 25, 71

[35] E. S. G. Shaqfeh and M. B. Mackaplow. A numerical study of the rheological properties of suspensions of rigid, non-brownian fibres. *Journal of Fluid Mechanics*, 329:155–186, 1996. 25, 26

[36] R. R. Sundararajakumar and D. L. Koch. Structure and properties of sheared fiber suspensions with mechanical contacts. *Journal of Non Newtonian Fluid Mechanics*, 54:205–239, 1997. 25, 26, 45

[37] F. Dupret and V. Verleye. Modelling the flow of fiber suspensions in narrow gaps. *Elsevier, Amsterdam*, pages 1347–1398, 1999. 25, 98, 106

[38] G. L. Hand. A theory of anisotropic fluids. *Journal of Fluid Mechanics*, 13:33–46, 1962. 25

[39] J. M. W. Munganga, B. D. Reddy, and K. J. Diatezua. Aspects of the thermodynamic stability of fibre suspension flows. *Journal of Non Newtonian Fluid Mechanics*, 92:135–150, 2000. 25

[40] F. P. Bretherton. The motion of rigid particles in a shear flow at low reynolds number. *Journal of Fluid Mechanics*, 14:284–304, 1962. 25

[41] X. J. Fan, N. Phan-Thien, and R. Zheng. A direct simulation of fiber suspensions. *Journal of Non-Newtonian Fluid Mechanics*, 74:113–135, 1998. 25, 26, 43, 56, 83

[42] F. Folgar, C. Tucker, and C. Lee. Simulation of compression molding for fiber-reinforced thermosetting polymers. *Journal of Fluid Engineering*, 106:114–125, 1984. 25

[43] N. Phan-Thien, X. J. Fan, R. I. Tanner, and R. Zheng. Folgar-tucker constant for a fibre suspension in a newtonian fluid. *Journal of Non Newtonian Fluid Mechanics*, 103:251–260, 2002. 25

[44] M. Rahnama, D. L. Koch, and C. Cohen. Observations of fiber orientation in suspensions subjected to planar extensional flows. *Physics of Fluids*, 7:1811–1817, 1995. 25

[45] D. H. Chung and T. H. Kwon. Fiber orientation in the processing of polymer composites. *Korea-Australia Rheology Journal*, 14:175–188, 2002. 25

[46] J. S. Cintra and C. L. Tucker. Orthotropic closure approximations for flow-induced fiber orientation. *Journal of Rheology*, 39:207–227, 1995. 25

[47] E. J. Hinch and L. G. Leal. Constitutive equations in suspension mechanics. Part1. General formulation. *Journal of Fluid Mechanics*, 71:481–195, 1975. 25

[48] G. P. Galdi and B. D. Reddy. Well-posedness of the problem of fiber suspension flows. *Journal of Non Newtonian Fluid Mechanics*, 83:205–230, 1999. 25

[49] F. P. Folgar and C. L. Tucker. Orientation behavior of fibers in concentrated suspensions. *Journal of Reinforced Plastic Composites*, 3:99, 1984. 25, 26, 102

[50] J. Hinch and G. Leal. The effect of brownian motion on the rheological properties of a suspension of non-spherical particles. *Journal of Fluid Mechanics*, 52:683–712, 1972. 25

[51] J. Hinch and G. Leal. Constitutive equations in suspension mechanics. Part ii. *Journal of Fluid Mechanics*, 76:187–208, 1976. 25

[52] J. Azaiez, K. Chiba, F. Chinesta, and A. Poitou. State-of-the-art on numerical simulation of fiber-reinforced thermoplastic forming processes. *Archives of Computational Methods in Engineering*, 9/2:141–198, 2002. 25

[53] E. Cueto, R. Monge, F. Chinesta, A. Poitou, I. Alfaro, and M. Mackley. Rheological modeling and forming process simulation of cnt nanocomposites. *International Journal of Material Forming*, 3/2:1327–1338, 2010. 25

[54] C. Tucker. Flow regimes for fiber suspensions in narrow gaps. *Journal of Non-Newtonian Fluid Mechanics*, 39:239–268, 1991. 25

[55] A. Ma, F. Chinesta, and M. Mackley. The rheology and modelling of chemically treated carbon nanotube suspensions. *Journal of Rheology*, 53/3:547–573, 2009. 25, 102

[56] C. J. S. Petrie. The rheology of fiber suspensions. *Journal of Non Newtonian Fluid Mechanics*, 87:369–402, 1999. 25

[57] M. P. Petrich and D. L. Koch. Interactions between contacting fibers. *Physics of Fluids*, 10:2111–2113, 1998. 26

[58] C. Servais, A. Luciani, and J.A. E. Manson. Fiber-fiber interaction in concentrated suspensions: Dispersed fiber bundles. *Journal of Rheology*, 43:1005–1018, 1999a. 26

[59] C. G. Joung, N. Phan-Thien, and X. J. Fan. Viscosity of curved fibers in suspension. *Journal of Non Newtonian Fluid Mechanics*, 102 (1):1–17, 2002. 26, 68

[60] L. H. Switzer and D. J. Klingenberg. Rheology of sheared flexible fiber suspensions via fiber-level simulations. *Journal of Rheology*, 47:759–778, 2003. 26

[61] Y. Yamane, Y. Kaneda, and M. Doi. The effect of interaction of rodlike particles in semi-dilute suspensions under shear flow. *Journal of the Physical Society of Japan*, 64:3265–3274, 1995. 26

[62] J. Férec, G. Ausias, M. C. Heuzey, and P. J. Carreau. Modeling fiber interactions in semiconcentrated fiber suspensions. *Journal of Rheology*, 53(1):49–72, 2009. 26, 47, 48, 102

[63] J. Wang, C.A. Silva, J.C. Viana, F.W.J. van Hattum, A.M. Cunha, and C. Tucker. Prediction of fiber orientation in a rotating compressing and expanding mold. *Polymer Engineering and Science*, pages 1405–1413, 2008. 26

[64] J. Wang, J. O'Gara, and C. Tucker. An objective model for slow orientation kinetics in concentrated fiber suspensions: Theory and rheological evidence. *Journal of Rheology*, 52/5:1179–1200, 2008. 26

[65] J. Phelps and C.Tucker. An anisotropic rotary diffusion model for fiber orientation in short and long fiber thermoplastics. *Journal of Non Newtonian Fluid Mechanics*, 156/3:165–176, 2009. 26

[66] A. Ma, F. Chinesta, A. Ammar, and M. Mackley. Rheological modelling of carbon nanotube aggregate suspensions. *Jounral of Rheology*, 52/6:1311–1330, 2008. 26, 102, 107

[67] G. Ausias, X. J. Fan, and R. I. Tanner. Direct simulations for concentrated fiber suspensions in transient and steady state shear flows. *Journal of Non-Newtonian Fluid Mechanics*, 135:46–57, 2006. 26, 33, 45, 102

[68] S. Le Corre, D. Caillerie, L. Orgeas, and D. Favier. Behavior of a net of fibers linked by viscous interactions: Theory and mechanical properties. *Journal of the Mechanics and Physics of Solids*, volume 52:395–421, 2004. 26, 33, 44

[69] S. Le Corre, P. Dumont, L. Orgeas, and D. Favier. Rheology of highly concentrated planar fiber suspensions. *Journal of Rheology*, volume 49:1029–1058, 2005. 26, 33

[70] R. Mezher, E. Abisset-Chavanne, J. Férec, G. Ausias, and F. Chinesta. Direct simulation of concentrated fiber suspensions subjected to bending effects. *Modelling and Simulation in Materials Science and Engineering*, 23 055007.:1–28, 2015. 26, 50, 102

[71] E. Abisset-Chavanne, R. Mezher, S. Le Corre, A. Ammar, and F. Chinesta. Kinetic theory microstructure modeling in concentrated suspensions. *Entropy*, 15:2805–2832, 2013. 26, 69, 119

[72] E. Abisset-Chavanne, F. Chinesta, J. Ferec, G. Ausias, and R. Keunings. On the multiscale description of dilute suspensions of non-brownian rigid clusters composed of rods. *Journal of Non Newtonian Fluid Mechanics, In press*. 26

[73] K. Ortman, D. Baird, P. Wapperom, and A. Whittington. Using startup of steady shear flow in a sliding plate rheometer to determine material parameters for the purpose of predicting long fiber orientation. *Journal of Rheology*, 56:955–981, 2012. 27

[74] U. Strautins and A. Latz. Flow-driven orientation dynamics of semifexible fiber systems. *Rheologica Acta*, 46:1057–1064, 2007. 27

[75] S. Toll and J. A. E. Manson. Dynamics of a planar concentrated suspension with non-hydrodynamic interaction. *Journal of Rheology*, 38(4):985–997, 1994. 33

[76] P. Dumont, S. Le Corre, L. Orgeas, and D. Favier. A numerical analysis of the evolution of bundle orientation in concentrated fiber-bundle suspensions. *Journal of Non Newtonian Fluid Mechanics*, 160:76–92, 2009. 33, 102

[77] S. Yamamoto and T. Matsuoka. Dynamic simulation of a platelike particle dispersed system. *Journal of Chemical Physics*, 107(8):3300–3308, 1997. 33

[78] S. Yamamoto and T. Matsuoka. A method for dynamic simulation of rigid and flexible fibers in a flow field. *Journal of Chemical Physics*, 98(1):644–650, 1993. 33

[79] C. Pozrikidis. Orientation statistics and effective viscosity of suspensions of elongated particles in simple shear flow. *European Journal of Mechanics B/Fluids*, 24:125–136, 2005. 33

[80] C. Mobuchon, P. J. Carreau, M. C. Heuzey, M. Sepehr, and G. Ausias. Shear and extensional properties of short glass fiber reinforced polypropylene. *Polymer Composites*, 26(3):247–263, 2005. 33

[81] M. Bornert, T. Bretheau, and P. Gilormini. *Homogénéisation en mécanique des matériaux 1 :Matériaux aléatoires élastiques et milieux périodiques*. Hermes Science Europe Paris, 2001. 38

[82] S. Kim and S. J. Karrila. *Microdynamics: Principles and Selected Applications*. Butterworth–Heinemann, Boston, 1991. 39, 40, 49, 126, 127

[83] R. Byron Bird, W. E. Stewart, and E. N. Lightfoot. *Transport Phenomena*. John Wiley and Sons, Inc., 2002. 39, 120

[84] Y. Yamane, Y. Kaneda, and M. Doi. Numerical-simulation of semidilute suspensions of rodlike particles in shear-flow. *Journal of Non Newtonian Fluid Mechanics*, 54:405–421, 1994. 43, 44

[85] O. G. Harlen, R. R. Sundararajakumar, and D. L. Koch. Numerical simulations of a sphere settling through a suspension of neutrally buoyant fibers. *Journal of Fluid Mechanics*, 388:355–388, 1999. 45

[86] M. Doi and S. F. Edwards. Dynamics of rod-like macromolecules in concentrated solution. Part 1. *Journal of the Chemical Society Faraday Transactions 2: Molecular and Chemical Physics*, 74:560–570, 1978. 47

[87] C. R. Sandstrom. *Interactions and orientation in concentrated suspensions of rigid rods: theory and experiment*. PhD thesis, University of Illinois, Urbana-Champaign, 1993. 47

[88] J. Férec, E. Abisset-Chavanne, G. Ausias, and F. Chinesta. On the use of interaction tensors to describe and predict rod interactions in rod suspensions. *Rheologica Acta, Springer*, 53:445–456, 2014. 47, 102

[89] S. Toll. Packing mechanics of fiber reinforcements. *Journal of Polymer Engineering and Science*, 38:1337–1350, 1998. 48, 76

[90] J. H. Irving and J. G. Kirkwood. The statistical mechanics of transport processes. iv. the equation of hydrodynamics. *Journal of Chemical Physics*, 18:817–829, 1950. 49

[91] S. T. Tassew and A. S. Lubell. Mechanical properties of glass fiber reinforced ceramic concrete. *Construction and Building Materials*, 51:215–224, 2014. 50

[92] A. I. Abd El-Rahman and C. L. Tucker. Mechanics of random discontinuous long-fiber thermoplastics Part I: Generation and characterization of initial geometry. *Journal of Applied Mechanics*, 80(5):0510071–05100710, 2013. 55, 57

[93] M. P. Allen and D. J. Tildesley. *Computer simulation of liquids*. Clarendon Press, 1987. 56, 57, 63

[94] A. I. Abd El-Rahman and C. L. Tucker. Mechanics of random discontinuous long-fiber thermoplastics. Part II: Direct simulation of uniaxial compression. *Journal of Rheology*, 57:1463–1489, 2013. 57

[95] G. Bossis, A. Meunier, and J. D. Sherwood. Stokesian dynamics simulations of particle trajectories near a plane. *Physics of Fluids a-Fluid Dynamics*, 3(8):1853–1858, 1991. 57

[96] M. Born and V. Karman. Overshoots in space lattices. *Journal of Physics A: Hadrons and Nuclei*, 13:297–309, 1912. 57

[97] M. Sepehr, G. Ausias, and P. J. Carreau. Rheological properties of short fiber filled polypropylene in transient shear flow. *Journal of Non Newtonian Fluid Mechanics*, 123 (1):19–32, 2004. 70, 71

[98] A. T. Mutel and M. R. Kamal. Characterization of the rheological behavior of fiber-filled polypropylene melts under steady and oscillatory shear using cone-and-plate and rotational parallel plate rheometry. *Journal of Polymer Composites*, 7 (5):283–294, 1986. 70

[99] H. M. Laun. Orientation effects and rheology of short glass fiber reinforced thermoplastics. *Colloids and Polymer Science*, 262:257–269, 1984. 70, 71

[100] B. Snook, L. M. Davidson, J. E. Butler, O. Pouliquen, and E. Guazzelli. Normal stress differences in suspensions of rigid fibers. *Journal of Fluid Mechanics*, 758:486–507, 2014. 71, 72, 73

[101] M. Sepehr, P. J. Carreau, M. Moan, and G. Ausias. Rheological properties of short fiber model suspensions. *Journal of Rheology*, 48(5):1023–1048, 2004. 82

[102] R. Keunings. Micro–macro methods for the multiscale simulation viscoelastic flow using molecular models of kinetic theory. *Rheology Reviews – British Society of Rheology*, pages 67–98, 2004. 93

[103] M. Kroger, A. Ammar, and F. Chinesta. Consistent closure schemes for statisical models of anisotropic fluids. *Jounal of Non-Newtonian Fluid Mechanics*, 149:40–55, 2008. 98, 106

[104] E. Pruliere, A. Ammar, N. El Kissi, and F. Chinesta. Recirculating flow involving short fiber suspensions: numerical difficulties and efficient advanced micro-macro solvers. *Archives of Computational Methods in Engineering State Art Review*, 16:1–30, 2009. 98, 106

[105] P. Grassia, J. Hinch, and L.C. Nitsche. Computer simulations of brownian motion of complex systems. *Journal of Fluid Mechanics*, 282:373–403, 1995. 98

[106] A. Ma, F. Chinesta, M. Mackley, and A. Ammar. The rheological modelling of carbon nanotube (CNT) suspensions in steady shear flows. *International Journal of Material Forming*, 2:83–88, 2008. 102

[107] F. Chinesta. From single–scale to two-scales kinetic theory descriptions of rods suspensions. *Archives of Computational Methods in Engineering*, 20:1–29, 2013. 105, 106

[108] R. B. Bird, R. C. Armstrong, and O. Hassager. *Dynamics of polymeric liquids, Volume 1, Fluid Mechanics*. John Wiley and Sons, 1987. 107

Thèse de Doctorat

Rabih MEZHER

Modeling and Simulation of concentrated suspensions of short, rigid and flexible fibers

Modélisation et Simulation de suspensions concentrées de fibres courtes, rigides et flexibles

Résumé

Les suspensions de nanoparticules - en particulier nanofibres et nanotubes - sont de plus en plus utilisées dans le cadre du développement de matériaux fonctionnels. Afin d'optimiser l'utilisation de ces matériaux et leurs procédés de fabrication, une connaissance fine de la microstructure et de son évolution lors d'un écoulement est primordiale. Pour cela, l'étude des suspensions se divise en deux axes de recherche : le régime dilué où la concentration est faible et chaque particule peut être décrite seule, et le régime concentré où l'on ne peut plus négliger l'interaction entre les particules, ni la formation d'agrégats. Le premier type de suspensions est bien connu ; le second reste encore problématique. Pour une description plus précise de la physique fine qui agit à l'échelle microscopique, des modèles basés sur la Simulation Numérique Directe (ou DNS) sont développés. Une DNS est basée sur le calcul dans un volume représentatif, du mouvement d'une centaine de fibres (particules) et de leurs interactions, à l'échelle microscopique lorsqu'un écoulement de cisaillement simple est appliqué. Ainsi les suspensions sont considérées avec des interactions entre les fibres et l'évolution statistique d'une population de fibres (forces d'interaction et le nombre de contacts entre les fibres) est décrite. Un code de calcul intensif 3D basé sur la DNS a été développé. Ce code calcule la cinématique associée aux suspensions de fibres concentrées (contenues dans un volume élémentaire) et prend en compte les forces d'interactions présentes à chaque pas de temps. Il existe une autre approche plus simplifiée à l'échelle mésoscospique pour traiter le régime concentré : la théorie cinétique. Cela est possible grâce à une fonction de densité de probabilité qui représente la probabilité de trouver une particule avec une orientation à un temps donné, dans l'espace. Lorsque la concentration du système devient très élevée, on considère un agrégat de fibre (au lieu de considérer une fibre, on suit l'évolution d'un agrégat composé de fibres enchevêtrées).

Abstract

Suspensions involving nanoparticles such as nanofibers and nanotubes are widely used today in the development of functional materials. In order to optimize the usage of these materials and their manufacturing processes, a fine knowledge of the microstructure's evolution in a flow is required. Thus, the study of such suspensions is divided into two main categories: the dilute regime where the concentration is low enough to describe each particle independently from its neighbors and the concentrated regime where the interaction between particles can no longer be neglected, nor the formation of aggregates (or clusters). The first type of suspensions is well known and treatable; the second one remains difficult to study. For a more precise and fine description of the physics at the microscopic scale, a solution consists in performing a Direct numerical simulation (or DNS). DNS is based on the computation, in a representative volume, of the motion of several hundreds of fibers and their interactions. It is a step by step process which derives kinematics as well as macroscopic properties, while taking into account the forces applied on each fiber at the microscopic scale. Thus the suspensions are considered along with interaction forces acting on each fiber and a statistical description is built (number of interactions, magnitude of forces, elastic energy...). During the thesis an extensive 3D simulation code based on DNS has been developed. It takes into account the kinematics of the concentrated fiber suspensions as well as the interaction forces involved. Another more simple way to simulate concentrated fiber suspensions in a given flow is to use kinetic theory approaches. The kinetic theory incorporates a statistical orientation distribution function, which represents the probability of having a particle in a given physical space, having a certain orientation, at a given time. The simplicity of this theory is that it ignores the individuality of the entities (particles, fibers, nanotubes, ...), by introducing a probability function that acts on the mesoscopic scale. Thus, when the concentration of the fibers is high enough, a cluster of fibers can be considered and the rheological properties can then be calculated.

Mots clés

Simulation Numérique Directe, Théorie Cinétique, Rhéologie, Modélisation Numérique, Mécanique des Fluides

Key Words

Direct Numerical Simulation, Kinetic Theory, Rheology, Numerical Modeling, Fluid Mechanics